A MULTISCALE EXAMINATION OF TWO-DIMENSIONAL AGENT-BASED PEDESTRIAN FLOW MODELS WITH SLOWDOWN INTERACTIONS

A Dissertation Presented to

the Faculty of the Department of Mathematics

University of Houston

In Partial Fulfillment

of the Requirements for the Degree

Doctor of Philosophy

By

Thomas Christian Weber

December 2016

A MULTISCALE EXAMINATION OF TWO-DIMENSIONAL AGENT-BASED PEDESTRIAN FLOW MODELS WITH SLOWDOWN INTERACTIONS

Thomas Christian Weber

Approved:

Dr. William Ott (Committee Chair)
Department of Mathematics, University of Houston

Committee Members:

Dr. Ilya Timofeyev
Department of Mathematics, University of Houston

Dr. Andrew Török
Department of Mathematics, University of Houston

Dr. Cory Hauck
Department of Mathematics, University of Tennessee

Dean, College of Natural Sciences and Mathematics
University of Houston

Acknowledgements

I would like to express my deepest gratitude to my doctoral advisors Professor William Ott and Professor Ilya Timofeyev for their encouragement, guidance, and inspiration throughout this work, and for introducing me to dynamical systems, stochastic processes, and agent-based modelling. I feel very fortunate to have had the opportunity to work with them on this project, and I hope that in the future I will have the opportunity to continue to collaborate with both of my advisors.

I would like to thank my committee members, Professor Andrew Török from the University of Houston and Professor Cory Hauck from the University of Tennessee for taking the time to read my dissertation, and for their valuable comments and suggestions.

I would like to thank the wonderful people of the University of Houston College of Mathematics for supporting me throughout the duration of my undergraduate and graduate education. I would especially like to thank Professors Philip Walker, Gordon Johnson, Mark Tomforde, Klaus Kaiser, David Blecher, William Ott, and Ilya Timofeyev for showing me that mathematics was far deeper, more interesting, and more fun than I had any right to hope.

To all of my family and friends: thank you. It can be hard to stay motivated with an undertaking of this size, but you all believed in me, and that belief helped me through the difficult times and brought me to where I am today.

I dedicate this dissertation to my wife, Kristina Pretzsch-Weber, without whose love and support I would not have been able to complete this work. I will always be grateful for all we continue to share. Always.

A MULTISCALE EXAMINATION OF TWO-DIMENSIONAL AGENT-BASED PEDESTRIAN FLOW MODELS WITH SLOWDOWN INTERACTIONS

An Abstract of a Dissertation

Presented to

the Faculty of the Department of Mathematics

University of Houston

In Partial Fulfillment

of the Requirements for the Degree

Doctor of Philosophy

By

Thomas Christian Weber

December 2016

Abstract

Cellular automata models and agent-based models have been areas of significant research over the last few decades. These models have been of particular use in the study of traffic and pedestrian flow, and many models have been proposed to study such problems as highway traffic, evacuation time, and proper placement of exits for optimal evacuation strategy. Because these models are difficult and resource intensive to simulate, however, macroscopic models that examine only gross properties of such flows have been preferred.

Building on recent attempts to derive macroscopic models for traffic and pedestrian flow, such as [14], [21], and [29], the present work, after examining a simple pedestrian model, presents an agent-based model for two groups of pedestrians moving on a two-dimensional lattice with a slowdown interaction. From this microscopic model, we derive a mesoscopic system of differential equations and a macroscopic system of inviscid conservation laws for the model. This macroscopic model is then simulated and compared to a simulation of the microscopic model.

Noting some differences between the microscopic and macroscopic results, we then derive a second-order diffusive system of partial differential equations. Additionally, the hyperbolicity of the inviscid macroscopic model is analyzed in some general cases, as well as one of the simulated specific cases. Finally, we discuss potential directions of future research in the area.

Contents

Chapter 1

Background, Motivation, and Outline

1.1 Background

1.1.1 Cellular Automata Models

The study of cellular automata models is a relatively recent phenomenon in the history of mathematics. In a speech given at the Hixon Symposium on September 20, 1948 [53], John von Neumann, one of the fathers of the field, addressed the lack of a rigorous mathematical theory of automata in the context of a comparison between the human nervous system and computing machines. In doing so, he proposed that the nervous system be considered a group of agents, each of which can be in finitely many states, that are able through their states to send signals to other agents. He posited that in order to rigorously study such systems, logic would need to move closer to the field of thermodynamics. This statement was quite prescient, as the theory of cellular

automata would be applied to exactly that field, though von Neumann's next work in cellular automata would involve, instead, hydrodynamics.

While he was not alone in birthing this field, his speech mentions one of the central problems of automata theory: the need to abstract. Citing Turing, he proposed considering an automaton as a "black box": an object that has a finite number of possible states and a rule for the changing of its state, with the internal operations involved in the changing of the state unspecified and unimportant. In the study of the nervous system, such abstraction is all but essential, as the internal workings of a neuron add far too much complication to the examination of the system as a whole, especially considering the enormous number of neurons involved in the system. Von Neumann viewed the problem of the workings of the individual neurons as the purview of physiology; the mathematician or logician would instead focus on the relationship between the operations of the individual components of the system and the operation of the system as a whole.

While these simple models can give rise to complex behavior and are suitable for modeling a variety of systems, they are in some ways extremely limited. As discussed by Chopard, Dupuis, et al. in their review of cellular automata models [15], the basic definition of a cellular automata model assumes homogeneity of rules across the defined lattice of cells, meaning that the next state of a given cell relies only on its current state and the states of its neighboring cells, ignoring its position on the lattice. Without modifications to the model, it is impossible to consider, for example, a configuration with a boundary. It is also impossible, without modification, for the behavioral rules for a cell to evolve in time. The finite state space of each cell further restricts the applicability of the system, as it may be useful to study a system in which a cell could contain any number of particles. A further restriction of these

early cellular automata models is that they are deterministic in nature: given the current configuration of the model, the configuration at the next time step is an absolute byproduct of the evolution rules of the system. While this is appropriate for some systems, it is often necessary for a system to be able to evolve into one of several possible states in a probabilistic manner.

With these modifications, Chopard, Dupuis, et al., in addition to reviewing the theory and general development of cellular automata models, review many different specific models, such as a model for ferromagnetism called the Ising model, a model for cell differentiation, models of gas flow, and the random walk, amongst others. Of particular relevance to the present work, however, is their study of a traffic flow model.

1.1.2 Traffic Flow Models

In the modern age, the increasing population and size of cities, along with the increase in the number of people who commute to their places of employment, has lead to an increased need for the study of vehicular traffic flow. In the simplest possible cellular automoata model for traffic flow, cells on a one dimensional lattice are treated as sites on a roadway which may at a given time contain a vehicle or be empty. The rule governing the updating of cells then dictates that if a cell is occupied and the next cell is not, then those cells will swap values after the next time step. This updating rule is called Rule 184 and is considered to be the most fundamental cellular automata model for traffic flow [52]. Using this model, we can simulate simple unidirectional traffic, though quite unrealistically, as the behavior of a vehicle depends only on its immediate neighbors and there is no variation in the speed of the observed vehicles.

Models with greater complexity are presented and studied in [18], [42], [43], [35], and many others. In [43], a new model is introduced in which vehicles can change speed based on their current velocities and observation of cells farther away than a single cell. This model, called the Nagel-Schreckenberg model, also introduces randomness in the form of randomly decreasing speeds: a vehicle with non-zero speed will decrease its speed at the next time step with some probability p. It is this randomness that allows the model to better approximate real world behavior, as the model otherwise quickly approaches a stationary pattern. This randomness also gives rise to one of the primary areas of interest in traffic flow models: the traffic jam, and its spontaneous generation from minor variations in the velocities of the vehicles. While [43] shows that traffic jams can arise from randomization of slowdown across all vehicles, [42], after removing all randomization from vehicles free to move at full speed, shows that jams can be created by vehicles that accelerate too slowly or brake too quickly. [35] studies a similar model, but with a delay added to the acceleration mechanism in cases where the vehicle is currently stopped or has recently braked, adding a short memory to the behavior of the vehicles. While these models study only single-lane, unidirectional traffic, models are given in [18] in which traffic is multilane and interacts with perpendicularly flowing traffic at stoplights.

One concern in the study of all of these models is mentioned in [35]: that the system of rules describing the interactions at the microscopic level must as closely as possible create behavior in agreement with the behavior of the natural phenomenon being studied. While this topic falls beyond the scope of the present work, it will be addressed briefly in Chapter 6.

An alternative to the use of cellular automata models to study traffic flow is the use of car-following models. In a car-following model, the velocity and position of each

vehicle is tracked at all times. Changes to the velocity of each vehicle are given by a rule that depends on the current velocity of the vehicle, the velocity of the vehicle ahead of it, and the distance to the vehicle ahead of it. In a more complex system, this rule may depend on the positions and velocities of multiple leading cars. Either way, the entire system can then be described by a system of ordinary differential equations. Such systems are studied in [45], [44], and [5], among others. While models such as these allow for more complex interaction rules, they are not as simple to implement, and so cellular automata models have been more widely applied to traffic flow problems. To study pedestrian flow, however, more complicated models will be useful. A survey of traffic flow models can be found in [17], and additional results can be found in [2] and [25].

1.1.3 Agent-Based Models

Adding an additional layer to the complexity of cellular automata systems, agent-based modeling takes, instead of the cell of cellular automata theory, the agent to be the fundamental unit of interaction. In cellular automata models, the value of a cell varies only in accord with its internal mechanism and the values of neighboring cells. In agent-based models, however, the fundamental component of interaction is the agent, which can move within the bounds of the model and, in doing so, change its own interaction rules over time.

In his 1969 paper, *Models of Segregation* [49], Thomas C. Schelling gives an early example of such a model. He posits an infinitely long line along which members of two groups have been randomly and fairly distributed. Each agent on the line has some preferred ratio of members of his own group to members of the other group in

a local neighborhood, and will move along the line in order to find a neighborhood at which this ratio is met. With this new distribution of agents, the process then repeats ad infinitum, or until a state of equilibrium is achieved. As with von Neumann, Schelling states that the main point of studying agent-based models is to examine the difference between the individual intent of the agents and the often quite different emergent behavior of the system. Indeed, in the studied case, this simple preference rule led to the segregation of the line into segments of uniform makeup.

As was the case with cellular automata models, adding a probabilistic element to agent-based models greatly expands the range of potential applications. In a 1969 article [51], Frank Spitzer defines an agent-based system in which the behavior of each agent is entirely deterministic, but the initial configuration is randomized. By doing so, the path of each agent becomes a stochastic process. He then increases the complexity further by allowing both a random initial distribution of agents and a random initial velocity vector for each agent. From these models, he derives a decription of the behavior of a large class of stochastic agent-based models, and shows that such systems can be used to model both Brownian motion and the Ornstein-Uhlenbeck process.

Stochastic agent-based models have found extensive applications in the sciences, and have been studied in great depth. Indeed, in his classic work *Interacting Particle Systems* [37], Thomas Liggett provides an in-depth study of models that are used to model magnetism, voting habits, the spread of an infectious disease, and gas flow on a lattice. He also expands the theory by studying interesting models on non-compact state spaces. In each model, however, there are common threads: given a simple system of particles that would, absent other interactions, be best described using the theory of Markov processes, impose upon the agents some type of interaction rule. In

doing so, the Markov property no longer holds for the individual agents in the system, but the system as a whole remains Markovian, though highly complex. By choosing interaction rules based on natural processes, we can use these sytems to model said processes with the ultimate goal of studying their long term behavior.

An overview of results in and applications of the study of agent-based models can be found in [13] and [31].

1.1.4 Pedestrian Flow Models

The study of agent-based modeling and the applications thereof have proliferated in the decades since the introduction of the theory. By allowing far more detailed and complex rules of interaction than cellular automata models, agent-based models can be used to study more complex systems. One such area in which agent-based models have been employed to great effect is in the study of pedestrian crowd dynamics. As pedestrians are far less limited and far more heterogeneous in their governing rules and interactions than are vehicles, the depth of complexity brought by agent-based models has been instrumental in this field of study.

An important early example of agent-based pedestrian models is the STREETS model presented in [48]. This work, which follows the underlying principle that it is the activity of the individuals that determines behavior, not the surroundings, defines a model in which pedestrians are drawn to certain locations based on desirabilty of the location and the population at the location, tempered by the cost or distance associated with the location. The model is populated using socio-economic data to create a statistically representative population, each member of which has goals and preferences with respect to the city layout. Deterministic behavior is defined for

the pedestrians in terms of pathfinding algorithms, and stochastic behavior is implemented to simulate preference for certain types of buildings, perceived attractiveness of buildings, and level of concentration and focus of the pedestrian. This gives some idea of the complexity built into even early agent-based pedestrian flow models.

Further works have constructed models for pedestrian flow in various different ways. In [10], a model is studied in which a pedestrian may move within a given lane of traffic or move into an adjacent lane, depending on whether the adjacent space is occupied. Burstedde et al. [12] add a "floor field" to their model of pedestrian flow, which replaces the complicated intelligence of the agent with a rule of adherence to laws dictated by this field. This field is allowed to change in time through decay and diffusion, and is also modified by the passage of the pedestrians themselves, allowing for the modeling of long distance interaction through residual "traces". In their work [6], Bandyopadhyay, Jie, et al. use Mixed Observable Markov Decision Processes to model the uncertainty an individual pedestrian would have as to the intent of other pedestrians, treating the behavioral rules of other pedestrians as unobserved variables. This leads to a model that greatly increases the ability of a pedestrian to avoid collisions, as demonstrated by their programming of a self-driving golf cart to follow this set of instructions.

Additional studies of pedesetrian flow models can be found in [11], [24], [27], [28], [40], [41], and [57].

1.1.5 Applications of Pedestrian Flow Models

One of the primary applications of pedestrian flow models is, of course, the study of phenomena related to pedestrian traffic. As is the case with traffic flow, pedestrian

flow can easily lead to jams, and many works have attempted to discern the conditions that give rise to such occurrences. A related topic of great practical interest is evacuation dynamics. It is of utmost importance that the design of buildings and rooms therein allow for optimal safety in the case of evacuation, and this is an area in which pedestrian flow models have been employed to great use. In [33], evacuation time in a room with a single door is shown to depend on how sensitive the pedestrians are to both the layout of the room and to the paths taken by other pedestrians. A model with two doors is also studied, and it is shown that the evacuation time depends on the distance between the doors, as putting the doors farther apart reduces jamming. In [26], the effects of multiple bottlenecks are examined in the context of merging of pedestrian flows in an evacuation, and it is found that optimizing the rate of a given bottleneck can adversely affect the evacuation rate of the system as a whole. In [32] obstacles are added to the configuration of the model, and pedestrians are given a choice between multiple exit points, some of which they may not be aware. This model is used to demonstrate that lack of awareness of the arrangement of a room and its exits can, in conjunction with a tendency to follow other pedestrians, increase the time it takes for a pedestrian to leave the room. Lack of information caused by obstruction of view is also studied in [56], in which agents are placed in L-shaped corriders, causing them to reevaluate their behavior at each turn based on new information gained. Another such evacuation model is studied in [39] with varying levels of complexity, studying the effects of different ranges of visibility and perceptions of relative danger on the behavior of the studied pedestrian model. A broad survey of results in evacuation theory can be found in [47].

The applications of this theory reach beyond the study of human foot traffic. In [12], the updating of the model due to the motion of the pedestrians is compared to the

process of chemotaxis, in which a motile organism moves according to relative concentrations of a particular chemical. Modeling of chemotaxis is achievable through these techniques, and can be used to study the behavior of various organisms, such as bacteria and ants (in, e.g., [16], [46], and [54]). Conversely, the authors of [33] use ideas from chemotaxis in the creation of their own models, which are then applied to the concepts of jamming and evacuation. Addressing a more recent area of concern, the authors of [6] explicitly state that a goal of their work is to improve safety and effectiveness of autonomous navigation.

1.1.6 The Scaling Problem

While cellular automata and agent-based models have been used extensively to study traffic and pedestrian flow, they have not been used exclusively. Indeed, these models provide what is called a microscopic model for the behavior of the observed systems: a model in which the behavior of every agent or cell is treated separately and the resulting behavior of the group as a whole is observed. This type of study, however, has some significant disadvantages, many of which are discussed in [9]. As previously mentioned [35], the rules chosen to describe the behavior of the agents or cells must match as closely as possible the decision making procedures of the entities being modeled. However, in the real world, we are only able to observe the overall emergent behavior of the system, and attempting to derive from this the decision making behavior of individual agents is a matter of guesswork. It is, conversely, also difficult to judge the behavior of the system as a whole from the knowledge of the rules observed by the agents of the system. While it is possible to observe emergent behavior through spatial, temporal, and iterative averaging, doing so increases the

amount of required resources for running such simulations drastically, and increasing the complexity of rules only worsens this problem. Indeed, this is one of the reasons that pedestrian flow models were not originally treated at this scale.

It is only natural, then, that the study of such system be not restricted to the microscopic scale. We can use macroscopic models, often comprised of systems of partial differential equations, to study aspects of the flow as a whole, such as density or mean speed. One of the first such attempts was made by Lighthill and Whitham in their 1955 paper, "On kinematic waves II: A theory of traffic flow on long, crowded roads" [38]. In this work, Lighthill and Whitham take as their model of traffic behavior the kinematic wave. Using this model, the authors study the effects of concentration of traffic on the mean speed, focusing on vehicular behavior following the changing of a red light to green and on the backwards propagation of traffic waves. They also expand their view to incorporate intersecting traffic. The authors themselves note a major caveat of using this method, however: it is only suitable for studying the limiting behavior of large populations. Additionally, using these models necessitates relinquishing the fine control afforded by miscroscopic models, though Kneidl, Thiemann, et. al. had some success in uniting the two scales in [34], in which a microscopic model and a macroscopic model are coupled, leading to a system in which the agents are aware of the macroscopic behavior, and the macroscopic model is able to take into account the effects of the microscopic programming, leading to a reduction in the difference between simulated evacuation times at the different scales.

Additional examples of such models can be found in [4], [7], [8], [30], and [55].

1.1.7 A Multiscale Approach

An obvious question thus arises: is there a way to program the behavior of the agents at the microscopic level but simulate and observe it at the macroscopic level, giving us the full complexity allowed by cellular automata models but the relative ease and speed of simulation afforded by differential equations? Some recent works in the field have attempted to do exactly this.

In [58], Zhang defines an agent-based car following model, in which the quantities of interest for the agents are speed, acceleration, distance between vehicles, and driver response time. By introducing smooth velocity and spacing field functions and expanding, a macroscopic momentum equation is derived. It is noted that it is also possible to derive this momentum equation through a Taylor expansion, and in doing so, derive a viscosity term through a second order expansion. The author further notes that the exact substitution of field equations and the approximation through expansion lead to the same result, but that there is no current understanding of why this should be so.

The writers of [1] attempt to apply Zhang's methods to a pedestrian flow model in two dimensions. From a two dimensional car-following model and a conservation law, they are able to derive an appropriate macroscopic form. The model thus derived is then simulated and is said to compare favorably to real-world observations in the case of jamming at evacuation points.

Two authors who have contributed considerably to the study of conversion between microscopic, kinetic, and macroscopic pedestrian flow models are C. Appert-Rolland and P. Degond. Some of their results can be found in [3], [19], [20], [21], [22], and [23], in which they and various other contributors study different forms of microscopic

models and the derived macroscopic models. One difficulty that repeatedly arises in these papers is the necessity of a suitable closure approximation when transitioning to the macroscopic model, and the viability of several such closures is examined.

A final paper that examines the derivation of macroscopic models from cellular automata models is found in "Pedestrian Flow Models with Slowdown Interactions", by Chertock, Kurganov, Polizzi, and Timofeyev. In this masterful work, a cellular automata model is devised in which two groups of pedestrians interact on a one-dimensional lattice, with rules for exclusion principle interactions between members of a single group and slowdown interactions for members of opposing groups. From this model is derived first a mesoscopic system of differenctial equations, and then a macroscopic system of PDEs describing the time-evolution of the densities of each group. It is noted that the derived macroscopic model is less diffusive than the microscopic model in simulations, and as was suggested in [58], the Taylor expansion of the mesoscopic model is used to derive a diffusive viscosity term. The new viscous system of equations is found to more accurately model the behavior of the microscopic model. Additionally, the hyperbolicity of the macroscopic model is examined. It is determined that the system will enter a non-hyperbolic regime under certain combinations of densities, leading to unnatural oscillations in the simulated data. Additional work by Timofeyev, along with Hauck and Sun, in the study of derived macroscopic models for traffic flow can be found in [29].

1.2 The Present Work

1.2.1 Motivation

The goal of the present work is to study a specific class of stochastic, two-dimensional agent-based pedestrian flow models defined on a discrete lattice, in which the behavior of the agents is determined by a velocity field, an exclusion principle, and a slowdown interaction, and from these models to derive deterministic mesoscopic and macroscopic models representing the emergent behavior of the stochastic models. As simulation of the macroscopic model is far less resource intensive than simulation of the microscopic model, the hope is that the derived model will be suitable for practical purposes.

The direction of this work has been heavily influenced by the work of Chertock, Kurganov, Polizzi, and Timofeyev in [14], in that this work applies their methodology to a broader class of agent-based models, namely, those in two dimensions with certain specific behaviors. Indeed, the behavior studied in their work can, with the proper one-dimensional lattice and velocity functions, be well represented using the techniques presented herein.

The prospective advantages provided by extending the one-dimensional model to a two-dimensional model are many. A two-dimensional model in which pedestrians are not restricted to lanes is a much more realistic representation of natural behavior, and should lead to more useful results for applications. While the models studied herein involve a maximum of two different groups, the results can be generalized to potentially any number of groups, each following a different velocity field and possessing different slowdown laws. This will allow the study of, for example, multiple

groups of pedestrians attempting to evacuate a building in which multiple exits are present.

1.2.2 Outline

In Chapter 2, we present a simple two-dimensional model with a velocity field and an exclusion principle interaction. This case is simpler than our ultimate goal, but is a good showcase for the techniques that are used. While all desired models are derived, no presentation is made of the results of simulating the models, as the actions of a single group on a lattice have been extensively studied in the past.

In Chapter 3, a more complex model is studied, this time incorporating two groups with a slowdown interaction defined for members of the opposite groups. This chapter proceeds in much the same manner as Chapter 2, but the resulting mesoscopic and macroscopic models are far more complicated and, therefore, interesting. Specifically, the macroscopic model is a system of partial differential equations whose properties are examined in greater depth in Chapter 5.

In Chapter 4, techniques for simulating the microscopic and mesoscopic/macroscopic models are outlined, as are several initial configurations of interest. These interesting systems are simulated using both models, and the results are presented and compared. Discrepancies between the models are noted and analyzed, as are the effects of certain parameters on these discrepancies.

In Chapter 5, based on the results presented in Chapters 3 and 4, we study properties of the macroscopic model that are likely to be problematic: hyperbolicity and diffusiveness. Hyperbolicity conditions for the system are derived, and specific models that give rise to hyperbolic and non-hyperbolic systems are examined. We also ex-

amine cells from some models presented in Chapter 4 to ascertain the hyperbolicity of the systems studied therein. A difference in the diffusiveness of the microscopic and macroscopic models noticed in Chapter 4 is further analyzed, and a diffusive correction is derived.

Finally, in Chapter 6, a summary of results is presented, and areas of potential future research are discussed.

Chapter 2

Single Group Model with Exclusion Interactions

Starting with a simple case, we examine the behavior of a single group of agents on a two-dimensional lattice moving according to a velocity field, with only an exclusion principle interaction between agents. The derived models will not be simulated, but will serve as a template for the models derived in the sequel.

2.1 Microscopic Agent-Based Model

We consider the time evolution of a single group of agents on an $M \times N$ lattice $\mathcal{L}$ with periodic boundary, along with a time independent vector field on $\mathcal{L}$ that defines a velocity at each point on the lattice. We represent the configuration of agents on

the lattice by $\sigma_{j,k,t} := \sigma(j,k,t)$, where

$$\sigma_{j,k,t} = \begin{cases} 1, & \text{if at time } t \text{ cell } (j,k) \text{ is occupied by an agent,} \\ 0, & \text{otherwise.} \end{cases} . \tag{2.1}$$

We apply the exclusion principle to the agents on the lattice: two agents cannot occupy the same cell at the same time.

We next take some velocity field $\boldsymbol{\phi}(j,k) = (\phi_1(j,k), \phi_2(j,k))$ on $\mathcal{L}$, and letting $V_{(a,b)\to(c,d)}(t)$ represent the rate of transition of an agent from cell (a,b) to cell (c,d) at time t, we define

$$V_{(j,k)\to(j\pm1,k)}(t) = \pm c_0 \phi_1(j,k) H(\pm\phi_1(j,k)), \tag{2.2}$$

and

$$V_{(j,k)\to(j,k\pm1)}(t) = \pm c_0 \phi_2(j,k) H(\pm\phi_2(j,k)), \tag{2.3}$$

where H is the Heaviside Function with $H(0) = 0$ and c_0 is some scaling parameter with $0 < c_0$. The Heaviside functions ensure that the rate of transition in a given direction is positive if and only if the component of the velocity vector in that direction is positive. The rate is zero, otherwise. We define all other transition rates of the form $V_{(a,b)\to(c,d)}(t)$ where $(a,b) \neq (c,d)$ to be zero, limiting movement by agents to vertical and horizontal movement only. We will refer to such transitions as elementary transitions.

The velocity field defined in Equations 2.2 and 2.3 are used to define the probability of an agent moving to a neighboring cell. The probability at time t of an agent from

cell (j,k) transferring to cell $(j \pm 1, k)$ during a small time interval Δt is given by

$$P_{(j,k)\to(j\pm1,k)}(t) = \Delta t V_{(j,k)\to(j\pm1,k)}(t)\sigma_{j,k,t}(1-\sigma_{j\pm1,k,t}), \tag{2.4}$$

while the probability of an agent from cell (j,k) transferring to cell $(j,k\pm1)$ is given by

$$P_{(j,k)\to(j,k\pm1)}(t) = \Delta t V_{(j,k)\to(j,k\pm1)}(t)\sigma_{j,k,t}(1-\sigma_{j,k\pm1,t}). \tag{2.5}$$

In these equations, the terms $\sigma_{j,k,t}(1-\sigma_{j\pm1,k,t})$ and $\sigma_{j,k,t}(1-\sigma_{j,k\pm1,t})$ ensure that the probability of transition is nonzero if and only if the originating cell is occupied and the target cell is not, thus implementing the exclusion principle.

2.2 Mesoscopic Deterministic Model

With these transition probabilities, $\boldsymbol{\sigma}_t := (\sigma_{j,k,t})$ is a continuous-time Markov chain. Its generator is given by

$$A\psi = \lim_{\Delta t\to 0} \frac{\mathbb{E}[\psi(\boldsymbol{\sigma}_{\Delta t})|\boldsymbol{\sigma}_0] - \psi(\boldsymbol{\sigma}_0)}{\Delta t}, \tag{2.6}$$

where $\boldsymbol{\sigma}_0$ is the initial configuration of the lattice, $\boldsymbol{\sigma}_{\Delta t}$ is the configuration at time Δt, ψ is any test function, and the expectation is taken over all possible transitions from $\boldsymbol{\sigma}_0$ to $\boldsymbol{\sigma}_{\Delta t}$. In the case that $\psi(\boldsymbol{\sigma}) = \sigma_{j,k,t}$ for some fixed j and k, we can write the action of the generator on ψ as

$$A\sigma_{j,k,t} = \lim_{\Delta t\to 0} \frac{\mathbb{E}[\sigma_{j,k,\Delta t}|\boldsymbol{\sigma}_0] - \sigma_{j,k,0}}{\Delta t} \tag{2.7}$$

$$= \lim_{\Delta t \to 0} \frac{\mathbb{E}[\sigma_{j,k,\Delta t} - \sigma_{j,k,0} | \boldsymbol{\sigma}_0]}{\Delta t} \tag{2.8}$$

$$= \lim_{\Delta t \to 0} \frac{1}{\Delta t} \sum_{s \in \Omega} (s_{j,k} - \sigma_{j,k,0}) P(\boldsymbol{\sigma}_{\Delta t} = s | \boldsymbol{\sigma}_0), \tag{2.9}$$

where Ω is the space of all possible configurations of the lattice.

With the probabilities defined above in Equations 2.4 and 2.5, we have that

$$P(\boldsymbol{\sigma}_{\Delta t} = s | \boldsymbol{\sigma}_0) = P_{(j,k) \to (j \pm 1, k)}(t) \tag{2.10}$$

if s can be obtained from $\boldsymbol{\sigma}_0$ by swapping the values of $\sigma_{j,k,0}$ and $\sigma_{j+1,k,0}$ or of $\sigma_{j,k,0}$ and $\sigma_{j-1,k,0}$ for some cell (j,k), and that

$$P(\boldsymbol{\sigma}_{\Delta t} = s | \boldsymbol{\sigma}_0) = P_{(j,k) \to (j,k \pm 1)}(t) \tag{2.11}$$

if s can be obtained from $\boldsymbol{\sigma}_0$ by swapping the values of $\sigma_{j,k,0}$ and $\sigma_{j,k+1,0}$ or of $\sigma_{j,k,0}$ and $\sigma_{j,k-1,0}$ for some cell (j,k). For all other $s \in \Omega$, the transition from $\boldsymbol{\sigma}_0$ to s would require more than one elementary transition or be impossible through any combination of elementary transitions, and thus for these cases,

$$P(\boldsymbol{\sigma}_{\Delta t} = s | \boldsymbol{\sigma}_0) = o(\Delta t), \tag{2.12}$$

where we say that a function $g(x) = o(f(x))$ if $\lim_{x \to 0} \frac{g(x)}{f(x)} = 0$. If we then denote by U the set of configurations of the lattice obtainable from $\boldsymbol{\sigma}_0$ by single elementary transitions, we have from Equation 2.9 that

$$A\sigma_{j,k,t} = \lim_{\Delta t \to 0} \frac{1}{\Delta t} \sum_{s \in \Omega} (s_{j,k} - \sigma_{j,k,0}) P(\boldsymbol{\sigma}_{\Delta t} = s | \boldsymbol{\sigma}_0) \tag{2.13}$$

$$= \lim_{\Delta t \to 0} \frac{1}{\Delta t} \sum_{s \in U} (s_{j,k} - \sigma_{j,k,0}) P(\boldsymbol{\sigma}_{\Delta t} = s | \boldsymbol{\sigma}_0)$$
$$+ \lim_{\Delta t \to 0} \frac{1}{\Delta t} \sum_{s \in \Omega \setminus U} (s_{j,k} - \sigma_{j,k,0}) P(\boldsymbol{\sigma}_{\Delta t} = s | \boldsymbol{\sigma}_0) \tag{2.14}$$

$$= \lim_{\Delta t \to 0} \frac{1}{\Delta t} \sum_{s \in U} (s_{j,k} - \sigma_{j,k,0}) P(\boldsymbol{\sigma}_{\Delta t} = s | \boldsymbol{\sigma}_0) + \lim_{\Delta t \to 0} \frac{1}{\Delta t} o(\Delta t) \tag{2.15}$$

$$= \lim_{\Delta t \to 0} \frac{1}{\Delta t} \sum_{s \in U} (s_{j,k} - \sigma_{j,k,0}) P(\boldsymbol{\sigma}_{\Delta t} = s | \boldsymbol{\sigma}_0). \tag{2.16}$$

Now, unless an agent transitions into or out of cell (j,k) in the transition from $\boldsymbol{\sigma}_0$ to s, we have that $s_{j,k} - \sigma_{j,k,0} = 0$. If an agent transitions into the cell, $s_{j,k} - \sigma_{j,k,0} = 1$, and if an agent transitions out of the cell, $s_{j,k} - \sigma_{j,k,0} = -1$. Thus Equation 2.16 can be simplified to

$$\begin{aligned} A\sigma_{j,k,t} = \lim_{\Delta t \to 0} \frac{1}{\Delta t} \big[& P_{(j-1,k)\to(j,k)}(t) - P_{(j,k)\to(j+1,k)}(t) + P_{(j+1,k)\to(j,k)}(t) \\ & - P_{(j,k)\to(j-1,k)}(t) + P_{(j,k-1)\to(j,k)}(t) - P_{(j,k)\to(j,k+1)}(t) \\ & + P_{(j,k+1)\to(j,k)}(t) - P_{(j,k)\to(j,k-1)}(t) \big], \end{aligned} \tag{2.17}$$

which, taking into account Equations 2.2-2.5, expands to

$$\begin{aligned} A\sigma_{j,k,t} = \lim_{\Delta t \to 0} \frac{1}{\Delta t} [& \Delta t c_0 \phi_1(j-1,k) H(\phi_1(j-1,k)) \sigma_{j-1,k,t}(1 - \sigma_{j,k,t}) \\ & - \Delta t c_0 \phi_1(j,k) H(\phi_1(j,k)) \sigma_{j,k,t}(1 - \sigma_{j+1,k,t}) \\ & - \Delta t c_0 \phi_1(j+1,k) H(-\phi_1(j+1,k)) \sigma_{j+1,k,t}(1 - \sigma_{j,k,t}) \\ & + \Delta t c_0 \phi_1(j,k) H(-\phi_1(j,k)) \sigma_{j,k,t}(1 - \sigma_{j-1,k,t}) \\ & + \Delta t c_0 \phi_2(j,k-1) H(\phi_2(j,k-1)) \sigma_{j,k-1,t}(1 - \sigma_{j,k,t}) \end{aligned}$$

$$
\begin{aligned}
&- \Delta t c_0 \phi_2(j,k) H(\phi_2(j,k)) \sigma_{j,k,t}(1-\sigma_{j,k+1,t}) \\
&- \Delta t c_0 \phi_2(j,k+1) H(-\phi_2(j,k+1)) \sigma_{j,k+1,t}(1-\sigma_{j,k,t}) \\
&+ \Delta t c_0 \phi_2(j,k) H(-\phi_2(j,k)) \sigma_{j,k,t}(1-\sigma_{j,k-1,t})] \qquad (2.18) \\
= &\, c_0 \phi_1(j-1,k) H(\phi_1(j-1,k)) \sigma_{j-1,k,t}(1-\sigma_{j,k,t}) \\
&- c_0 \phi_1(j,k) H(\phi_1(j,k)) \sigma_{j,k,t}(1-\sigma_{j+1,k,t}) \\
&- c_0 \phi_1(j+1,k) H(-\phi_1(j+1,k)) \sigma_{j+1,k,t}(1-\sigma_{j,k,t}) \\
&+ c_0 \phi_1(j,k) H(-\phi_1(j,k)) \sigma_{j,k,t}(1-\sigma_{j-1,k,t}) \\
&+ c_0 \phi_2(j,k-1) H(\phi_2(j,k-1)) \sigma_{j,k-1,t}(1-\sigma_{j,k,t}) \\
&- c_0 \phi_2(j,k) H(\phi_2(j,k)) \sigma_{j,k,t}(1-\sigma_{j,k+1,t}) \\
&- c_0 \phi_2(j,k+1) H(-\phi_2(j,k+1)) \sigma_{j,k+1,t}(1-\sigma_{j,k,t}) \\
&+ c_0 \phi_2(j,k) H(-\phi_2(j,k)) \sigma_{j,k,t}(1-\sigma_{j,k-1,t}). \qquad (2.19)
\end{aligned}
$$

Recalling that the generator satisfies the property

$$
\frac{d}{dt}\mathbb{E}\psi = \mathbb{E}A\psi, \qquad (2.20)
$$

and applying this property to the test function $\psi(\boldsymbol{\sigma}) = \sigma_{j,k,t}$ results in the following equation for the time evolution of $\rho_{j,k,t} := \mathbb{E}[\sigma_{j,k,t}]$:

$$
\begin{aligned}
\frac{d}{dt}\rho_{j,k,t} = \mathbb{E}\,[&c_0 \phi_1(j-1,k) H(\phi_1(j-1,k)) \sigma_{j-1,k,t}(1-\sigma_{j,k,t}) \\
&- c_0 \phi_1(j,k) H(\phi_1(j,k)) \sigma_{j,k,t}(1-\sigma_{j+1,k,t}) \\
&- c_0 \phi_1(j+1,k) H(-\phi_1(j+1,k)) \sigma_{j+1,k,t}(1-\sigma_{j,k,t})
\end{aligned}
$$

$$
\begin{aligned}
&+ c_0\phi_1(j,k)H(-\phi_1(j,k))\sigma_{j,k,t}(1-\sigma_{j-1,k,t}) \\
&+ c_0\phi_2(j,k-1)H(\phi_2(j,k-1))\sigma_{j,k-1,t}(1-\sigma_{j,k,t}) \\
&- c_0\phi_2(j,k)H(\phi_2(j,k))\sigma_{j,k,t}(1-\sigma_{j,k+1,t}) \\
&- c_0\phi_2(j,k+1)H(-\phi_2(j,k+1))\sigma_{j,k+1,t}(1-\sigma_{j,k,t}) \\
&+ c_0\phi_2(j,k)H(-\phi_2(j,k))\sigma_{j,k,t}(1-\sigma_{j,k-1,t})\big]\,. \qquad (2.21)
\end{aligned}
$$

We can derive a closure approximation for this equation by assuming approximate independence of second moments, i.e. that

$$\mathbb{E}[\sigma_{j,k,t}\sigma_{j+1,k,t}] \approx \mathbb{E}[\sigma_{j,k,t}]\mathbb{E}[\sigma_{j+1,k,t}] \qquad (2.22)$$

and that

$$\mathbb{E}[\sigma_{j,k,t}\sigma_{j,k+1,t}] \approx \mathbb{E}[\sigma_{j,k,t}]\mathbb{E}[\sigma_{j,k+1,t}]. \qquad (2.23)$$

A closure of this type has previously been used and justified in [14], [36], and [50]. In this case, a closed system can be obtained, and the resulting mesoscopic model for the time evolution of the density $\rho_{j,k,t}$ is

$$
\begin{aligned}
\frac{d}{dt}\rho_{j,k,t} &= c_0\phi_1(j-1,k)H(\phi_1(j-1,k))\rho_{j-1,k,t}(1-\rho_{j,k,t}) \\
&- c_0\phi_1(j,k)H(\phi_1(j,k))\rho_{j,k,t}(1-\rho_{j+1,k,t}) \\
&- c_0\phi_1(j+1,k)H(-\phi_1(j+1,k))\rho_{j+1,k,t}(1-\rho_{j,k,t}) \\
&+ c_0\phi_1(j,k)H(-\phi_1(j,k))\rho_{j,k,t}(1-\rho_{j-1,k,t}) \\
&+ c_0\phi_2(j,k-1)H(\phi_2(j,k-1))\rho_{j,k-1,t}(1-\rho_{j,k,t})
\end{aligned}
$$

$$
\begin{aligned}
&- c_0\phi_2(j,k)H(\phi_2(j,k))\rho_{j,k,t}(1-\rho_{j,k+1,t}) \\
&- c_0\phi_2(j,k+1)H(-\phi_2(j,k+1))\rho_{j,k+1,t}(1-\rho_{j,k,t}) \\
&+ c_0\phi_2(j,k)H(-\phi_2(j,k))\rho_{j,k,t}(1-\rho_{j,k-1,t}),
\end{aligned} \tag{2.24}
$$

with $\rho_{j,k,t} \in [0,1]$ for all j, k, and t. This system is deterministic and is defined on the same lattice $\mathcal{L}$ as the microscopic model.

2.3 Macroscopic PDE Model

We now treat sites $(j,k) \in \mathcal{L}$ as square cells with fixed side length $h > 0$. Let Ω denote the subdomain of $\mathbb{R}^2$ corresponding to the lattice $\mathcal{L}$, i.e., $\Omega = [0,M] \times [0,N]$ with the total number of cells depending on h. We consider a rescaling of time $t \to ht$ and derive a coarse-grained PDE model as the cell size tends to zero and the number of cells tends to infinity.

We rewrite the Equation 2.24 in the following flux form, taking the time rescaling into account:

$$
\frac{d\rho_{j,k,t}}{dt} = -\frac{F_{j,j+1} - F_{j-1,j} + G_{k,k+1} - G_{k-1,k}}{h}, \tag{2.25}
$$

where

$$
\begin{aligned}
F_{j,j+1} &= c_0\phi_1(j,k)H(\phi_1(j,k))\rho_{j,k,t}(1-\rho_{j+1,k}) \\
&\quad + c_0\phi_1(j+1,k)H(-\phi_1(j+1,k))\rho_{j+1,k}(1-\rho_{j,k,t}),
\end{aligned} \tag{2.26}
$$

$$
\begin{aligned}
G_{k,k+1} &= c_0\phi_2(j,k)H(\phi_2(j,k))\rho_{j,k,t}(1-\rho_{j,k+1}) \\
&\quad + c_0\phi_2(j,k+1)H(-\phi_2(j,k+1))\rho_{j,k+1}(1-\rho_{j,k,t}).
\end{aligned} \tag{2.27}
$$

Here $F_{j,j+1}$ represents the flux in the horizontal direction while $G_{k,k+1}$represents the flux in the vertical direction. Multiplying Equation 2.25 by $\varphi_{j,k} := \varphi(jh, kh)$, where $\varphi \in C_0^1(\bar{\Omega})$ is a test function, and summing over the cells of Ω gives

$$\sum_{j,k} \varphi_{j,k} \frac{d\rho_{j,k,t}}{dt} = -\sum_{j,k} \left[\varphi_{j,k} \frac{F_{j,j+1} - F_{j-1,j}}{h} + \varphi_{j,k} \frac{G_{k,k+1} - G_{k-1,k}}{h} \right] \tag{2.28}$$

Using summation by parts and the fact that $\varphi \in C_0^1(\bar{\Omega})$, this can be rewritten as

$$\begin{aligned} \sum_{j,k} \varphi_{j,k} \frac{d\rho_{j,k,t}}{dt} &= -\sum_{j,k} \left[-\frac{\varphi_{j+1,k} - \varphi_{j,k}}{h} F_{j,j+1} - \frac{\varphi_{j,k+1} - \varphi_{j,k}}{h} G_{k,k+1} \right] \\ &= \sum_{j,k} \left[F_{j,j+1} \frac{\varphi_{j+1,k} - \varphi_{j,k}}{h} + G_{k,k+1} \frac{\varphi_{j,k+1} - \varphi_{j,k}}{h} \right]. \end{aligned} \tag{2.29}$$

We define pedestrian densities on Ω as follows. Reusing the notation ρ for convenience, define the function $\rho(x, y, t)$ to be a continuous piecewise linear interpolation of $\rho_{j,k,t}(t)$ and take the limit as $h \to 0^+$. We will denote $\rho(x, y, t)$ by $\rho_{x,y,t}$. Due to the boundedness of both $\rho_{x,y,t}$ and $\frac{d\rho_{j,k,t}}{dt}$, we obtain a weak formulation of the coarse-grained model:

$$\iint_{\Omega} \varphi(x, y) \frac{\partial}{\partial t} \rho_{x,y,t} dx dy = \iint_{\Omega} \left[F(\rho_{x,y,t}) \frac{\partial}{\partial x} \varphi(x, y) + G(\rho_{x,y,t}) \frac{\partial}{\partial y} \varphi(x, y) \right] dx dy, \tag{2.30}$$

where $F(\rho_{x,y,t})$ and $G(\rho_{x,y,t})$ are defined as the corresponding limits of $F_{j,j+1}$ and $G_{k,k+1}$ from Equations 2.26 and 2.27, respectively, when spacial scaling is taken into

account; i.e.,

$$\begin{aligned} F(\rho_{x,y,t}) &= \lim_{h\to 0} c_0\phi_1(x,y)\rho_{x,y,t}(1-\rho_{x,y,t})[H(\phi_1(x,y)) + H(-\phi_1(x+h,y))] \\ &= c_0\phi_1(x,y)\rho_{x,y,t}(1-\rho_{x,y,t})[H(\phi_1(x,y)) + H(-\phi_1(x,y))] \\ &= c_0\phi_1(x,y)\rho_{x,y,t}(1-\rho_{x,y,t}) \qquad (2.31) \\ G(\rho_{x,y,t}) &= \lim_{h\to 0} c_0\phi_2(x,y)\rho_{x,y,t}(1-\rho_{x,y,t})[H(\phi_2(x,y)) + H(-\phi_2(x,y+h))] \\ &= c_0\phi_2(x,y)\rho_{x,y,t}(1-\rho_{x,y,t})[H(\phi_2(x,y)) + H(-\phi_2(x,y))] \\ &= c_0\phi_2(x,y)\rho_{x,y,t}(1-\rho_{x,y,t}) \qquad (2.32) \end{aligned}$$

with the last equivalence in each case due to the fact that

$$f(x)[H(f(x)) + H(-f(x))] = f(x) \qquad (2.33)$$

for all functions f. Applying integration by parts and again using the fact that $\varphi \in C_0^1(\bar{\Omega})$ gives us

$$\iint_\Omega \varphi(x,y)\frac{\partial}{\partial t}\rho_{x,y,t}dxdy = \iint_\Omega \left[-\frac{\partial}{\partial x}F(\rho_{x,y,t})\varphi(x,y) - \frac{\partial}{\partial y}G(\rho_{x,y,t})\varphi(x,y)\right]dxdy \qquad (2.34)$$

Because φ is arbitrary, Equation 2.34 can be written as the following partial differential equation:

$$\rho_t + F(\rho)_x + G(\rho)_y = 0. \qquad (2.35)$$

Equation 2.35 can also be written in the form

$$\rho_t + \mathbf{u}(\rho)\cdot\nabla\rho = 0, \qquad (2.36)$$

where $\mathbf{u}$ is given by

$$\mathbf{u}(\rho) = (F_x(\rho), G_y(\rho)). \tag{2.37}$$

We can then see that this is, in fact, a non-linear advection equation. Additionally, if we rewrite Equation 2.35 in the form

$$\rho_t + \nabla \cdot (c_0 \rho(1-\rho)\boldsymbol{\phi}) = 0. \tag{2.38}$$

we see that the equation is a non-linear conservation law. Indeed, as we assume the boundary of the region Ω to be periodic, we have that the total flux of any observed vector field out of the boundary must be zero. In particular, we would have that

$$\iint_\Omega \nabla \cdot (c_0 \rho(1-\rho)\boldsymbol{\phi})\, dxdy = 0, \tag{2.39}$$

by the Divergence Theorem. Integrating both sides of Equation 2.38 then gives

$$\iint_\Omega \rho_t dxdy = 0. \tag{2.40}$$

Rewriting Equation 2.41 as

$$\frac{\partial}{\partial t} \iint_\Omega \rho dxdy = 0, \tag{2.41}$$

we see that Equation 2.38 is a conservation equation for the total mass of pedestrians. Indeed, this will be the case under any boundary conditions for which Equation 2.39 holds.

Chapter 3

Two Group Model with Slowdown Interactions

We now look at the more complex case of two groups moving on the lattice $\mathcal{L}$ defined in Chapter 2 with slow-down interactions between members of different groups, that we will call Group A and Group B.

3.1 Microscopic Agent-Based Model

We represent the configuration of agents from Groups A and B, respectively, on the lattice by $\sigma^A_{j,k,t} := \sigma^A(j,k,t)$ and $\sigma^B_{j,k,t} := \sigma^B(j,k,t)$. Here,

$$\sigma^A_{j,k,t} = \begin{cases} 1, & \text{if at time } t \text{ cell } (j,k) \text{ is occupied by a pedestrian} \\ & \text{from Group A,} \\ 0, & \text{otherwise.} \end{cases} \tag{3.1}$$

and

$$\sigma^B_{j,k,t} = \begin{cases} 1, & \text{if at time } t \text{ cell } (j,k) \text{ is occupied by a pedestrian} \\ & \text{from Group B,} \\ 0, & \text{otherwise.} \end{cases} . \tag{3.2}$$

In this case, we assume that agents from different groups can occupy the same cell but continue to disallow two agents from the same group to simultaneously occupy a cell. Allowing agents from opposing groups to occupy the same cell but imposing a reduction on their velocities when they do so is done to mimic the more complicated interaction one would observe in nature, in which the pedestrians involved would attempt to sidestep each other, as in [14]. This slowdown interaction allows us to simulate this natural interaction without greatly increasing the complexity of our model.

Taking some velocity fields $\phi^A(j,k) = (\phi^A_1(j,k), \phi^A_2(j,k))$ and $\phi^B(j,k) = (\phi^B_1(j,k), \phi^B_2(j,k))$ defined on $\mathcal{L}$, we consider a slow-down interaction by prescribing the velocity

$$V^A(j,k,\sigma) = (V^A_1(j,k,\sigma), V^A_2(j,k,\sigma)) \tag{3.3}$$

for agents in Group A to each cell based on the configurations of adjacent cells. Letting $V^A_{(a,b)\to(c,d)}(t)$ represent the rate of transition of an agent in Group A from cell

(a, b) to cell (c, d) at time t, we define

$$V^A_{(j,k)\to(j\pm1,k)}(t) = \begin{cases} \pm c_0\phi^A_1(j,k)H(\pm\phi^A_1(j,k)), & \text{if } \sigma^B_{j,k} = \sigma^B_{j\pm1,k} = 0, \\ \pm c_1\phi^A_1(j,k)H(\pm\phi^A_1(j,k)), & \text{if } \sigma^B_{j,k} = 0, \sigma^B_{j\pm1,k} = 1, \\ \pm c_2\phi^A_1(j,k)H(\pm\phi^A_1(j,k)), & \text{if } \sigma^B_{j,k} = 1, \sigma^B_{j\pm1,k} = 0, \\ \pm c_3\phi^A_1(j,k)H(\pm\phi^A_1(j,k)), & \text{if } \sigma^B_{j,k} = \sigma^B_{j\pm1,k} = 1 \end{cases}, \tag{3.4}$$

and

$$V^A_{(j,k)\to(j,k\pm1,)}(t) = \begin{cases} \pm c_0\phi^A_2(j,k)H(\pm\phi^A_2(j,k)), & \text{if } \sigma^B_{j,k} = \sigma^B_{j,k\pm1} = 0, \\ \pm c_1\phi^A_2(j,k)H(\pm\phi^A_2(j,k)), & \text{if } \sigma^B_{j,k} = 0, \sigma^B_{j,k\pm1} = 1, \\ \pm c_2\phi^A_2(j,k)H(\pm\phi^A_2(j,k)), & \text{if } \sigma^B_{j,k} = 1, \sigma^B_{j,k\pm1} = 0, \\ \pm c_3\phi^A_2(j,k)H(\pm\phi^A_2(j,k)), & \text{if } \sigma^B_{j,k} = \sigma^B_{j,k\pm1} = 1 \end{cases}. \tag{3.5}$$

These velocities can be simplified to the form

$$\begin{aligned} V^A_{(j,k)\to(j\pm1,k)}(t) = {} & \pm\phi^A_1(j,k)H(\pm\phi^A_1(j,k)) \\ & \times \left[c_0(1-\sigma^B_{j,k})(1-\sigma^B_{j\pm1,k}) + c_1(1-\sigma^B_{j,k})\sigma^B_{j\pm1,k}\right. \\ & \left. + c_2\sigma^B_{j,k}(1-\sigma^B_{j\pm1,k}) + c_3\sigma^B_{j,k}\sigma^B_{j\pm1,k}\right], \end{aligned} \tag{3.6}$$

$$\begin{aligned} V^A_{(j,k)\to(j,k\pm1,)}(t) = {} & \pm\phi^A_2(j,k)H(\pm\phi^A_2(j,k)) \\ & \times \left[c_0(1-\sigma^B_{j,k})(1-\sigma^B_{j,k\pm1}) + c_1(1-\sigma^B_{j,k})\sigma^B_{j,k\pm1}\right. \\ & \left. + c_2\sigma^B_{j,k}(1-\sigma^B_{j,k\pm1}) + c_3\sigma^B_{j,k}\sigma^B_{j,k\pm1}\right], \end{aligned} \tag{3.7}$$

with terms such as $\sigma^B_{j,k}(1-\sigma^B_{j,k\pm1})$ acting as logical operators to select the appropriate slowdown constant. Through the assignation of scaling constants c_0, c_1, c_2 and c_3 to the velocity in the cases in which both cells are unoccupied by members of the

opposing group, the target cell is occupied by a member of the opposing group, the current cell is occupied by a member of the opposing group, and both cells are occupied by members of the opposing group, respectively, we are allowed to define the strength of the slowdown interaction by modifying the values of these constants, with a smaller scalar value corresponding to a stronger slowdown interaction. The constants should then logically obey the relationship

$$c_3 < c_2 \leq c_1 < c_0, \tag{3.8}$$

as one would expect a stronger interaction as the number of interacting pedestrians from opposing groups increases.

The velocities of agents in Group B are defined in a similar manner, giving us

$$\begin{aligned} V^B_{(j,k)\to(j\pm1,k)}(t) = {} & \pm\phi^B_1(j,k)H(\pm\phi^B_1(j,k)) \\ & \times \left[c_0(1-\sigma^A_{j,k})(1-\sigma^A_{j\pm1,k}) + c_1(1-\sigma^A_{j,k})\sigma^A_{j\pm1,k}\right. \\ & \left. +c_2\sigma^A_{j,k}(1-\sigma^A_{j\pm1,k}) + c_3\sigma^A_{j,k}\sigma^A_{j\pm1,k}\right], \end{aligned} \tag{3.9}$$

$$\begin{aligned} V^B_{(j,k)\to(j,k\pm1,)}(t) = {} & \pm\phi^B_2(j,k)H(\pm\phi^B_2(j,k)) \\ & \times \left[c_0(1-\sigma^A_{j,k})(1-\sigma^A_{j,k\pm1}) + c_1(1-\sigma^A_{j,k})\sigma^A_{j,k\pm1}\right. \\ & \left. +c_2\sigma^A_{j,k}(1-\sigma^A_{j,k\pm1}) + c_3\sigma^A_{j,k}\sigma^A_{j,k\pm1}\right]. \end{aligned} \tag{3.10}$$

In the sequel, we shall only derive formulas for agents in Group A, as formulas for agents in Group B are derived using the same techniques.

The velocities defined in Equations 3.6 and 3.7 and the constants described in Equation 3.8 are used to determine the probability of a pedestrian to move to a neighboring cell. The probability of transition $(j,k) \to (j \pm 1, k)$ for a member of Group A during

a small time interval Δt is given by

$$P^A_{(j,k)\to(j\pm1,k)}(t) = \Delta t V^A_{(j,k)\to(j\pm1,k)}(t)\sigma^A_{j,k,t}(1-\sigma^A_{j\pm1,k,t}), \tag{3.11}$$

while the probability of transition $(j,k) \to (j,k\pm1)$ for a member of Group A is given by

$$P^A_{(j,k)\to(j,k\pm1)}(t) = \Delta t V^A_{(j,k)\to(j,k\pm1,)}(t)\sigma^A_{j,k,t}(1-\sigma^A_{j,k\pm1,t}), \tag{3.12}$$

with $\sigma^A_{j,k,t}(1-\sigma^A_{j\pm1,k,t})$ and $\sigma^A_{j,k,t}(1-\sigma^A_{j,k\pm1,t})$ fulfilling analogous roles to $\sigma_{j,k,t}(1-\sigma_{j\pm1,k,t})$ and $\sigma_{j,k,t}(1-\sigma_{j,k\pm1,t})$ in Equations 2.4 and 2.5.

3.2 Mesoscopic Deterministic Model

Because $\boldsymbol{\sigma}_t := \{\sigma^A_{j,k,t}, \sigma^B_{j,k,t}\}$ is a continuous-time Markov chain, its generator is given by

$$A\psi = \lim_{\Delta t\to 0} \frac{\mathbb{E}[\psi(\boldsymbol{\sigma}_{\Delta t})|\boldsymbol{\sigma}_0] - \psi(\boldsymbol{\sigma}_0)}{\Delta t}, \tag{3.13}$$

where $\boldsymbol{\sigma}_0$ is the initial configuration of Group A and Group B on the lattice, $\boldsymbol{\sigma}_{\Delta t}$ is the configuration at time Δt, ψ is any test function, and the expectation is taken over all possible transitions from $\boldsymbol{\sigma}_0$ to $\boldsymbol{\sigma}_{\Delta t}$. In the case that $\psi(\boldsymbol{\sigma}) = \sigma^A_{j,k,t}$ for some fixed j and k, we can write the action of the generator on ψ as

$$A\sigma_{j,k,t} = \lim_{\Delta t\to 0} \frac{1}{\Delta t} \sum_{s\in\Omega^A} (s_{j,k} - \sigma^A_{j,k,0}) P(\boldsymbol{\sigma}^A_{\Delta t} = s|\boldsymbol{\sigma}^A_0), \tag{3.14}$$

where Ω^A is the space of all possible configurations of Group A on the lattice. As before, we have that

$$P(\boldsymbol{\sigma}^A_{\Delta t} = s|\boldsymbol{\sigma}^A_0) = P^A_{(j,k)\to(j\pm1,k)}(t) \tag{3.15}$$

if s can be obtained from $\boldsymbol{\sigma}^A_0$ by swapping the values of $\sigma^A_{j,k,0}$ and $\sigma^A_{j+1,k,0}$ or of $\sigma^A_{j,k,0}$ and $\sigma^A_{j-1,k,0}$ for some cell (j,k), and that

$$P(\boldsymbol{\sigma}^A_{\Delta t} = s|\boldsymbol{\sigma}^A_0) = P^A_{(j,k)\to(j,k\pm1)}(t) \tag{3.16}$$

if s can be obtained from $\boldsymbol{\sigma}^A_0$ by swapping the values of $\sigma^A_{j,k,0}$ and $\sigma^A_{j,k+1,0}$ or of $\sigma^A_{j,k,0}$ and $\sigma^A_{j,k-1,0}$ for some cell (j,k). For all other $s \in \Omega^A$, the transition from $\boldsymbol{\sigma}_0$ to s would require more than one elementary transition or be impossible through any combination of elementary transitions, and thus for these cases,

$$P(\boldsymbol{\sigma}^A_{\Delta t} = s|\boldsymbol{\sigma}^A_0) = o(\Delta t). \tag{3.17}$$

If we then denote by U^A the set of configurations of Group A on the lattice obtainable from $\boldsymbol{\sigma}^A_0$ by single elementary transitions, we have that Equation 3.14 can be simplified to

$$A\sigma^A_{j,k,t} = \lim_{\Delta t\to 0} \frac{1}{\Delta t} \sum_{s\in U^A} (s_{j,k} - \sigma^A_{j,k,0}) P(\boldsymbol{\sigma}^A_{\Delta t} = s|\boldsymbol{\sigma}^A_0). \tag{3.18}$$

Again, unless an agent transitions into or out of cell (j,k) in the transition from $\boldsymbol{\sigma}^A_0$ to s, we have that $s_{j,k} - \sigma^A_{j,k,0} = 0$. If an agent transitions into the cell, $s_{j,k} - \sigma^A_{j,k,0} = 1$, and if an agent transitions out of the cell, $s_{j,k} - \sigma^A_{j,k,0} = -1$. Thus Equation 3.18 can

be further simplified into the form

$$\begin{aligned} A\sigma^A_{j,k,t} = \lim_{\Delta t\to 0}\frac{1}{\Delta t}\big[&P^A_{(j-1,k)\to(j,k)}(t) - P^A_{(j,k)\to(j+1,k)}(t) + P^A_{(j+1,k)\to(j,k)}(t) \\ &- P^A_{(j,k)\to(j-1,k)}(t) + P^A_{(j,k-1)\to(j,k)}(t) - P^A_{(j,k)\to(j,k+1)}(t) \\ &+P^A_{(j,k+1)\to(j,k)}(t) - P^A_{(j,k)\to(j,k-1)}(t)\big], \end{aligned} \tag{3.19}$$

which expands, through appropriate substitutions of Equations 3.9-3.12, to

$$\begin{aligned} A\sigma^A_{j,k,t} = {}& \phi^A_1(j-1,k)H(\phi^A_1(j-1,k))\sigma^A_{j-1,k,t}(1-\sigma^A_{j,k,t}) \\ &\times\big[c_0(1-\sigma^B_{j-1,k,t})(1-\sigma^B_{j,k,t}) + c_1(1-\sigma^B_{j-1,k,t})\sigma^B_{j,k,t} \\ &+c_2\sigma^B_{j-1,k,t}(1-\sigma^B_{j,k,t}) + c_3\sigma^B_{j-1,k,t}\sigma^B_{j,k,t}\big] \\ &- \phi^A_1(j,k)H(\phi^A_1(j,k))\sigma^A_{j,k,t}(1-\sigma^A_{j+1,k,t}) \\ &\times\big[c_0(1-\sigma^B_{j,k,t})(1-\sigma^B_{j+1,k,t}) + c_1(1-\sigma^B_{j,k,t})\sigma^B_{j+1,k,t} \\ &+c_2\sigma^B_{j,k,t}(1-\sigma^B_{j+1,k,t}) + c_3\sigma^B_{j,k,t}\sigma^B_{j+1,k,t}\big] \\ &- \phi^A_1(j+1,k)H(-\phi^A_1(j+1,k))\sigma^A_{j+1,k,t}(1-\sigma^A_{j,k,t}) \\ &\times\big[c_0(1-\sigma^B_{j+1,k,t})(1-\sigma^B_{j,k,t}) + c_1(1-\sigma^B_{j+1,k,t})\sigma^B_{j,k,t} \\ &+c_2\sigma^B_{j+1,k,t}(1-\sigma^B_{j,k,t}) + c_3\sigma^B_{j+1,k,t}\sigma^B_{j,k,t}\big] \\ &+ \phi^A_1(j,k)H(-\phi^A_1(j,k))\sigma^A_{j,k,t}(1-\sigma^A_{j-1,k,t}) \\ &\times\big[c_0(1-\sigma^B_{j,k,t})(1-\sigma^B_{j-1,k,t}) + c_1(1-\sigma^B_{j,k,t})\sigma^B_{j-1,k,t} \\ &+c_2\sigma^B_{j,k,t}(1-\sigma^B_{j-1,k,t}) + c_3\sigma^B_{j,k,t}\sigma^B_{j-1,k,t}\big] \\ &+ \phi^A_2(j,k-1)H(\phi^A_2(j,k-1))\sigma^A_{j,k-1,t}(1-\sigma^A_{j,k,t}) \\ &\times\big[c_0(1-\sigma^B_{j,k-1,t})(1-\sigma^B_{j,k,t}) + c_1(1-\sigma^B_{j,k-1})\sigma^B_{j,k,t} \\ &+c_2\sigma^B_{j,k-1}(1-\sigma^B_{j,k,t}) + c_3\sigma^B_{j,k-1,t}\sigma^B_{j,k,t}\big] \end{aligned}$$

$$
\begin{aligned}
&- \phi_2^A(j,k) H(\phi_2^A(j,k)) \sigma^A_{j,k,t}(1-\sigma^A_{j,k+1,t}) \\
&\qquad \times \left[c_0(1-\sigma^B_{j,k,t})(1-\sigma^B_{j,k+1,t}) + c_1(1-\sigma^B_{j,k,t})\sigma^B_{j,k+1,t}\right. \\
&\qquad \left. + c_2\sigma^B_{j,k,t}(1-\sigma^B_{j,k+1,t}) + c_3\sigma^B_{j,k,t}\sigma^B_{j,k+1,t}\right] \\
&- \phi_2^A(j,k+1,t) H(-\phi_2^A(j,k+1,t)) \sigma^A_{j,k+1,t}(1-\sigma^A_{j,k,t}) \\
&\qquad \times \left[c_0(1-\sigma^B_{j,k+1,t})(1-\sigma^B_{j,k,t}) + c_1(1-\sigma^B_{j,k+1,t})\sigma^B_{j,k,t}\right. \\
&\qquad \left. + c_2\sigma^B_{j,k+1,t}(1-\sigma^B_{j,k,t}) + c_3\sigma^B_{j,k+1,t}\sigma^B_{j,k,t}\right] \\
&+ \phi_2^A(j,k) H(-\phi_2^A(j,k)) \sigma^A_{j,k,t}(1-\sigma^A_{j,k-1,t}) \\
&\qquad \times \left[c_0(1-\sigma^B_{j,k,t})(1-\sigma^B_{j,k-1,t}) + c_1(1-\sigma^B_{j,k,t})\sigma^B_{j,k-1,t}\right. \\
&\qquad \left. + c_2\sigma^B_{j,k,t}(1-\sigma^B_{j,k-1,t}) + c_3\sigma^B_{j,k,t}\sigma^B_{j,k-1,t}\right]. \qquad (3.20)
\end{aligned}
$$

Applying the property of the generator given in Equation 2.20 to this equation results in the following equation for the time evolution of $\rho^A_{j,k,t} := \mathbb{E}[\sigma^A_{j,k,t}]$:

$$
\begin{aligned}
\frac{d}{dt}\rho^A_{j,k} = \mathbb{E}\Big[&\phi_1^A(j-1,k) H(\phi_1^A(j-1,k)) \sigma^A_{j-1,k,t}(1-\sigma^A_{j,k,t}) \\
&\qquad \times \left[c_0(1-\sigma^B_{j-1,k,t})(1-\sigma^B_{j,k,t}) + c_1(1-\sigma^B_{j-1,k,t})\sigma^B_{j,k,t}\right. \\
&\qquad \left. + c_2\sigma^B_{j-1,k,t}(1-\sigma^B_{j,k,t}) + c_3\sigma^B_{j-1,k,t}\sigma^B_{j,k,t}\right] \\
&- \phi_1^A(j,k) H(\phi_1^A(j,k)) \sigma^A_{j,k,t}(1-\sigma^A_{j+1,k,t}) \\
&\qquad \times \left[c_0(1-\sigma^B_{j,k,t})(1-\sigma^B_{j+1,k,t}) + c_1(1-\sigma^B_{j,k,t})\sigma^B_{j+1,k,t}\right. \\
&\qquad \left. + c_2\sigma^B_{j,k,t}(1-\sigma^B_{j+1,k,t}) + c_3\sigma^B_{j,k,t}\sigma^B_{j+1,k,t}\right] \\
&- \phi_1^A(j+1,k) H(-\phi_1^A(j+1,k)) \sigma^A_{j+1,k,t}(1-\sigma^A_{j,k,t}) \\
&\qquad \times \left[c_0(1-\sigma^B_{j+1,k,t})(1-\sigma^B_{j,k,t}) + c_1(1-\sigma^B_{j+1,k,t})\sigma^B_{j,k,t}\right. \\
&\qquad \left. + c_2\sigma^B_{j+1,k,t}(1-\sigma^B_{j,k,t}) + c_3\sigma^B_{j+1,k,t}\sigma^B_{j,k,t}\right]
\end{aligned}
$$

$$
\begin{aligned}
&+ \phi_1^A(j,k)H(-\phi_1^A(j,k))\sigma_{j,k,t}^A(1-\sigma_{j-1,k,t}^A) \\
&\qquad \times \left[c_0(1-\sigma_{j,k,t}^B)(1-\sigma_{j-1,k,t}^B) + c_1(1-\sigma_{j,k,t}^B)\sigma_{j-1,k,t}^B\right. \\
&\qquad \left.+c_2\sigma_{j,k,t}^B(1-\sigma_{j-1,k,t}^B) + c_3\sigma_{j,k,t}^B\sigma_{j-1,k,t}^B\right] \\
&+ \phi_2^A(j,k-1)H(\phi_2^A(j,k-1))\sigma_{j,k-1,t}^A(1-\sigma_{j,k,t}^A) \\
&\qquad \times \left[c_0(1-\sigma_{j,k-1,t}^B)(1-\sigma_{j,k,t}^B) + c_1(1-\sigma_{j,k-1,t}^B)\sigma_{j,k,t}^B\right. \\
&\qquad \left.+c_2\sigma_{j,k-1,t}^B(1-\sigma_{j,k,t}^B) + c_3\sigma_{j,k-1,t}^B\sigma_{j,k,t}^B\right] \\
&- \phi_2^A(j,k)H(\phi_2^A(j,k))\sigma_{j,k,t}^A(1-\sigma_{j,k+1,t}^A) \\
&\qquad \times \left[c_0(1-\sigma_{j,k,t}^B)(1-\sigma_{j,k+1,t}^B) + c_1(1-\sigma_{j,k,t}^B)\sigma_{j,k+1,t}^B\right. \\
&\qquad \left.+c_2\sigma_{j,k,t}^B(1-\sigma_{j,k+1,t}^B) + c_3\sigma_{j,k,t}^B\sigma_{j,k+1,t}^B\right] \\
&- \phi_2^A(j,k+1)H(-\phi_2^A(j,k+1))\sigma_{j,k+1,t}^A(1-\sigma_{j,k,t}^A) \\
&\qquad \times \left[c_0(1-\sigma_{j,k+1,t}^B)(1-\sigma_{j,k,t}^B) + c_1(1-\sigma_{j,k+1,t}^B)\sigma_{j,k,t}^B\right. \\
&\qquad \left.+c_2\sigma_{j,k+1,t}^B(1-\sigma_{j,k,t}^B) + c_3\sigma_{j,k+1,t}^B\sigma_{j,k,t}^B\right] \\
&+ \phi_2^A(j,k)H(-\phi_2^A(j,k))\sigma_{j,k,t}^A(1-\sigma_{j,k-1,t}^A) \\
&\qquad \times \left[c_0(1-\sigma_{j,k,t}^B)(1-\sigma_{j,k-1,t}^B) + c_1(1-\sigma_{j,k,t}^B)\sigma_{j,k-1,t}^B\right. \\
&\qquad \left.\left.+c_2\sigma_{j,k,t}^B(1-\sigma_{j,k-1,t}^B) + c_3\sigma_{j,k,t}^B\sigma_{j,k-1,t}^B\right]\right]. \qquad (3.21)
\end{aligned}
$$

We can derive a closure approximation of the system comprised of this equation and the corresponding equation for $\frac{d}{dt}\rho_{j,k,t}^B$ by assuming that all random variables appearing in the previous equation are approximately independent, giving us, for example, that

$$\mathbb{E}[\sigma_{j,k,t}^A\sigma_{j+1,k,t}^A] \approx \mathbb{E}[\sigma_{j,k,t}^A]\mathbb{E}[\sigma_{j+1,k,t}^A] \qquad (3.22)$$

and that

$$\mathbb{E}[\sigma^A_{j,k,t}\sigma^B_{j,k,t}] \approx \mathbb{E}[\sigma^A_{j,k,t}]\mathbb{E}[\sigma^B_{j,k,t}]. \tag{3.23}$$

Under this assumption, we once again have a closed system, and the resulting mesoscopic model for the time evolution of the density of Group A can be given as

$$\begin{aligned}
\frac{d}{dt}\rho^A_{j,k} = {} & \phi^A_1(j-1,k)H(\phi^A_1(j-1,k,t))\rho^A_{j-1,k,t}(1-\rho^A_{j,k,t}) \\
& \times \big[c_0(1-\rho^B_{j-1,k,t})(1-\rho^B_{j,k,t}) + c_1(1-\rho^B_{j-1,k,t})\rho^B_{j,k,t} \\
& + c_2\rho^B_{j-1,k,t}(1-\rho^B_{j,k,t}) + c_3\rho^B_{j-1,k,t}\rho^B_{j,k,t}\big] \\
& - \phi^A_1(j,k)H(\phi^A_1(j,k))\rho^A_{j,k,t}(1-\rho^A_{j+1,k,t}) \\
& \times \big[c_0(1-\rho^B_{j,k,t})(1-\rho^B_{j+1,k,t}) + c_1(1-\rho^B_{j,k,t})\rho^B_{j+1,k,t} \\
& + c_2\rho^B_{j,k,t}(1-\rho^B_{j+1,k,t}) + c_3\rho^B_{j,k,t}\rho^B_{j+1,k,t}\big] \\
& - \phi^A_1(j+1,k)H(-\phi^A_1(j+1,k))\rho^A_{j+1,k,t}(1-\rho^A_{j,k,t}) \\
& \times \big[c_0(1-\rho^B_{j+1,k,t})(1-\rho^B_{j,k,t}) + c_1(1-\rho^B_{j+1,k,t})\rho^B_{j,k,t} \\
& + c_2\rho^B_{j+1,k,t}(1-\rho^B_{j,k,t}) + c_3\rho^B_{j+1,k,t}\rho^B_{j,k,t}\big] \\
& + \phi^A_1(j,k)H(-\phi^A_1(j,k))\rho^A_{j,k,t}(1-\rho^A_{j-1,k,t}) \\
& \times \big[c_0(1-\rho^B_{j,k,t})(1-\rho^B_{j-1,k,t}) + c_1(1-\rho^B_{j,k,t})\rho^B_{j-1,k,t} \\
& + c_2\rho^B_{j,k,t}(1-\rho^B_{j-1,k,t}) + c_3\rho^B_{j,k,t}\rho^B_{j-1,k,t}\big] \\
& + \phi^A_2(j,k-1)H(\phi^A_2(j,k-1))\rho^A_{j,k-1,t}(1-\rho^A_{j,k,t}) \\
& \times \big[c_0(1-\rho^B_{j,k-1,t})(1-\rho^B_{j,k,t}) + c_1(1-\rho^B_{j,k-1,t})\rho^B_{j,k,t} \\
& + c_2\rho^B_{j,k-1,t}(1-\rho^B_{j,k,t}) + c_3\rho^B_{j,k-1,t}\rho^B_{j,k,t}\big] \\
& - \phi^A_2(j,k)H(\phi^A_2(j,k))\rho^A_{j,k,t}(1-\rho^A_{j,k+1,t}) \\
& \times \big[c_0(1-\rho^B_{j,k,t})(1-\rho^B_{j,k+1,t}) + c_1(1-\rho^B_{j,k,t})\rho^B_{j,k+1,t}
\end{aligned}$$

$$
\begin{aligned}
&\quad + c_2\rho^B_{j,k,t}(1-\rho^B_{j,k+1,t}) + c_3\rho^B_{j,k,t}\rho^B_{j,k+1,t}\big] \\
&- \phi^A_2(j,k+1)H(-\phi^A_2(j,k+1))\rho^A_{j,k+1,t}(1-\rho^A_{j,k,t}) \\
&\quad \times \big[c_0(1-\rho^B_{j,k+1,t})(1-\rho^B_{j,k,t}) + c_1(1-\rho^B_{j,k+1,t})\rho^B_{j,k,t} \\
&\quad + c_2\rho^B_{j,k+1,t}(1-\rho^B_{j,k,t}) + c_3\rho^B_{j,k+1,t}\rho^B_{j,k,t}\big] \\
&+ \phi^A_2(j,k)H(-\phi^A_2(j,k))\rho^A_{j,k,t}(1-\rho^A_{j,k-1,t}) \\
&\quad \times \big[c_0(1-\rho^B_{j,k,t})(1-\rho^B_{j,k-1,t}) + c_1(1-\rho^B_{j,k,t})\rho^B_{j,k-1,t} \\
&\quad + c_2\rho^B_{j,k,t}(1-\rho^B_{j,k-1,t}) + c_3\rho^B_{j,k,t}\rho^B_{j,k-1,t}\big]\,. \qquad (3.24)
\end{aligned}
$$

This system is defined on the same lattice $\mathcal{L}$ as the microscopic model.

3.3 Macroscopic PDE Model

We now treat sites $(j,k) \in \mathcal{L}$ as square cells with fixed side length $h > 0$. Let Ω denote the subdomain of $\mathbb{R}^2$ corresponding to the lattice $\mathcal{L}$, i.e., $\Omega = [0,M] \times [0,N]$ with the total number of cells depending on h. We consider a rescaling of time $t \to ht$ and derive a coarse-grained PDE model as the cell size tends to zero and the number of cells tends to infinity.

We rewrite Equation 3.24 in the following flux form, taking the time rescaling into account:

$$
\frac{d\rho^A_{j,k,t}}{dt} = -\frac{F^A_{j,j+1} - F^A_{j-1,j} + G^A_{k,k+1} - G^A_{k-1,k}}{h}, \qquad (3.25)
$$

where

$$
\begin{aligned}
F^A_{j,j+1} &= \phi^A_1(j,k)H(\phi^A_1(j,k))\rho^A_{j,k,t}(1-\rho^A_{j+1,k,t}) \\
&\quad \times \big[c_0(1-\rho^B_{j,k,t})(1-\rho^B_{j+1,k,t}) + c_1(1-\rho^B_{j,k,t})\rho^B_{j+1,k,t}
\end{aligned}
$$

$$
\begin{aligned}
&\quad + c_2\rho^B_{j,k,t}(1-\rho^B_{j+1,k,t}) + c_3\rho^B_{j,k,t}\rho^B_{j+1,k,t}\big] \\
&+ \phi^A_1(j+1,k)H(-\phi^A_1(j+1,k,t))\rho^A_{j+1,k,t}(1-\rho^A_{j,k,t}) \\
&\quad \times \big[c_0(1-\rho^B_{j+1,k,t})(1-\rho^B_{j,k,t}) + c_1(1-\rho^B_{j+1,k,t})\rho^B_{j,k,t} \\
&\quad + c_2\rho^B_{j+1,k,t}(1-\rho^B_{j,k,t}) + c_3\rho^B_{j+1,k,t}\rho^B_{j,k,t}\big], \qquad (3.26)
\end{aligned}
$$

$$
\begin{aligned}
G^A_{k,k+1} &= \phi^A_2(j,k)H(\phi^A_2(j,k))\rho^A_{j,k,t}(1-\rho^A_{j,k+1,t}) \\
&\quad \times \big[c_0(1-\rho^B_{j,k,t})(1-\rho^B_{j,k+1,t}) + c_1(1-\rho^B_{j,k,t})\rho^B_{j,k+1,t} \\
&\quad + c_2\rho^B_{j,k,t}(1-\rho^B_{j,k+1,t}) + c_3\rho^B_{j,k,t}\rho^B_{j,k+1,t}\big] \\
&+ \phi^A_2(j,k+1)H(-\phi^A_2(j,k+1))\rho^A_{j,k+1,t}(1-\rho^A_{j,k,t}) \\
&\quad \times \big[c_0(1-\rho^B_{j,k+1,t})(1-\rho^B_{j,k,t}) + c_1(1-\rho^B_{j,k+1,t})\rho^B_{j,k,t} \\
&\quad + c_2\rho^B_{j,k+1,t}(1-\rho^B_{j,k,t}) + c_3\rho^B_{j,k+1,t}\rho^B_{j,k,t}\big]. \qquad (3.27)
\end{aligned}
$$

Multiplying Equation 3.25 by $\varphi_{j,k} := \varphi(jh, kh)$, where $\varphi \in C^1_0(\bar{\Omega})$ is a test function, and summing over the cells of Ω gives

$$
\sum_{j,k} \varphi_{j,k}\frac{d\rho^A_{j,k,t}}{dt} = -\sum_{j,k}\left[\varphi_{j,k}\frac{F^A_{j,j+1}-F^A_{j-1,j}}{h} + \varphi_{j,k}\frac{G^A_{k,k+1}-G^A_{k-1,k}}{h}\right] \qquad (3.28)
$$

Using summation by parts and the fact that $\varphi \in C^1_0(\bar{\Omega})$, this can be rewritten as

$$
\begin{aligned}
\sum_{j,k} \varphi_{j,k}\frac{d\rho_{j,k,t}}{dt} &= -\sum_{j,k}\left[-\frac{\varphi_{j+1,k}-\varphi_{j,k}}{h}F^A_{j,j+1} - \frac{\varphi_{j,k+1}-\varphi_{j,k}}{h}G^A_{k,k+1}\right] \\
&= \sum_{j,k}\left[F^A_{j,j+1}\frac{\varphi_{j+1,k}-\varphi_{j,k}}{h} + G^A_{k,k+1}\frac{\varphi_{j,k+1}-\varphi_{j,k}}{h}\right]. \qquad (3.29)
\end{aligned}
$$

We define pedestrian densities on Ω as follows. Reusing the notation ρ^A for convenience, define the function $\rho^A(x,y,t)$ as a continuous piecewise linear interpolation of

$\rho^A_{j,k}(t)$ and take the limit as $h \to 0^+$. Due to the boundedness of both ρ^A and $\frac{d\rho^A_{j,k,t}}{dt}$, we obtain a weak formulation of the coarse-grained model:

$$\iint\limits_{\Omega} \varphi(x,y)\frac{\partial}{\partial t}\rho^A(x,y,t)dxdy = \iint\limits_{\Omega}\left(F^A(\rho^A)\frac{\partial}{\partial x}\varphi + G^A(\rho^A)\frac{\partial}{\partial y}\varphi\right)dxdy, \tag{3.30}$$

where $F^A(\rho)$ and $G^A(\rho)$ are defined as the corresponding limits of $F^A_{j,j+1}$ and $G^A_{k,k+1}$ in Equations 3.26 and 3.27, i.e.,

$$F^A(\rho^A) = \phi^A_1\rho^A(1-\rho^A)\left[(c_0-c_1-c_2+c_3)(\rho^B)^2 + (c_1+c_2-2c_0)\rho^B + c_0\right], \tag{3.31}$$

$$G^A(\rho^A) = \phi^A_2\rho^A(1-\rho^A)\left[(c_0-c_1-c_2+c_3)(\rho^B)^2 + (c_1+c_2-2c_0)\rho^B + c_0\right]. \tag{3.32}$$

We can now write the full system of PDEs as

$$\rho^A_t + [\phi^A_1 f(\rho^A)g(\rho^B)]_x + [\phi^A_2 f(\rho^A)g(\rho^B)]_y = 0, \tag{3.33}$$

$$\rho^B_t + [\phi^B_1 f(\rho^B)g(\rho^A)]_x + [\phi^B_2 f(\rho^B)g(\rho^A)]_y = 0, \tag{3.34}$$

where

$$f(u) = u(1-u), g(u) = (c_0-c_1-c_2+c_3)u^2 + (c_1+c_2-2c_0)u + c_0. \tag{3.35}$$

We can write the system given in Equation 3.33 as a system of coupled conservation laws in the form

$$\rho^A_t + \nabla\cdot\left(f(\rho^A)g(\rho^B)\boldsymbol{\phi}^A\right) = 0, \tag{3.36}$$

$$\rho^B_t + \nabla\cdot\left(f(\rho^B)g(\rho^A)\boldsymbol{\phi}^B\right) = 0. \tag{3.37}$$

By again applying the Divergence Theorem, we can show that given appropriate boundary conditions, such as a periodic boundary, we can show that

$$\frac{\partial}{\partial t}\iint_{\Omega}\rho^{A}dxdy = 0, \tag{3.38}$$

$$\frac{\partial}{\partial t}\iint_{\Omega}\rho^{B}dxdy = 0, \tag{3.39}$$

and thus the pedestrian masses for both groups are conserved.

We can, alternatively, write the system given in Equation 3.33 as

$$\frac{\partial}{\partial t}\begin{bmatrix}\rho^{A}\\ \rho^{B}\end{bmatrix} + \frac{\partial}{\partial x}\begin{bmatrix}\phi_1^{A} f(\rho^{A})g(\rho^{B})\\ \phi_1^{B} f(\rho^{B})g(\rho^{A})\end{bmatrix} + \frac{\partial}{\partial y}\begin{bmatrix}\phi_2^{A} f(\rho^{A})g(\rho^{B})\\ \phi_2^{B} f(\rho^{B})g(\rho^{A})\end{bmatrix} = \mathbf{0}. \tag{3.40}$$

Properties of this system, such as hyperbolicity, are discussed in Chapter 5.

Chapter 4

Simulation of Two Group Models

We now turn to simulations of the microscopic and mesoscopic models introduced in the previous chapter in order to gauge the effectiveness of the derived deterministic model. As the mesoscopic model can be viewed as a first-order discretization of the macroscopic model, the macroscopic model will not be treated separately.

4.1 Simulation Techniques

We simulate the evolution of the stochastic agent-based model defined in Section 3.1 using a method that will be referred to as Progressive Modified Tau-Leaping. The algorithm for generating a realization of the system using Progressive Modified Tau-Leaping is as follows:

1. Set the time $t = 0$.

2. Fix a time step τ.

3. Choose an initial state $\left\{\boldsymbol{\sigma}_0^A, \boldsymbol{\sigma}_0^B\right\}$.

4. Form a randomly ordered list of all agents on the lattice.

5. For each agent in the list, perform the following procedure:

   (a) Form a list R_k of all transition rates for elementary transtions of the agent.

   (b) Define $Q_n = \sum_{k=1}^{n} R_k$.

   (c) Calculate the total rate $Q = \sum_k R_k$.

   (d) Sample a random number u from the uniform distribution on $(0, 1]$.

   (e) Determine which elementary transition R_k occurs by finding k such that $Q_{k-1} < uQ \leq Q_k$.

   (f) Modify $\left\{\boldsymbol{\sigma}_0^A, \boldsymbol{\sigma}_0^B\right\}$ by making this transition.

6. Set $t = t + \tau$.

7. Return to Step 4.

A more traditional but more computationally expensive method for simulating the time evolution of such a system is the Kinetic Monte Carlo method. The algorithm for a rejection-free Kinetic Monte Carlo simulation is as follows:

1. Set the time $t = 0$.

2. Choose an initial state $\left\{\boldsymbol{\sigma}_0^A, \boldsymbol{\sigma}_0^B\right\}$.

3. Form a list r_k of all transition rates for all possible transitions T_i of the system.

4. Define $R_n = \sum_{k=1}^{n} r_k$ for $n = 1, \ldots, N$ where N is the total number of transitions. Denote $R = R_N$.

5. Sample a random number u from the uniform distribution on $(0, 1]$.

6. Determine which transition occurs by finding R_k such that $R_{k-1} < uQ_k \leq R_k$.

7. Modify $\left\{\boldsymbol{\sigma}_0^A, \boldsymbol{\sigma}_0^B\right\}$ by making this transition.

8. Sample a new random number u from the uniform distribution on $(0, 1]$.

9. Set $t = t + R^{-1} \log u^{-1}$.

10. Return to Step 3.

A comparison of the Kinetic Monte Carlo and Progressive Modified Tau-Leaping methods is provided in Appendix A. The comparison of these methods shows that the Progressive Modified Tau-Leaping method produces results statistically identical to the Kinetic Monte Carlo method with $\tau = 0.05$, and decreasing τ does not significantly improve the similarity. Thus in the following stochastic simulations, Progressive Modified Tau-Leaping results with $\tau = 0.05$ were averaged over 1000 realizations to produce approximations for the densities ρ^A and ρ^B. The mesoscopic deterministic system given in Equation 3.24 was simulated in MATLAB using the ode45 solver. Both stochastic and deterministic simulations were allowed to run to a maximum time of $t = 350$, with samples being taken at each timestep of $\Delta t = 1$.

4.2 Square Groups of Uniform Density

We will begin by examining the effects of the strength of the slowdown interaction, as determined by the constants c_0, c_1, c_2, and c_3 from Equation 3.8, on the stochastic model and on the mesoscopic model. To do this, we will study the evolution of the same initial configuration of groups under different constant values. In the three cases we consider, we will examine the behavior when $c_0 = 1$, $c_1 = c_2 = \frac{1}{\alpha}$, and $c_3 = \frac{1}{2\alpha}$,

assigning a different value to α in each case. In this way, an increased value of α will represent an increase in the strength of the slowdown interaction, with larger values of α corresponding to greater "friction" between the groups of pedestrians. We will consider the cases

$$\alpha = 2, 3, \text{ and } 4. \tag{4.1}$$

In all cases, the stochastic model is averaged over 1000 realizations.

4.2.1 Lattice and Velocity Fields

We let $\mathcal{L}$ be a 200 by 200 lattice. We define functions $\Psi^A(j,k)$ and $\Psi^B(j,k)$ on $\mathcal{L}$ by

$$\Psi^A(j,k) = (180-j)^2 + (180-k^2) \tag{4.2}$$

and

$$\Psi^B(j,k) = (21-j)^2 + (21-k^2), \tag{4.3}$$

respectively. We then take our velocity fields $\phi^A(j,k)$ and $\phi^B(j,k)$ to be

$$\phi^A(j,k) = -\frac{\nabla\Psi^A(j,k)}{||\nabla\Psi^A(j,k)||_1} \tag{4.4}$$

$$= \left(\frac{180-j}{|(180-j)|+|(180-k)|}, \frac{180-k}{|(180-j)|+|(180-k)|}\right) \tag{4.5}$$

and

$$\phi^B(j,k) = -\frac{\nabla\Psi^B(j,k)}{||\nabla\Psi^B(j,k)||_1} \tag{4.6}$$

$$= \left(\frac{21-j}{|(21-j)|+|(21-k)|}, \frac{21-k}{|(21-j)|+|(21-k)|}\right). \tag{4.7}$$

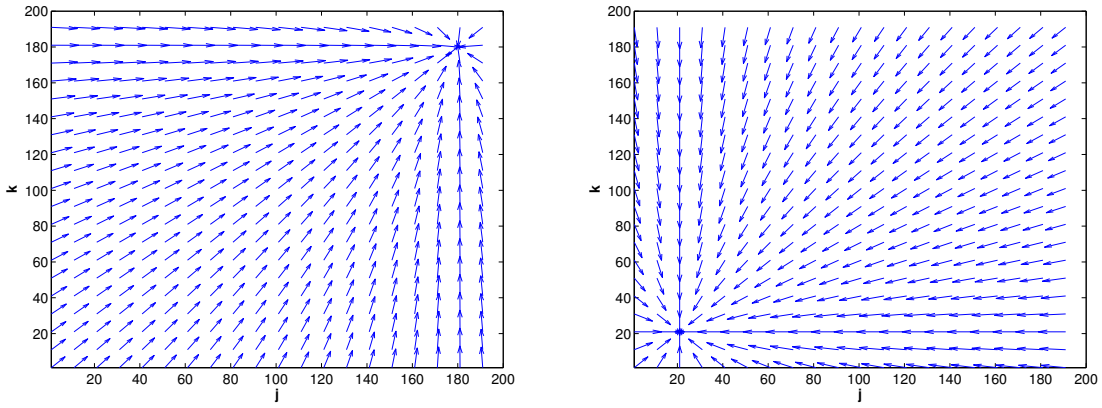

(a) $\boldsymbol{\phi}^A$ on $\mathcal{L}$ (b) $\boldsymbol{\phi}^B$ on $\mathcal{L}$

Figure 4.1: Velocity Fields from Equations 4.5 and 4.7
(j and k refer to coordinates of cells on $\mathcal{L}$ in all Figures)

With this velocity field, agents from Group A will move towards the point $(180, 180)$ and agents from Group B will move towards the point $(21, 21)$. Note briefly that the use of the 1-norm is merely a pragmatic decision, as it prevents the total probability of transition from being greater than 1 without requiring careful selection of the scaling constants. Plots of these velocity fields are shown in Figure 4.1.

4.2.2 Initial Configuration

We let

$$\sigma^A_{j,k,0} = \begin{cases} 1, & 81 \leq j \leq 100 \text{ and } 81 \leq k \leq 100, \\ 0, & \text{otherwise}, \end{cases} \tag{4.8}$$

and let

$$\sigma^B_{j,k,0} = \begin{cases} 1, & 101 \leq j \leq 120 \text{ and } 101 \leq k \leq 120, \\ 0, & \text{otherwise}. \end{cases} \tag{4.9}$$

This configuration was used for all simulations in this section.

4.2.3 Model 1: $\alpha = 2$

We start with a relatively small value of $\alpha = 2$, meaning that the slowdown interaction will be relatively weak. In this case, we see that the stochastic and deterministic models produce very similar results, especially in the short term. In Figures 4.2, 4.3, and 4.4, we show the densities for the groups on the lattice at various times.

While these images are good for showing the shape of the overall pattern, they make it difficult to distinguish some fine differences between the models. Plotting the density of a single group along the diagonal of the lattice gives us a clearer picture of the similarities and differences in the models, and we do so in Figures 4.5, 4.6, and 4.7.

4.2.4 Model 2: $\alpha = 3$

By increasing the value of α, we strengthen the slowdown interaction between the groups. In Figures 4.8, 4.9, and 4.10, we again show the densities for the groups on the lattice at various times, and in Figures 4.11, 4.12, and 4.13, we again examine the density of a single group along the diagonal of the lattice.

4.2.5 Model 3: $\alpha = 4$

We conclude our study of the effects of the value of α on the accuracy of the mesoscopic model by considering the case $\alpha = 4$. In Figures 4.14, 4.15, and 4.16, we again show the densities for the groups on the lattice at various times, and in Figures 4.17, 4.18, and 4.19, we again examine the density of a single group along the diagonal of the lattice.

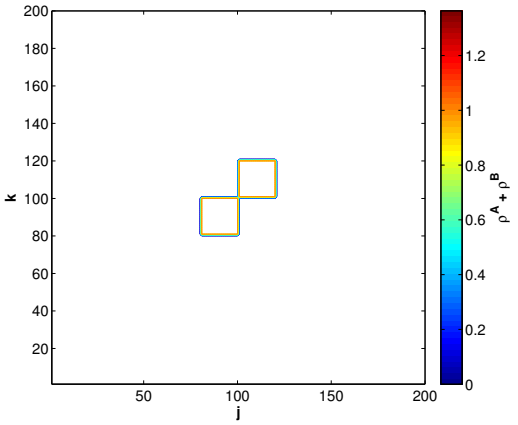

(a) Stochastic, $t = 0$

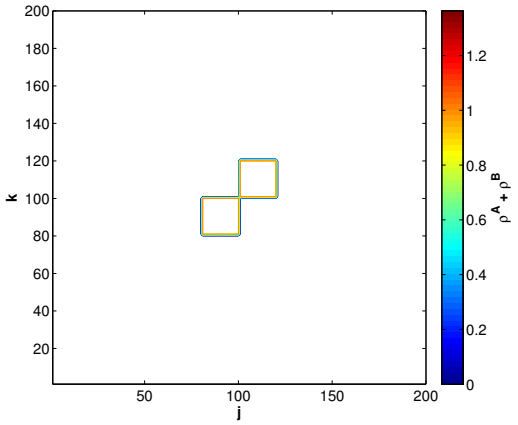

(b) Deterministic, $t = 0$

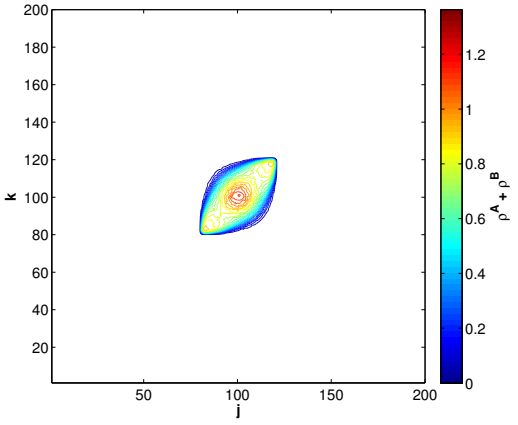

(c) Stochastic, $t = 30$

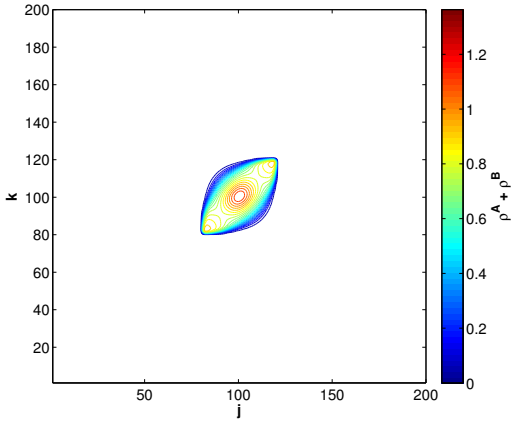

(d) Deterministic, $t = 30$

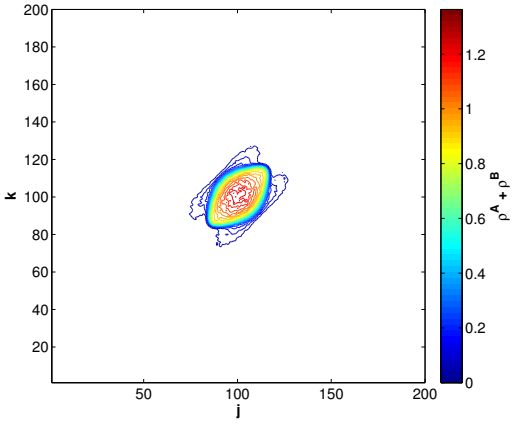

(e) Stochastic, $t = 60$

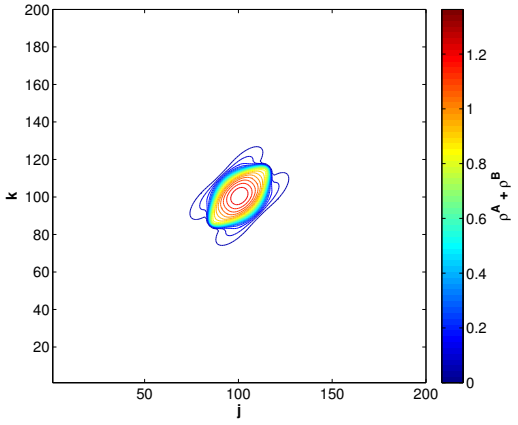

(f) Deterministic, $t = 60$

Figure 4.2: ρ^A and ρ^B, Stochastic and Deterministic, Times $t = 0, 30, 60$ $\alpha = 2$ (Units for t, ρ^A, and ρ^B are arbitrary in all Figures)

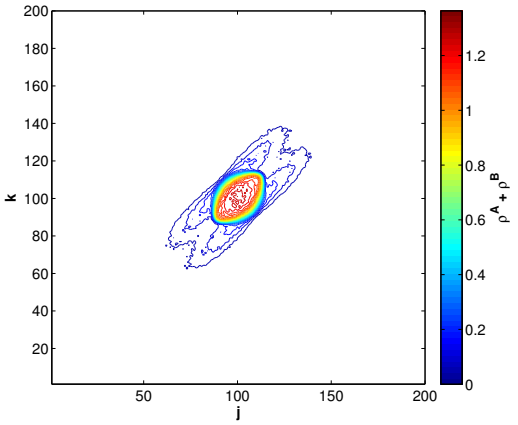

(a) Stochastic, $t = 90$

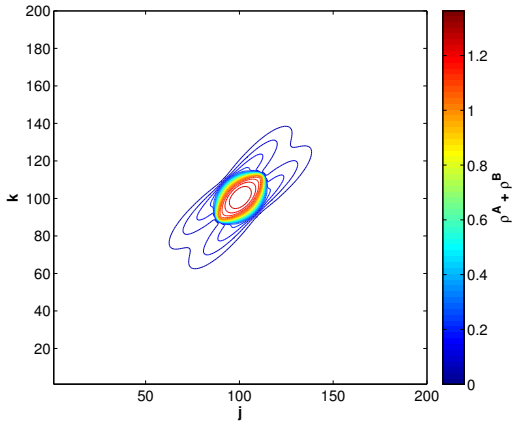

(b) Deterministic, $t = 90$

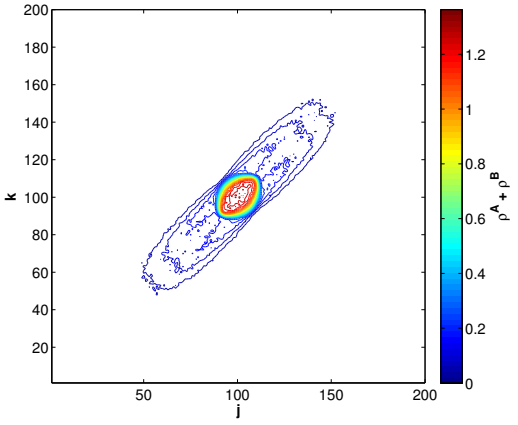

(c) Stochastic, $t = 120$

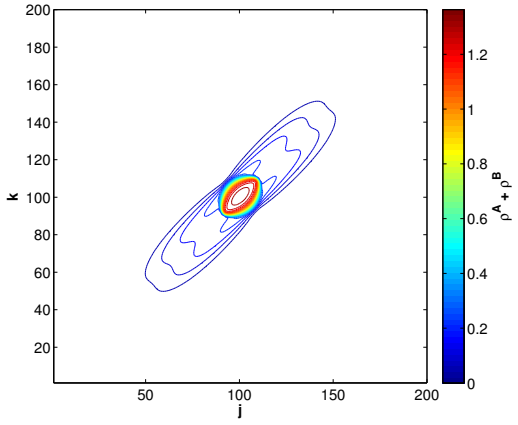

(d) Deterministic, $t = 120$

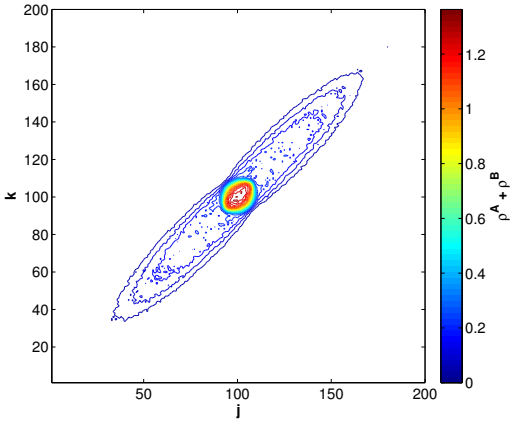

(e) Stochastic, $t = 150$

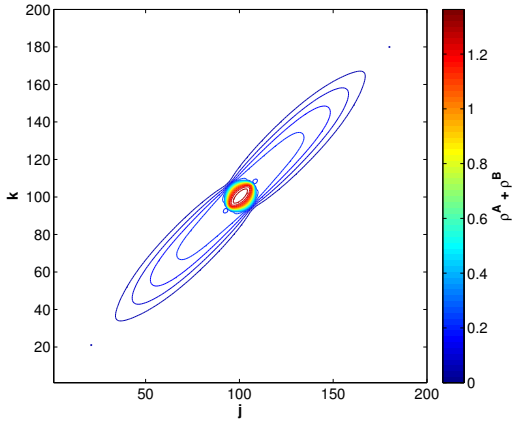

(f) Deterministic, $t = 150$

Figure 4.3: ρ^A and ρ^B, Stochastic and Deterministic, Times $t = 90, 120, 150$ $\alpha = 2$

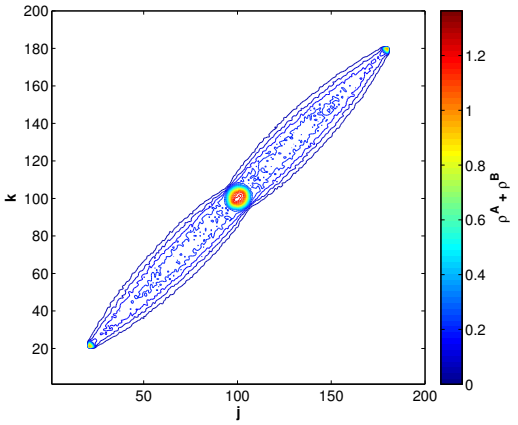

(a) Stochastic, $t = 180$

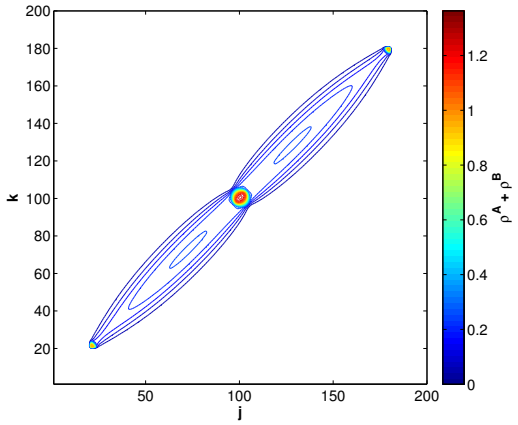

(b) Deterministic, $t = 180$

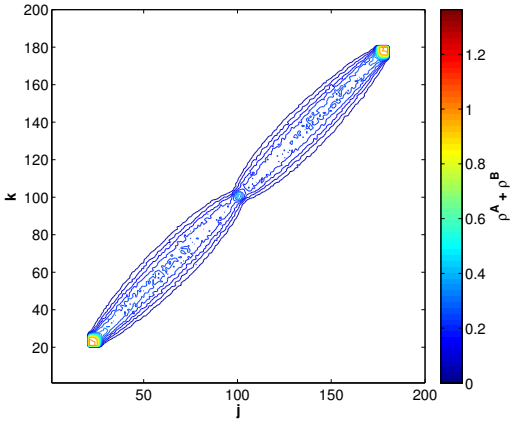

(c) Stochastic, $t = 210$

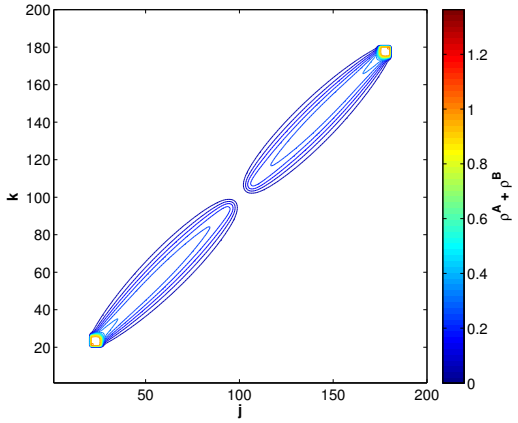

(d) Deterministic, $t = 210$

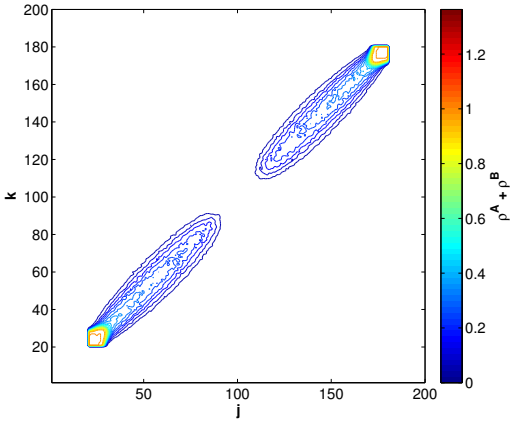

(e) Stochastic, $t = 240$

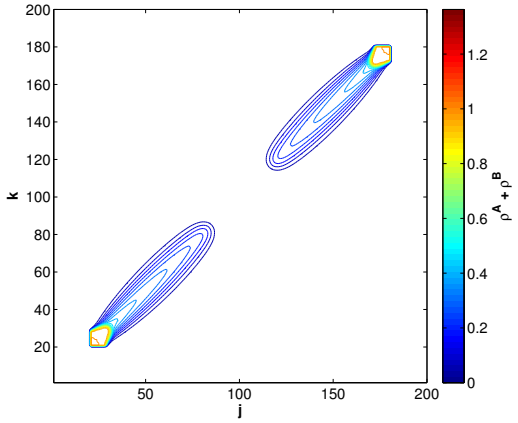

(f) Deterministic, $t = 240$

Figure 4.4: ρ^A and ρ^B, Stochastic and Deterministic, Times $t = 180, 210, 240$ $\alpha = 2$

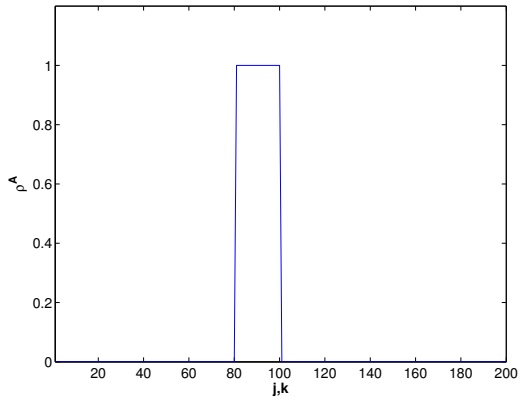

(a) Stochastic, $t = 0$

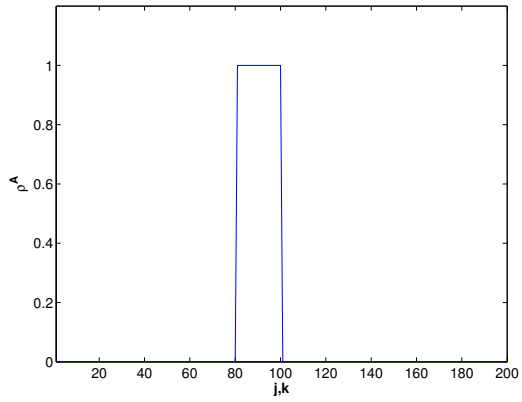

(b) Deterministic, $t = 0$

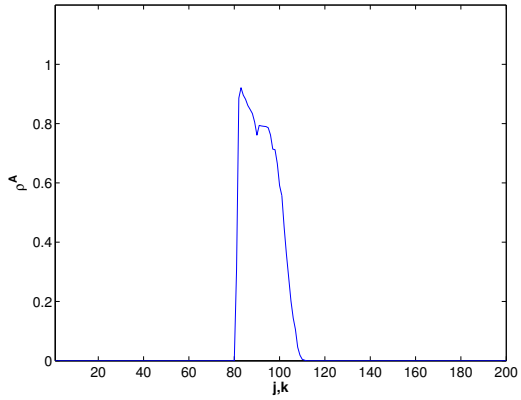

(c) Stochastic, $t = 30$

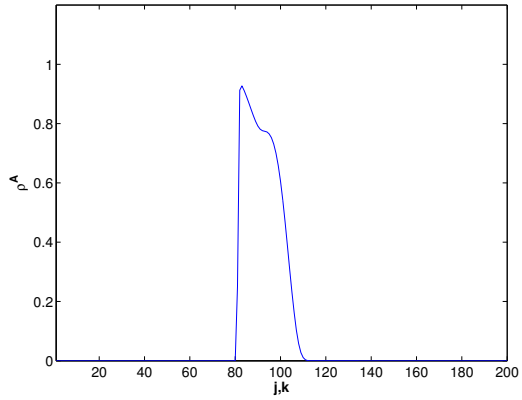

(d) Deterministic, $t = 30$

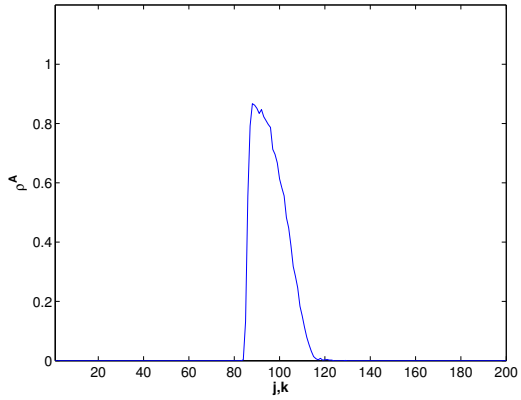

(e) Stochastic, $t = 60$

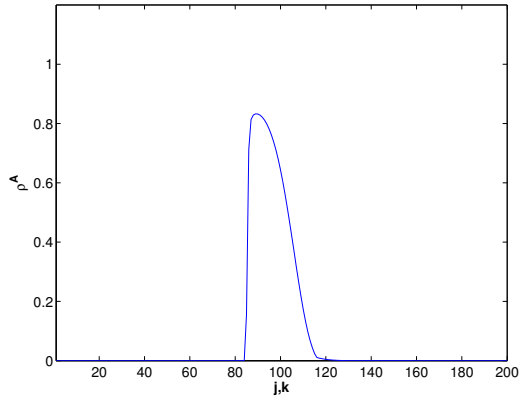

(f) Deterministic, $t = 60$

Figure 4.5: $\rho^A_{j,j,t}$, Stochastic and Deterministic, Times $t = 0, 30, 60$
$\alpha = 2$

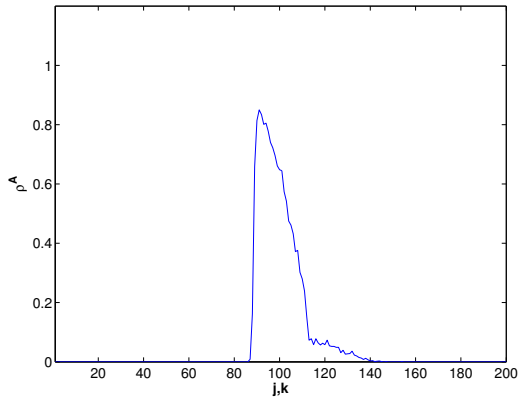

(a) Stochastic, $t = 90$

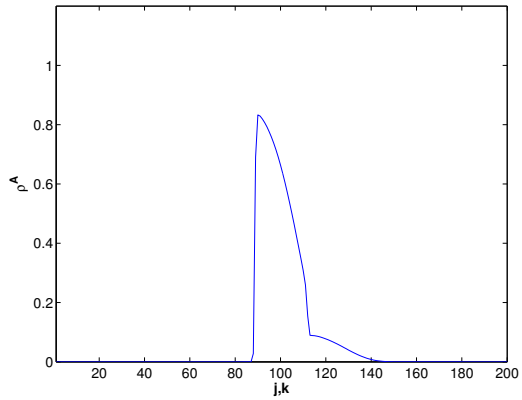

(b) Deterministic, $t = 90$

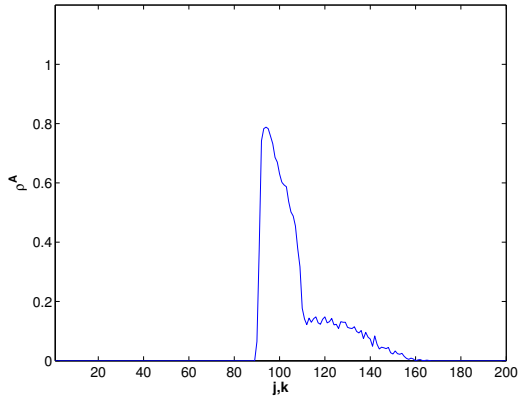

(c) Stochastic, $t = 120$

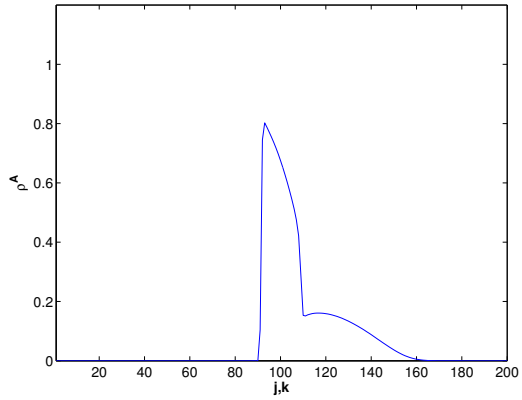

(d) Deterministic, $t = 120$

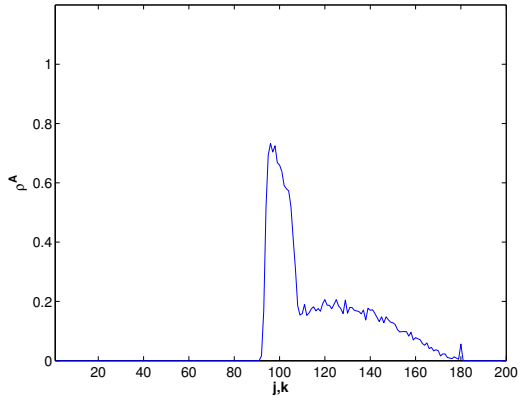

(e) Stochastic, $t = 150$

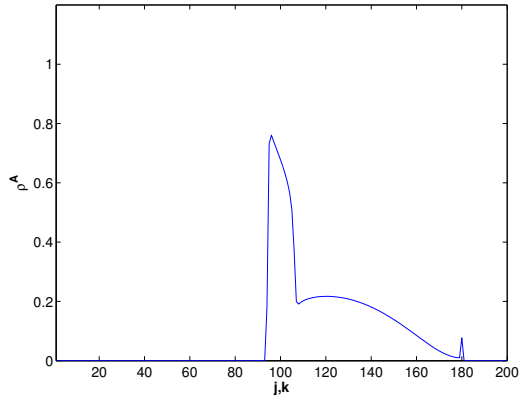

(f) Deterministic, $t = 150$

Figure 4.6: $\rho^A_{j,j,t}$, Stochastic and Deterministic, Times $t = 90, 120, 150$
$\alpha = 2$

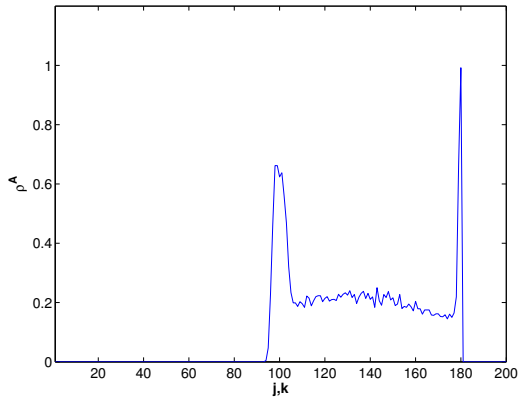

(a) Stochastic, $t = 180$

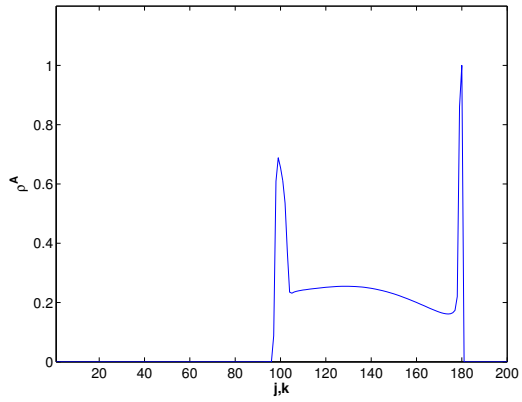

(b) Deterministic, $t = 180$

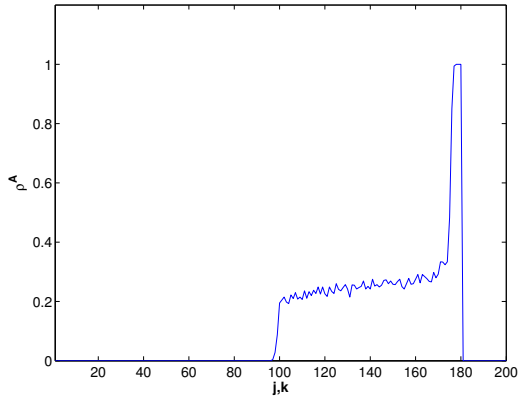

(c) Stochastic, $t = 210$

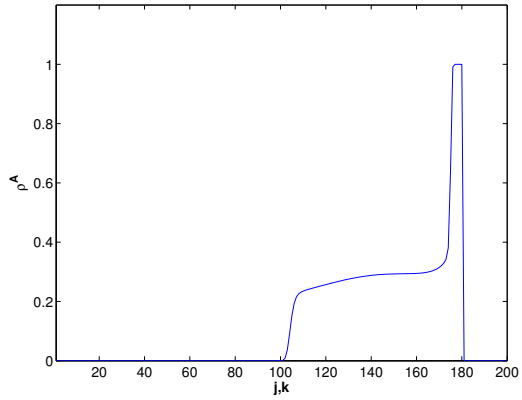

(d) Deterministic, $t = 210$

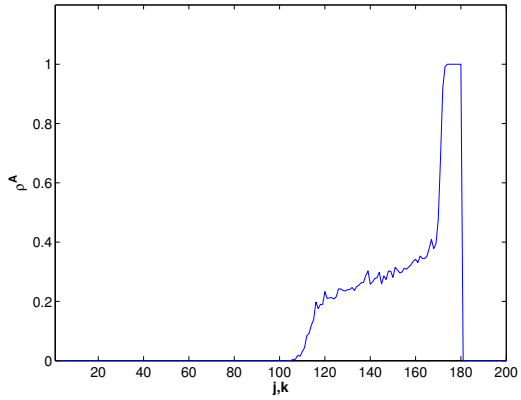

(e) Stochastic, $t = 240$

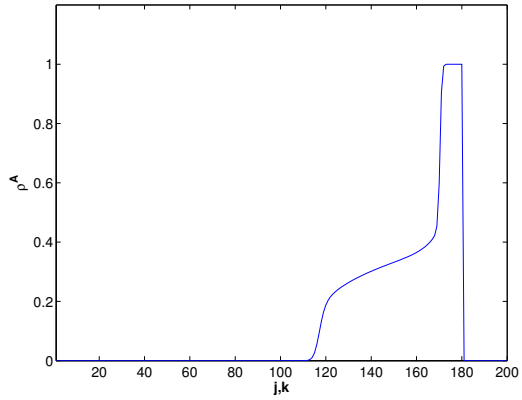

(f) Deterministic, $t = 240$

Figure 4.7: $\rho^A_{j,j,t}$, Stochastic and Deterministic, Times $t = 180, 210, 240$ $\alpha = 2$

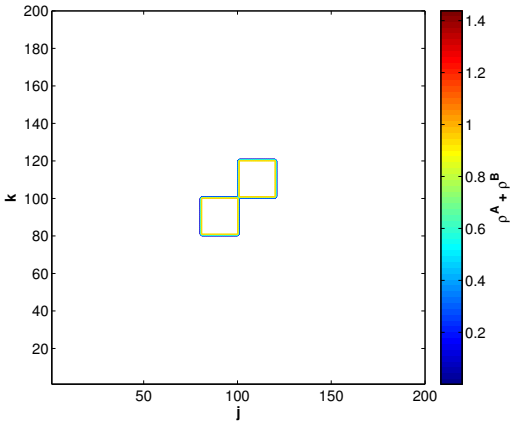

(a) Stochastic, $t = 0$

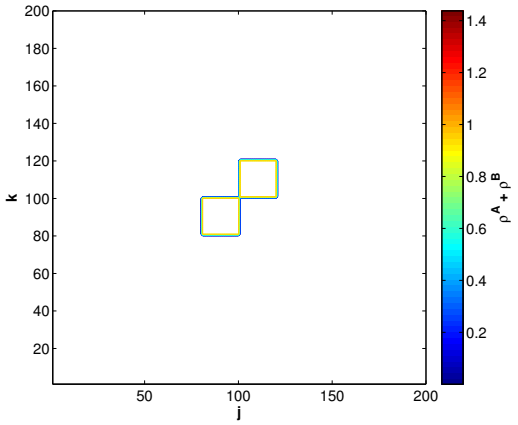

(b) Deterministic, $t = 0$

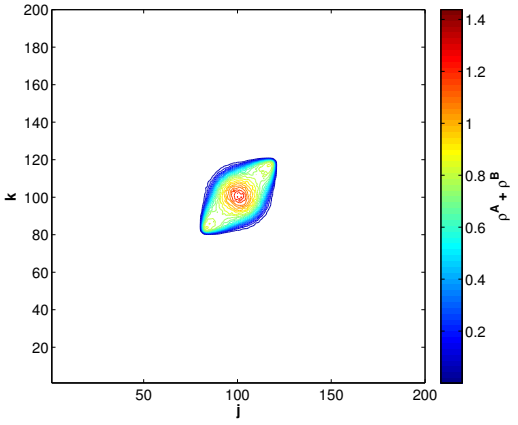

(c) Stochastic, $t = 35$

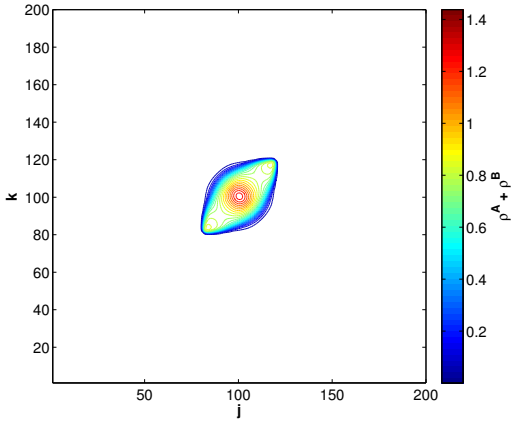

(d) Deterministic, $t = 35$

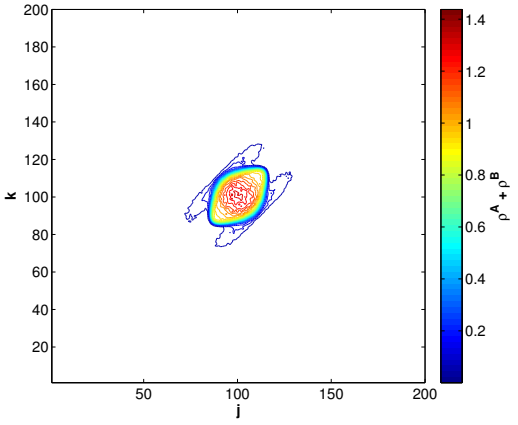

(e) Stochastic, $t = 70$

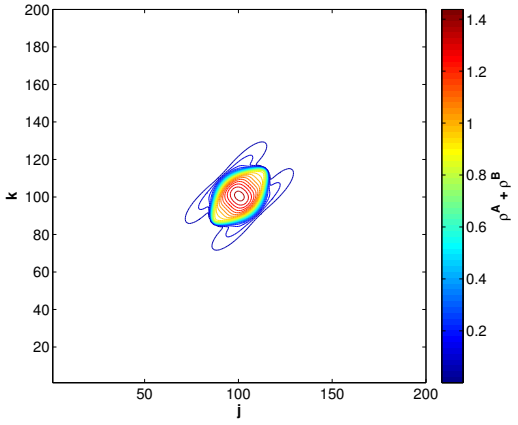

(f) Deterministic, $t = 70$

Figure 4.8: ρ^A and ρ^B, Stochastic and Deterministic, Times $t = 0, 35, 70$
$\alpha = 3$

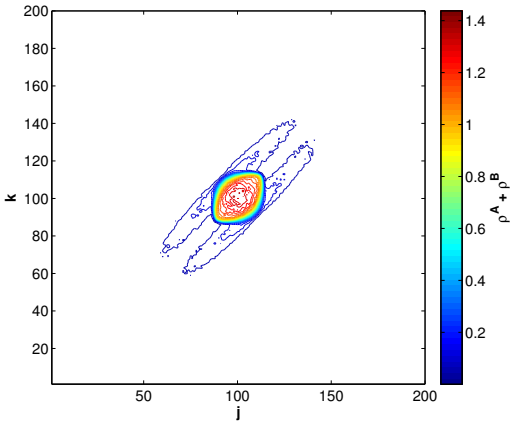

(a) Stochastic, $t = 105$

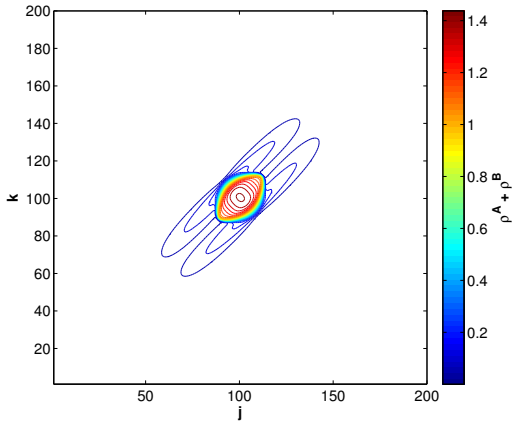

(b) Deterministic, $t = 105$

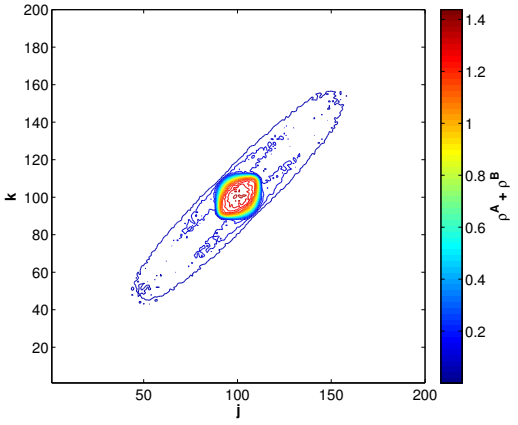

(c) Stochastic, $t = 140$

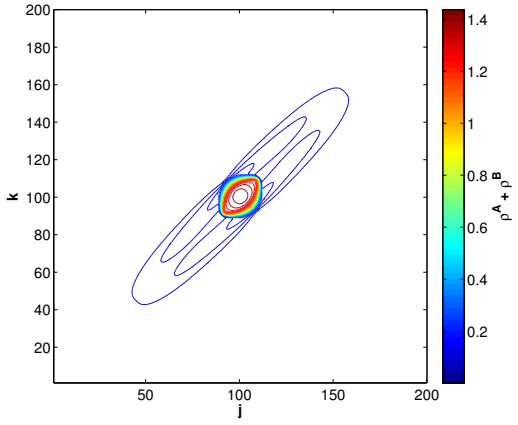

(d) Deterministic, $t = 140$

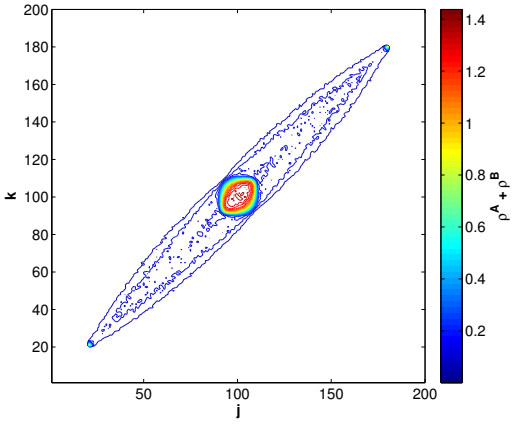

(e) Stochastic, $t = 175$

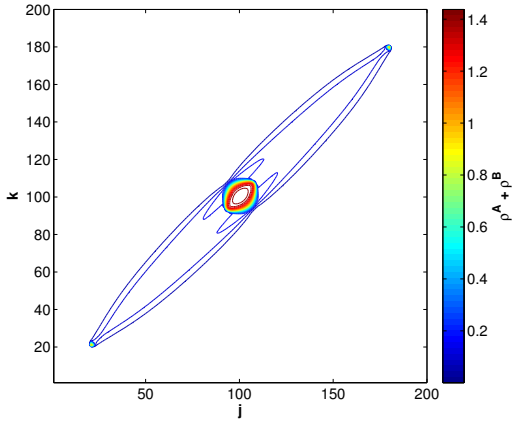

(f) Deterministic, $t = 175$

Figure 4.9: ρ^A and ρ^B, Stochastic and Deterministic, Times $t = 105, 140, 175$ $\alpha = 3$

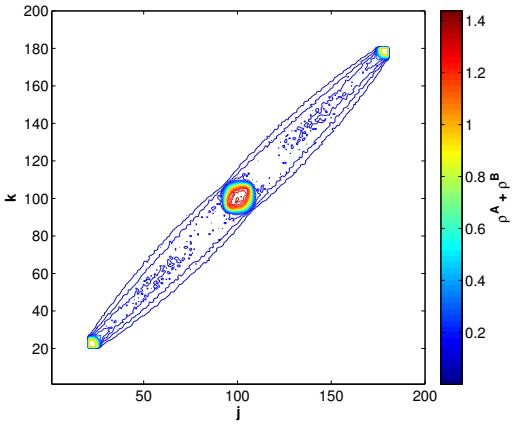

(a) Stochastic, $t = 210$

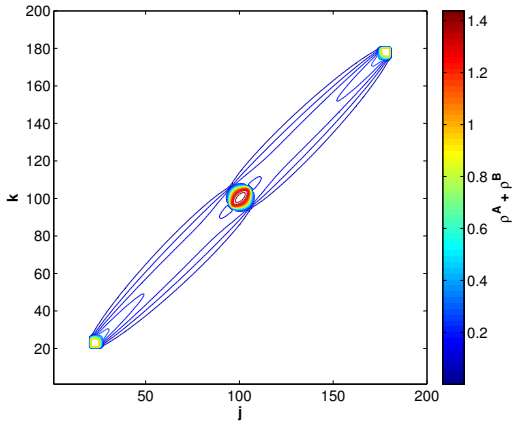

(b) Deterministic, $t = 210$

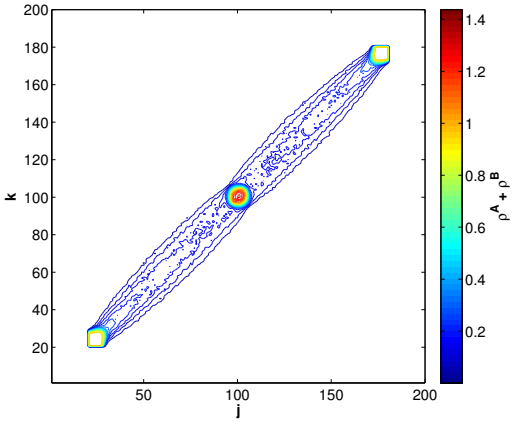

(c) Stochastic, $t = 245$

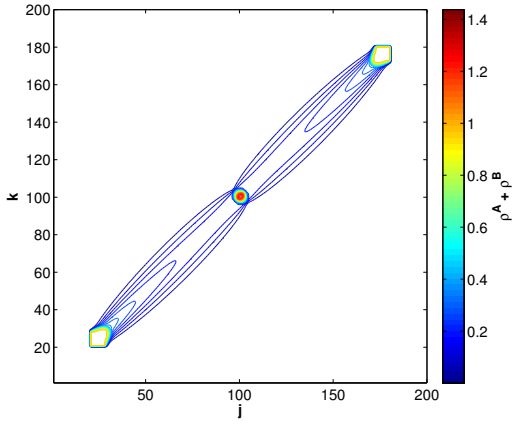

(d) Deterministic, $t = 245$

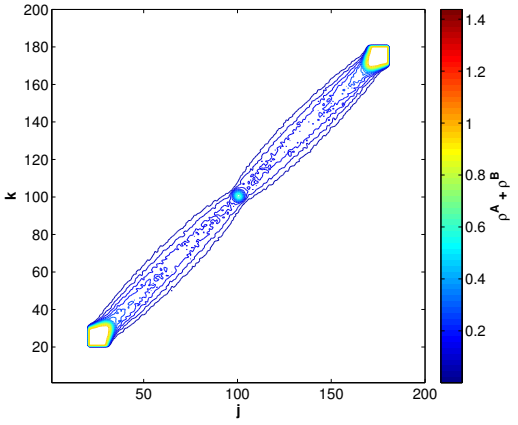

(e) Stochastic, $t = 280$

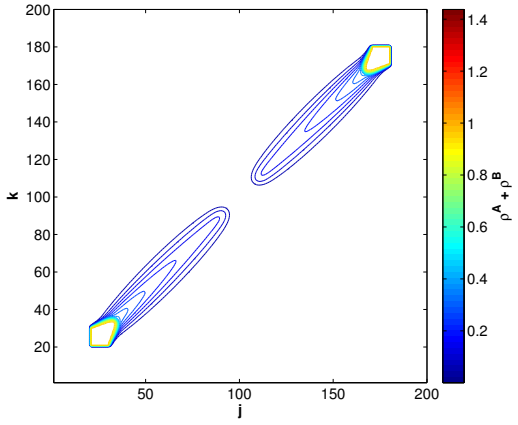

(f) Deterministic, $t = 280$

Figure 4.10: ρ^A and ρ^B, Stochastic and Deterministic, Times $t = 210, 245, 280$ $\alpha = 3$

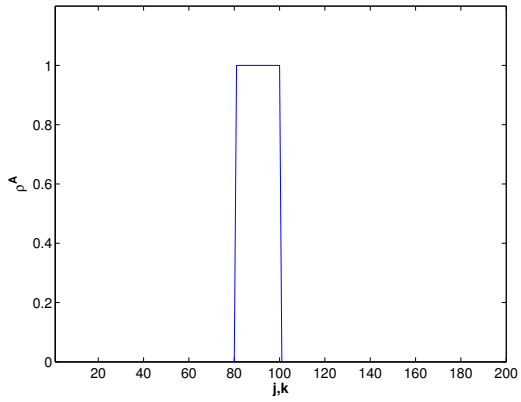

(a) Stochastic, $t = 0$

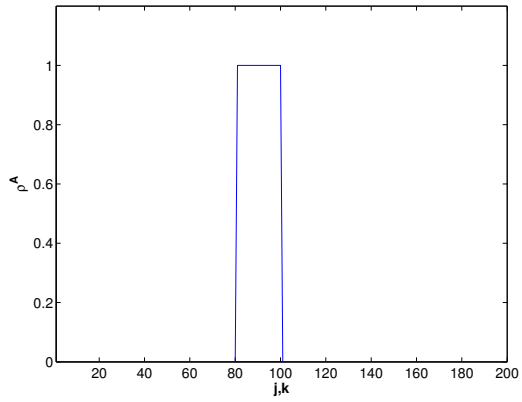

(b) Deterministic, $t = 0$

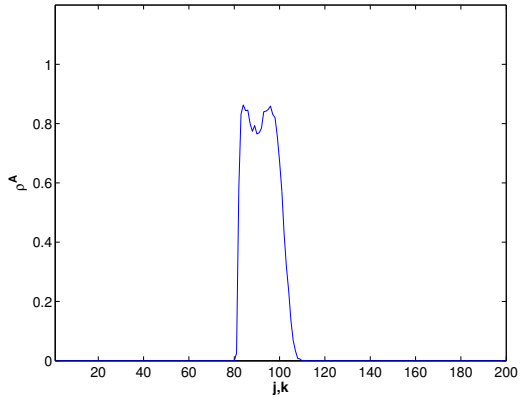

(c) Stochastic, $t = 35$

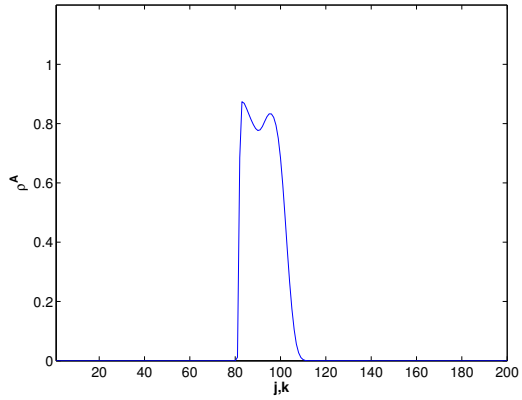

(d) Deterministic, $t = 35$

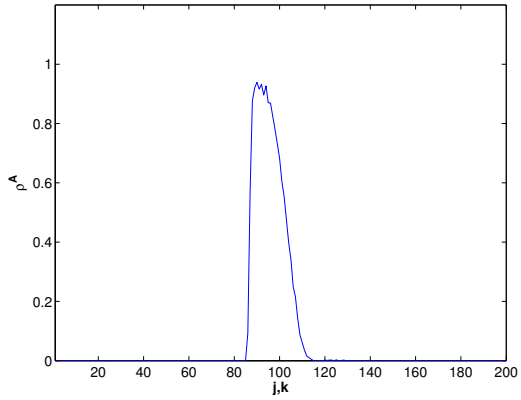

(e) Stochastic, $t = 70$

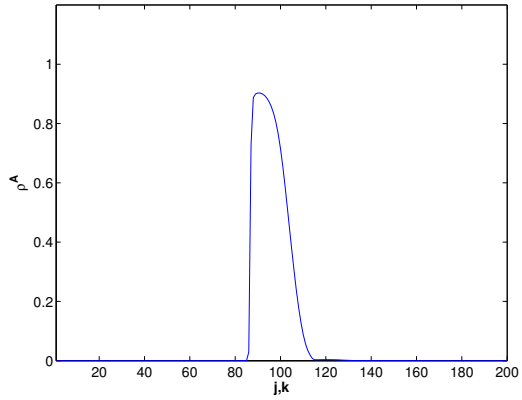

(f) Deterministic, $t = 70$

Figure 4.11: $\rho^A_{j,j,t}$, Stochastic and Deterministic, Times $t = 0, 35, 70$
$\alpha = 3$

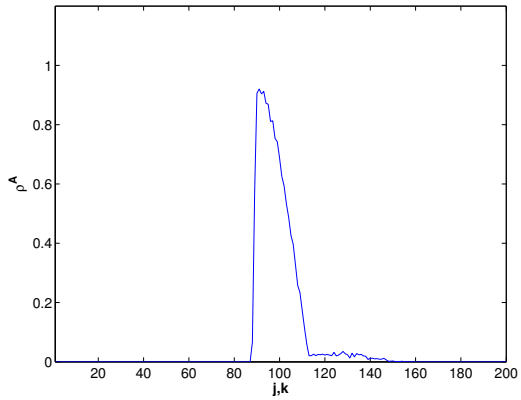

(a) Stochastic, $t = 105$

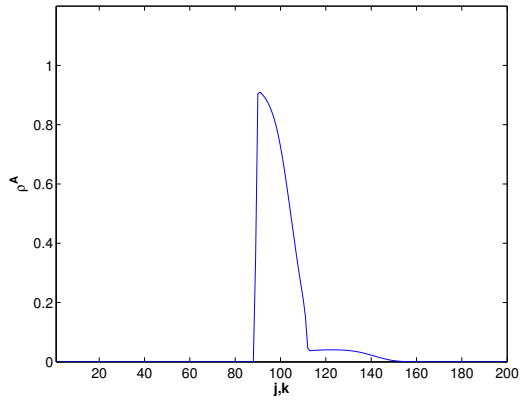

(b) Deterministic, $t = 105$

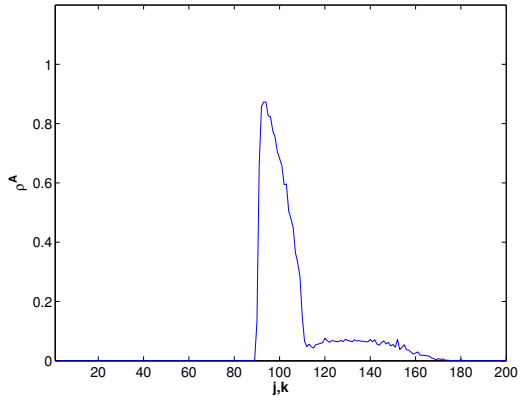

(c) Stochastic, $t = 140$

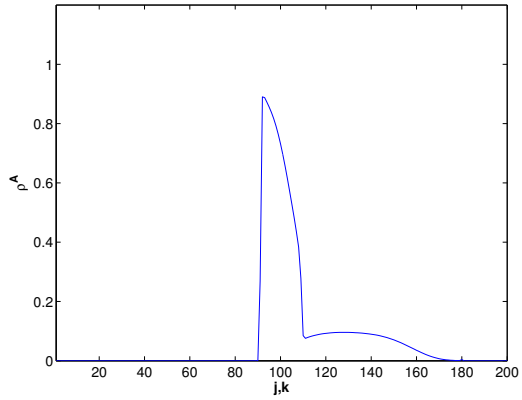

(d) Deterministic, $t = 140$

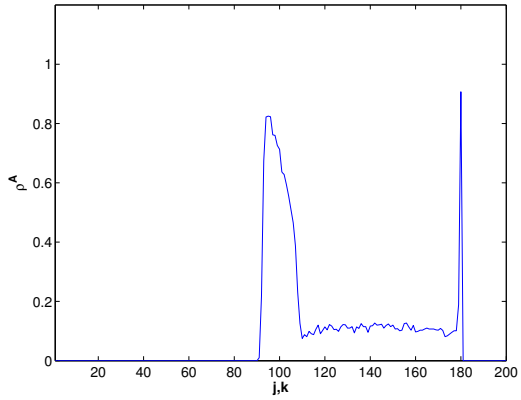

(e) Stochastic, $t = 175$

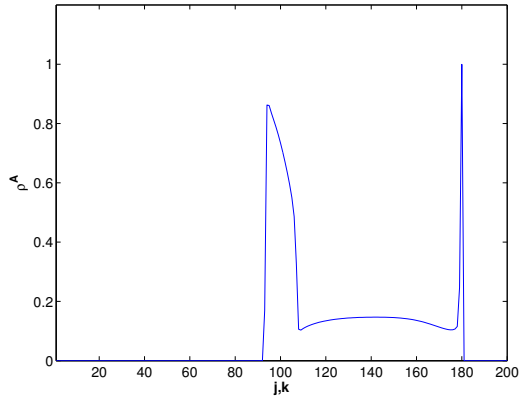

(f) Deterministic, $t = 175$

Figure 4.12: $\rho^A_{j,j,t}$, Stochastic and Deterministic, Times $t = 105, 140, 175$
$\alpha = 3$

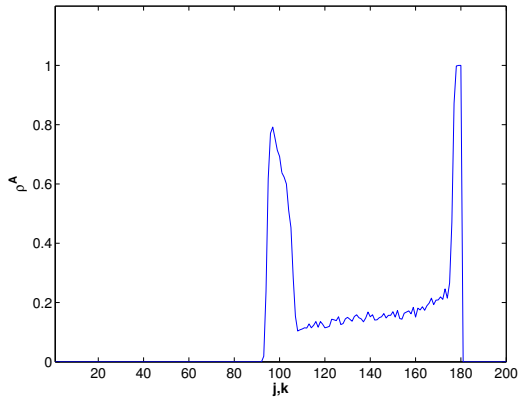

(a) Stochastic, $t = 210$

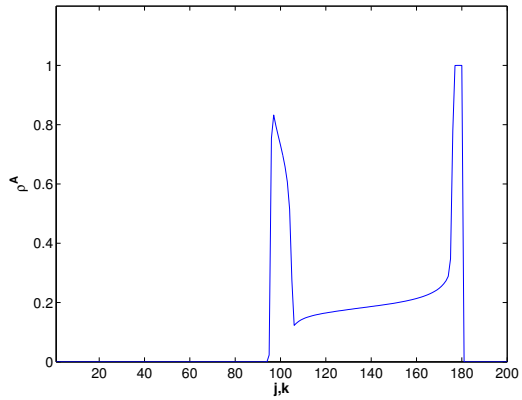

(b) Deterministic, $t = 210$

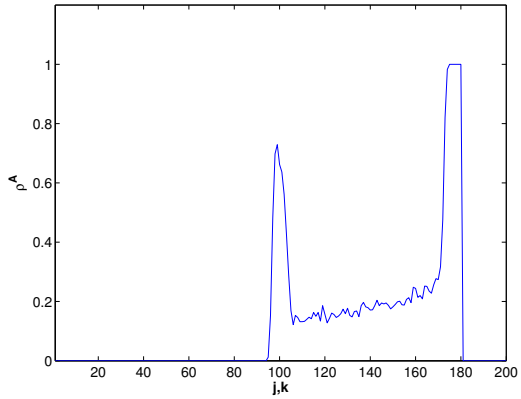

(c) Stochastic, $t = 245$

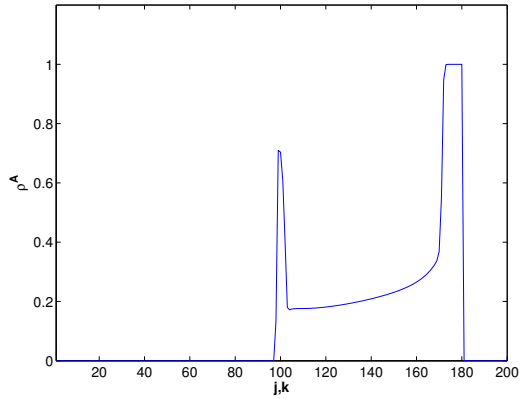

(d) Deterministic, $t = 245$

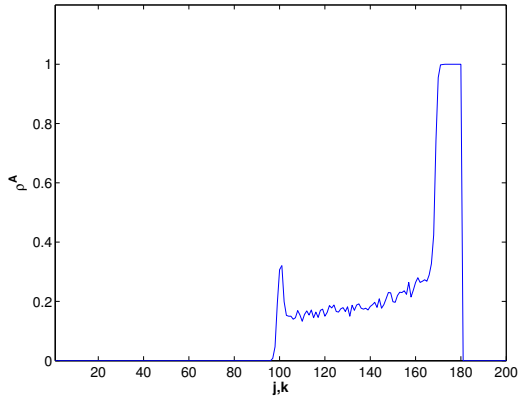

(e) Stochastic, $t = 280$

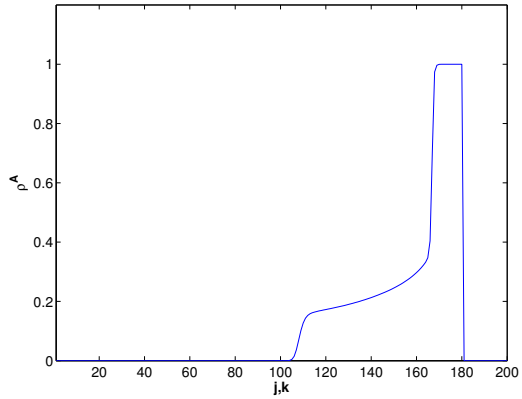

(f) Deterministic, $t = 280$

Figure 4.13: $\rho^A_{j,j,t}$, Stochastic and Deterministic, Times $t = 210, 245, 280$
$\alpha = 3$

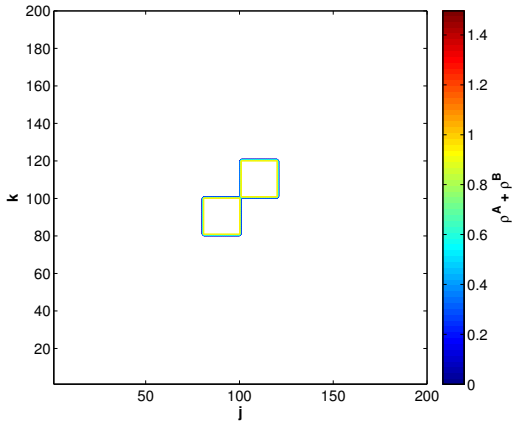

(a) Stochastic, $t = 0$

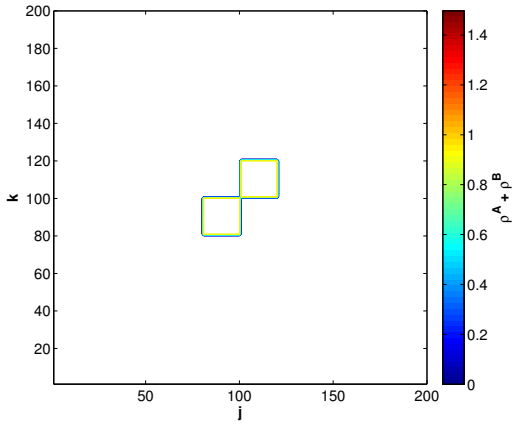

(b) Deterministic, $t = 0$

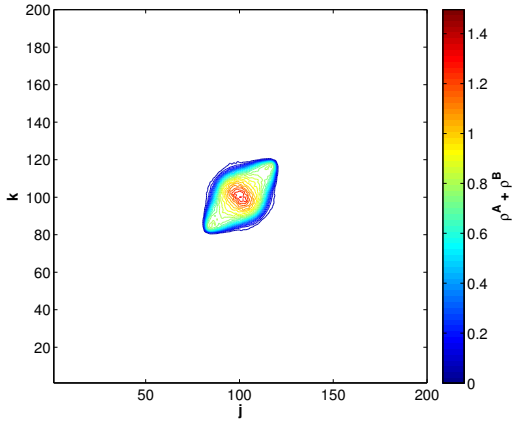

(c) Stochastic, $t = 40$

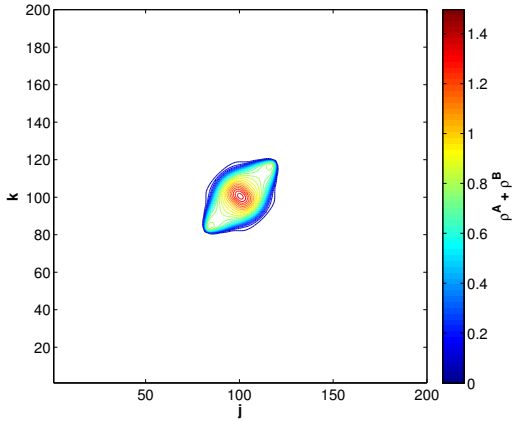

(d) Deterministic, $t = 40$

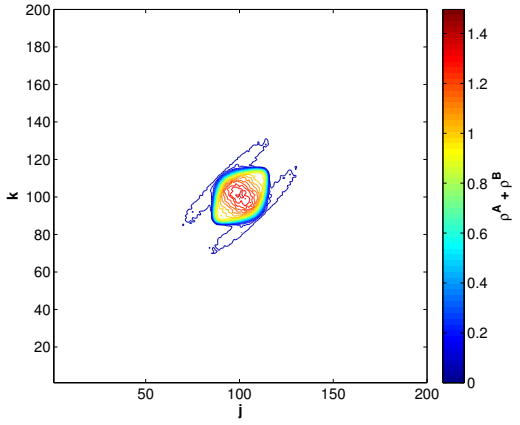

(e) Stochastic, $t = 80$

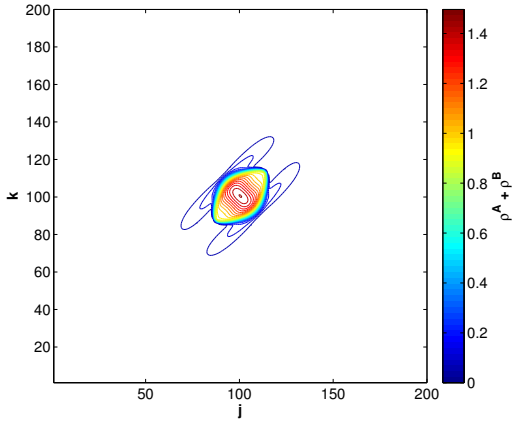

(f) Deterministic, $t = 80$

Figure 4.14: ρ^A and ρ^B, Stochastic and Deterministic, Times $t = 0, 40, 80$ $\alpha = 4$

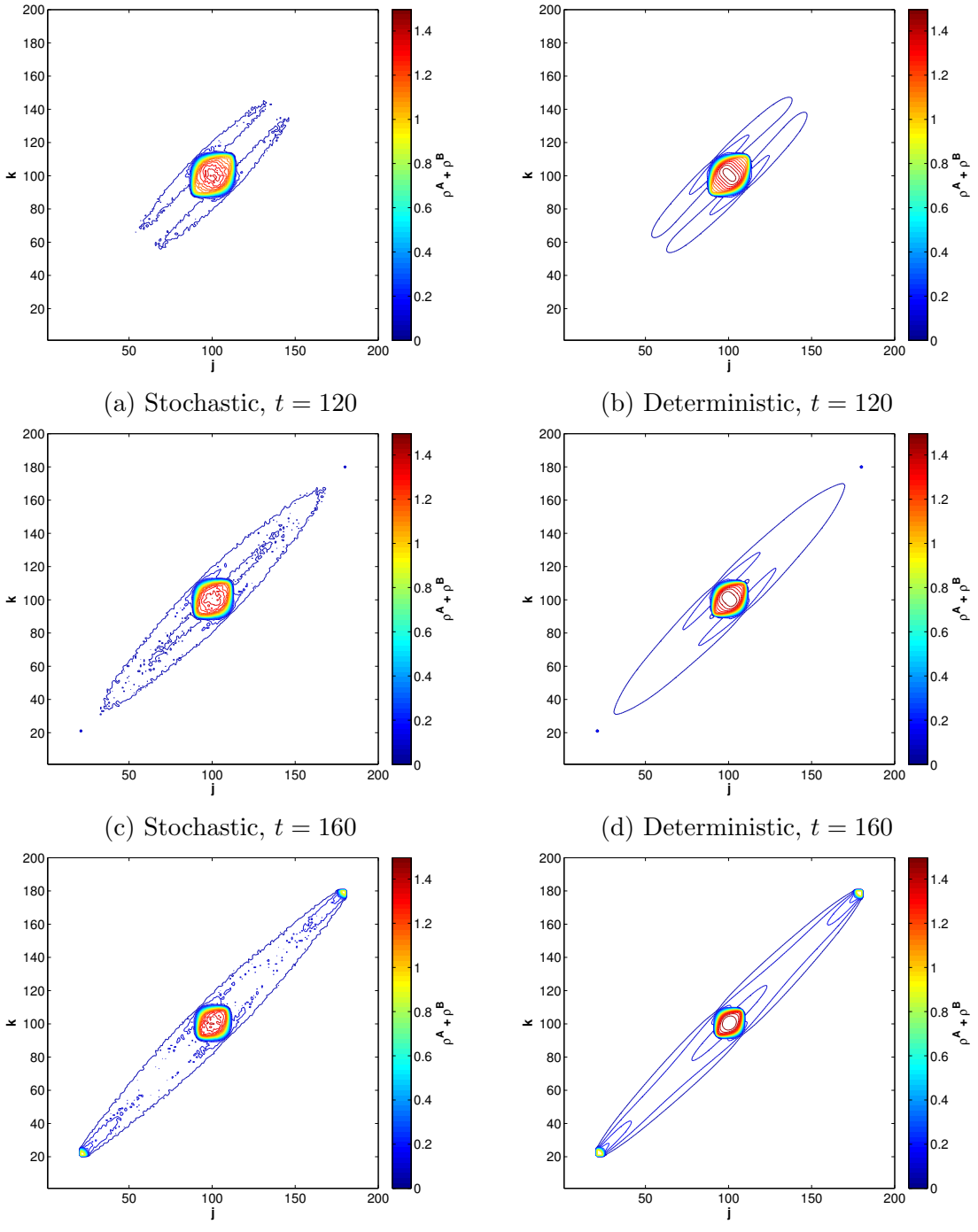

(a) Stochastic, $t = 120$

(b) Deterministic, $t = 120$

(c) Stochastic, $t = 160$

(d) Deterministic, $t = 160$

(e) Stochastic, $t = 200$

(f) Deterministic, $t = 200$

Figure 4.15: ρ^A and ρ^B, Stochastic and Deterministic, Times $t = 120, 160, 200$ $\alpha = 4$

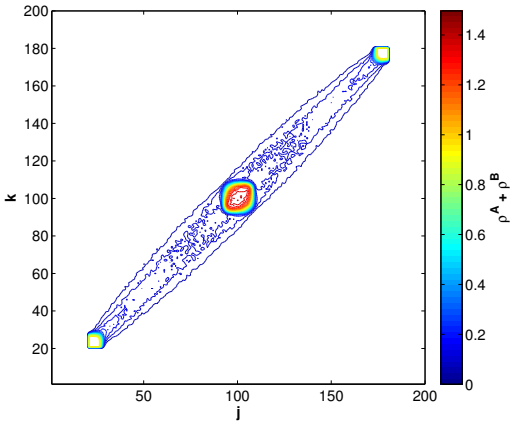

(a) Stochastic, $t = 240$

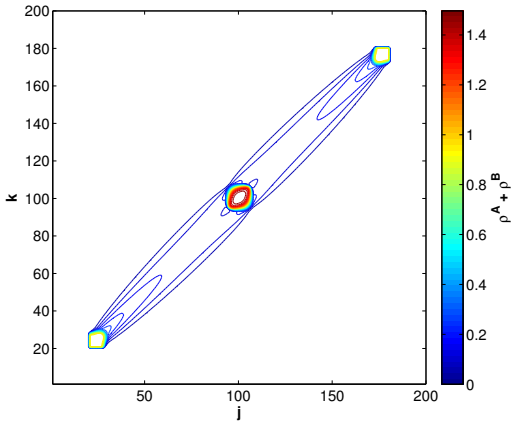

(b) Deterministic, $t = 240$

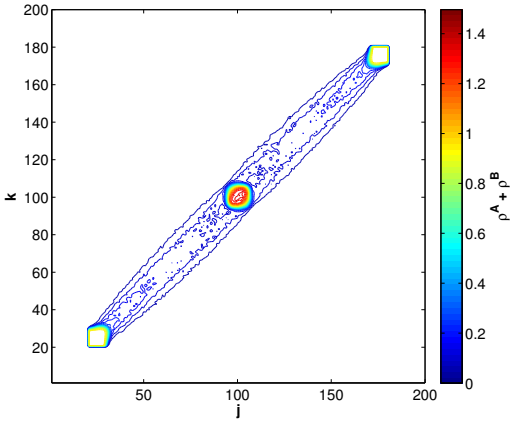

(c) Stochastic, $t = 280$

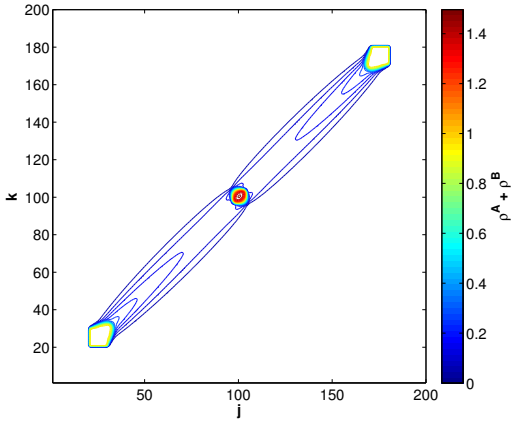

(d) Deterministic, $t = 280$

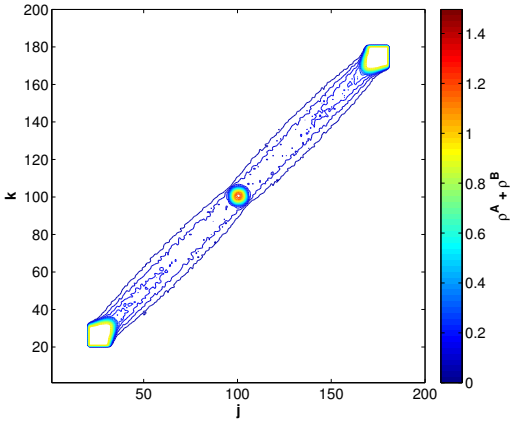

(e) Stochastic, $t = 320$

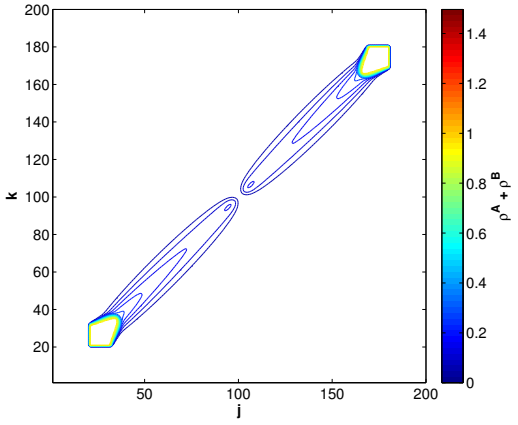

(f) Deterministic, $t = 320$

Figure 4.16: ρ^A and ρ^B, Stochastic and Deterministic, Times $t = 240, 280, 320$ $\alpha = 4$

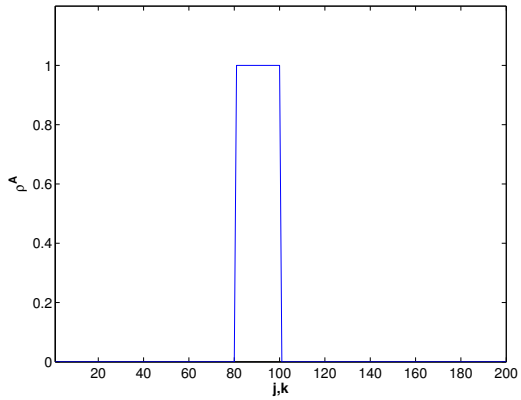

(a) Stochastic, $t = 0$

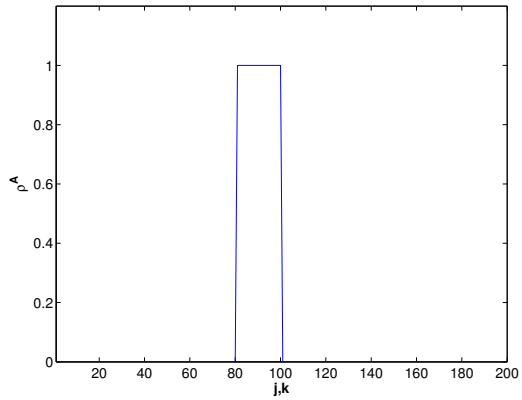

(b) Deterministic, $t = 0$

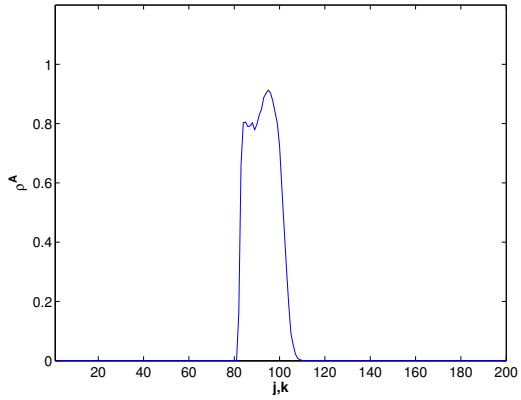

(c) Stochastic, $t = 40$

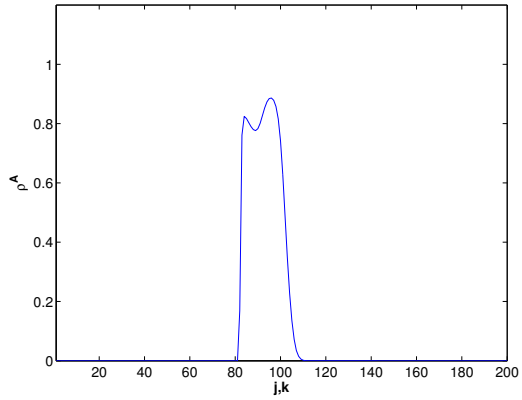

(d) Deterministic, $t = 40$

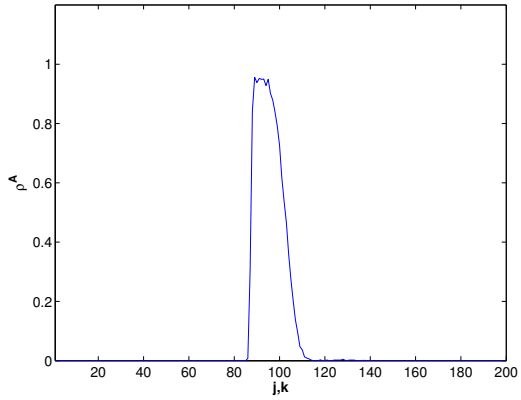

(e) Stochastic, $t = 80$

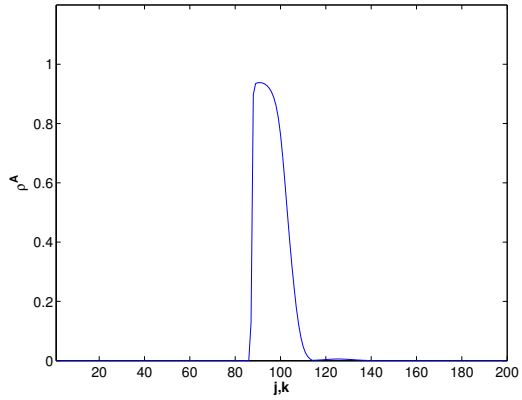

(f) Deterministic, $t = 80$

Figure 4.17: $\rho^A_{j,j,t}$, Stochastic and Deterministic, Times $t = 0, 40, 80$
$\alpha = 4$

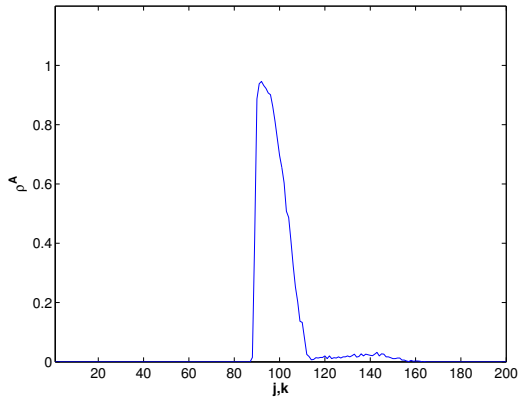

(a) Stochastic, $t = 120$

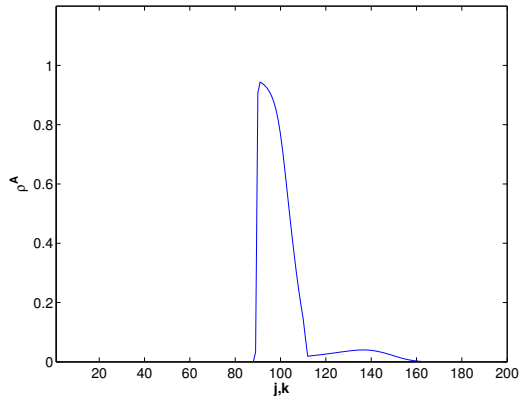

(b) Deterministic, $t = 120$

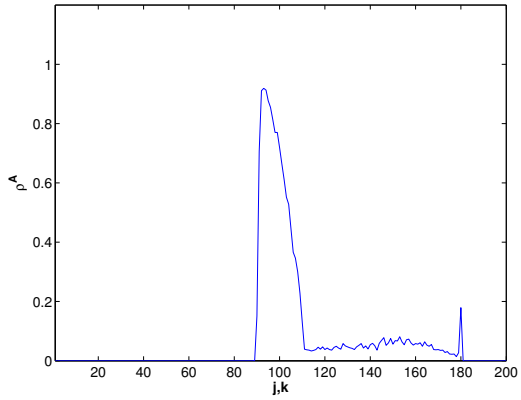

(c) Stochastic, $t = 160$

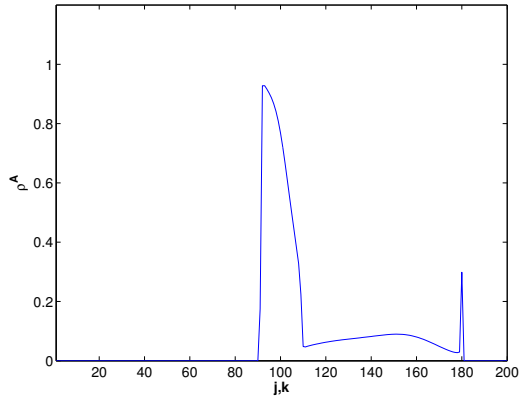

(d) Deterministic, $t = 160$

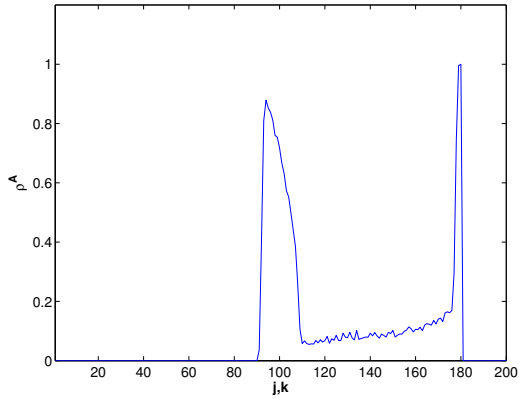

(e) Stochastic, $t = 200$

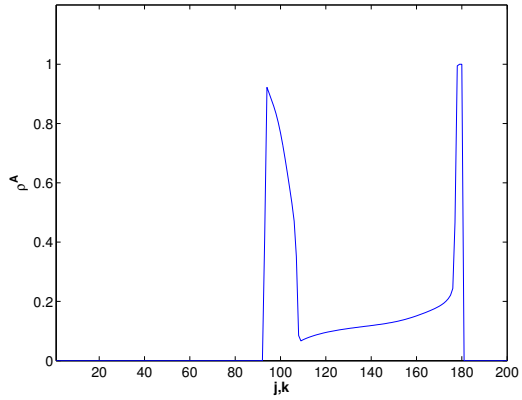

(f) Deterministic, $t = 200$

Figure 4.18: $\rho^A_{j,j,t}$, Stochastic and Deterministic, Times $t = 120, 160, 200$ $\alpha = 4$

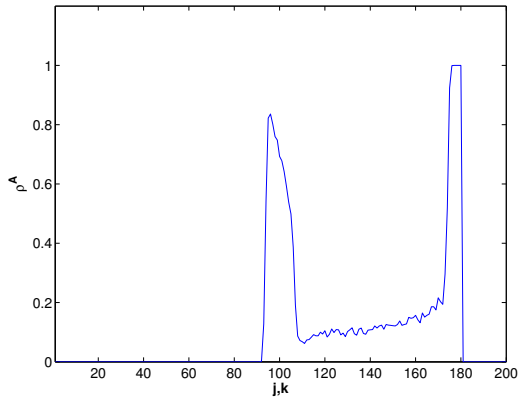

(a) Stochastic, $t = 240$

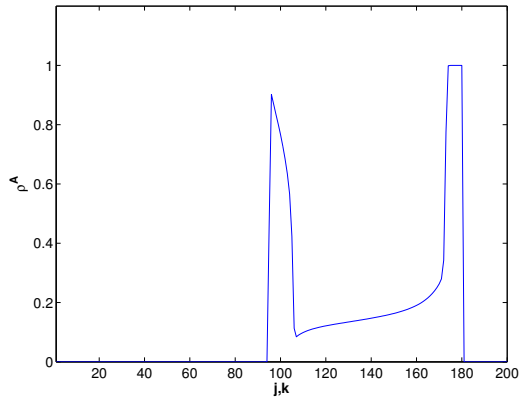

(b) Deterministic, $t = 240$

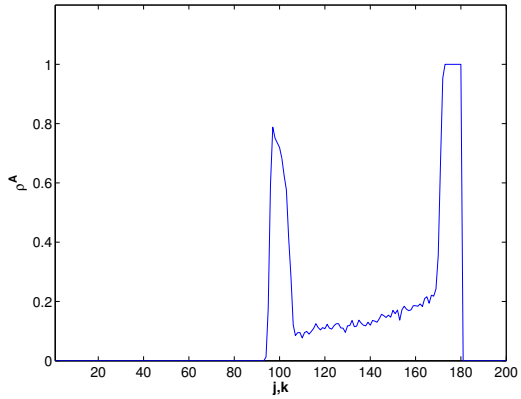

(c) Stochastic, $t = 280$

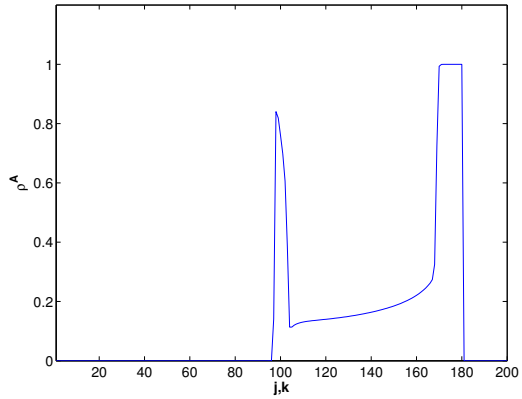

(d) Deterministic, $t = 280$

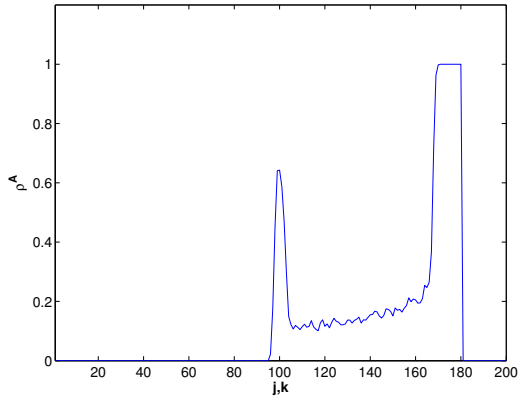

(e) Stochastic, $t = 320$

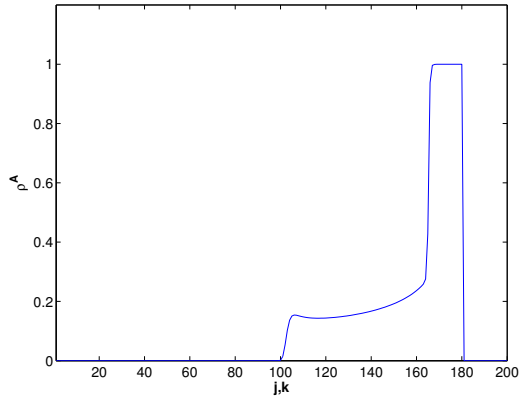

(f) Deterministic, $t = 320$

Figure 4.19: $\rho^A_{j,j,t}$, Stochastic and Deterministic, Times $t = 240, 280, 320$
$\alpha = 3$

4.2.6 Analysis of Results

In all three models, we see that as the two groups migrate towards their target points, a blockage begins to form at the center of the lattice. While some agents pass around the blockage, the majority of the agents are slowed down in the center of the lattice. As time progresses, the blockage first expands, then dissipates, allowing the remaining agents to pass through.

In all three models, we see very close agreement between the stochastic and deterministic models over the short term. As time progresses, however, we notice some common discrepancies between the stochastic and deterministic models. In all cases, we see that agents are able to pass through the central blockage more quickly in the deterministic model than in the stochastic model. This leads to the blockage collapsing sooner and faster accumulation of density at the target point in the deterministic model.

Varying the value of α results in differences to the individual model and to the discrepancies between the models. The most readily apparent effect of increasing α is an increase in the amount of time it takes for the central blockage to dissolve. As the strength of the slowdown interaction increases, it requires more time for agents to pass through the central blockage, and as such the density at the blockage stays higher for a longer period of time, and densities accumulate at the target points more slowly.

While the stochastic and deterministic models agree fairly well qualitatively for small values of t in all three models, the differences between the models appear more rapidly as α increases. Indeed, when $\alpha = 3$ or $\alpha = 4$, the central blockage dissipates much more quickly in the stochastic model than in the deterministic model. As observed

in [14] in the context of a traffic model, this is due to the fact that the approximate independence assumptions given in Equations 3.22 and 3.23 break down rapidly as the strength of the slowdown interaction increases.

4.3 Square Groups of Non-Uniform Density

We next examine the effects of the initial conditions on the stochastic and deterministic model, specifically by testing the effects of initial groups of non-uniform density. As we are only studying the effects of the initial configuration, we will fix $\alpha = 2$. We simulate to a maximum time of $t = 20$, as beyond this time, the effects of the non-uniform nature of the initial conditions quickly becomes lost.

4.3.1 Lattice, Velocity Fields, and Constants

We let $\mathcal{L}$ be a 100 by 100 lattice. We define functions $\Psi^A(j,k)$ and $\Psi^B(j,k)$ on $\mathcal{L}$ by

$$\Psi^A(j,k) = (80-j)^2 + (80-k^2) \tag{4.10}$$

and

$$\Psi^B(j,k) = (21-j)^2 + (21-k^2), \tag{4.11}$$

respectively. We then take our velocity fields $\phi^A(j,k)$ and $\phi^B(j,k)$ by

$$\phi^A(j,k) = -\frac{\nabla\Psi^A(j,k)}{||\nabla\Psi^A(j,k)||_1} \tag{4.12}$$

$$= \left(\frac{80-j}{|(80-j)|+|(80-k)|}, \frac{80-k}{|(80-j)|+|(80-k)|}\right) \tag{4.13}$$

and

$$\phi^B(j,k) = -\frac{\nabla\Psi^B(j,k)}{||\nabla\Psi^B(j,k)||_1} \tag{4.14}$$

$$= \left(\frac{21-j}{|(21-j)|+|(21-k)|}, \frac{21-k}{|(21-j)|+|(21-k)|}\right). \tag{4.15}$$

With this velocity field, agents from Group A will move towards the point $(80, 80)$ and agents from Group B will move towards the point $(21, 21)$. The graphs of these velocity fields are simpliy scaled versions of those given in Figure 4.1, and so are not provided here.

4.3.2 Initial Configuration

For the deterministic model, we simply let

$$\rho^A_{j,k,0} = \begin{cases} \frac{1}{4}\left\lceil 2\left(1+\cos\left(\frac{4\pi}{19}(i+j-62)\right)\right)\right\rceil, & 31 \le j \le 50 \text{ and } 31 \le k \le 50, \\ 0, & \text{otherwise,} \end{cases} \tag{4.16}$$

and let

$$\rho^B_{j,k,0} = \begin{cases} \frac{1}{4}\left\lceil 2\left(1+\cos\left(\frac{4\pi}{19}(i+j-102)\right)\right)\right\rceil, & 51 \le j \le 70 \text{ and } 51 \le k \le 70, \\ 0, & \text{otherwise.} \end{cases} \tag{4.17}$$

To replicate this initial configuration in the stochastic model, we average over 20000 realizations, each with an initial setup constructed in the following manner:

- For all cells (j, k) such that $31 \le j \le 50$ and $31 \le k \le 50$,

    1. Sample u from the uniform distribution on $(0, 1]$.

2. If $u < \frac{1}{4}\left\lceil 2\left(1+\cos\left(\frac{4\pi}{19}(i+j-62)\right)\right)\right\rceil$, set $\sigma^A_{j,k,0} = 1$.

3. Otherwise, set $\sigma^A_{j,k,0} = 0$.

- For all cells (j,k) such that $51 \leq j \leq 70$ and $51 \leq k \leq 70$,

1. Sample u from the uniform distribution on $(0,1]$.

2. If $u < \frac{1}{4}\left\lceil 2\left(1+\cos\left(\frac{4\pi}{19}(i+j-102)\right)\right)\right\rceil$, set $\sigma^B_{j,k,0} = 1$.

3. Otherwise, set $\sigma^B_{j,k,0} = 0$.

Because the initial conditions are recalculated for each realization, the initial configuration approaches that of the deterministic model as we average over large numbers of realizations.

4.3.3 Simulation Results

As before, Figures 4.20 and 4.21 show the densities for the groups on the lattice at various times, while Figures 4.22, and 4.23 show the density of a single group along the diagonal of the lattice.

4.3.4 Analysis of Results

As we saw in models with uniform initial conditions, the stochastic and deterministic models agree very well over short periods of time. As mentioned previously, the system quickly loses memory of its non-uniform initial conditions, with regions of high density and low density quickly normalizing. However, at any given time, it is clear that the oscillations of the stochastic simulation are sharper than those of the deterministic simulation. This is due to the stochastic model being more diffusive, as

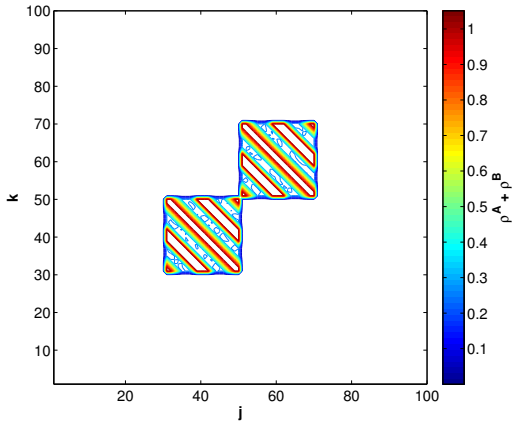

(a) Stochastic, $t = 0$

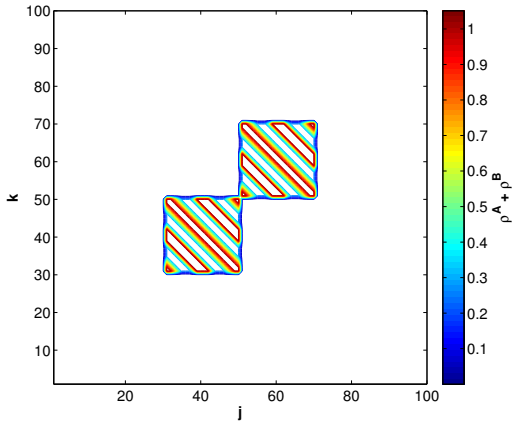

(b) Deterministic, $t = 0$

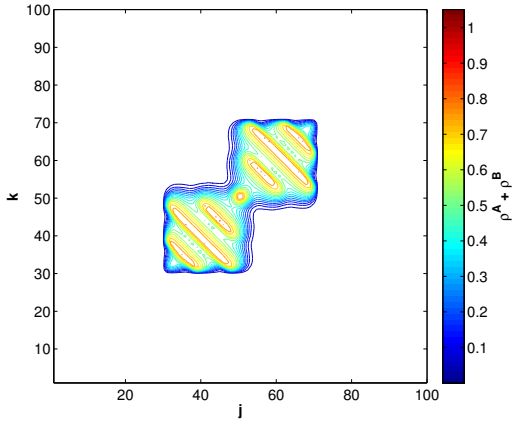

(c) Stochastic, $t = 4$

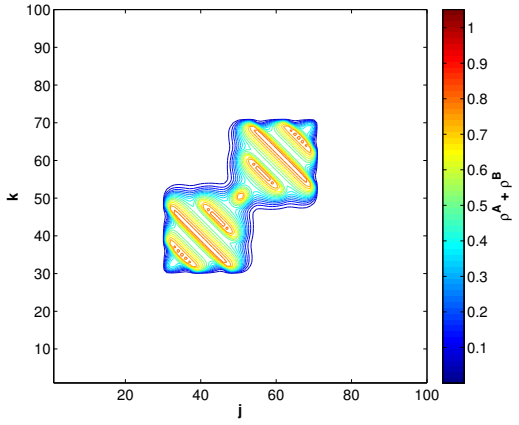

(d) Deterministic, $t = 4$

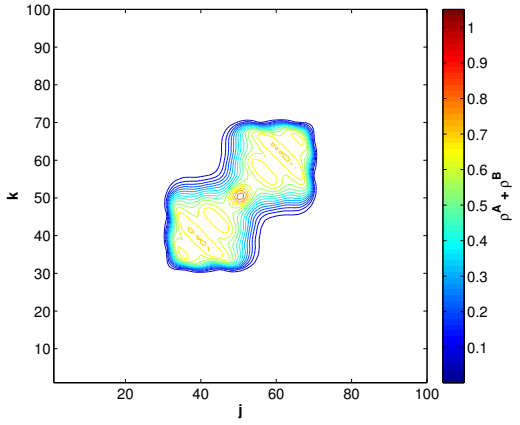

(e) Stochastic, $t = 8$

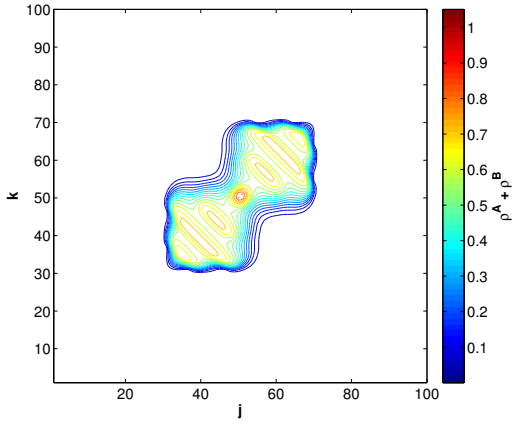

(f) Deterministic, $t = 8$

Figure 4.20: ρ^A and ρ^B, Stochastic and Deterministic, Times $t = 0, 4, 8$ $\alpha = 2$

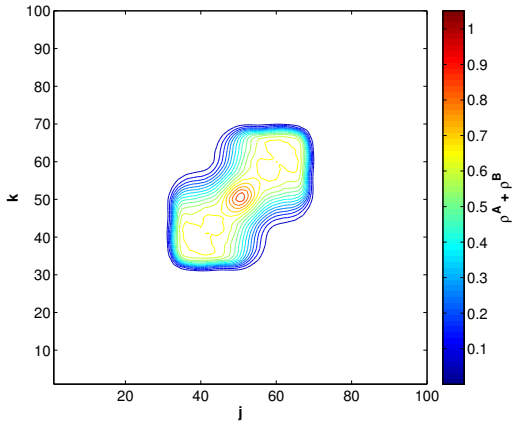

(a) Stochastic, $t = 12$

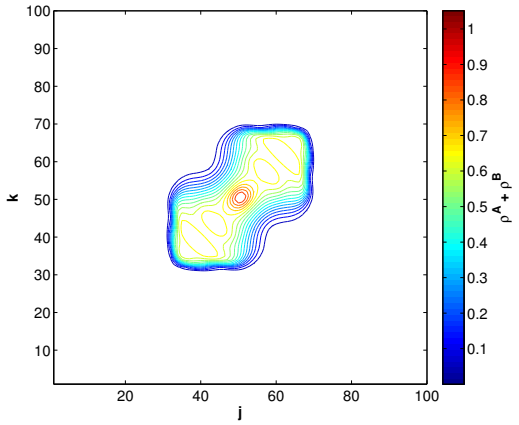

(b) Deterministic, $t = 12$

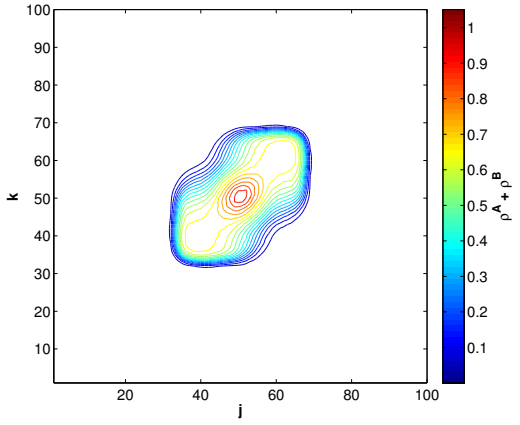

(c) Stochastic, $t = 16$

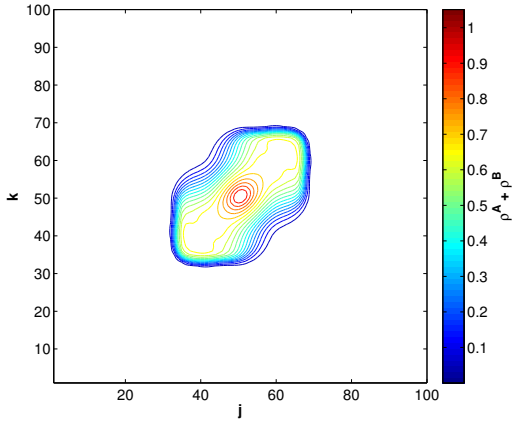

(d) Deterministic, $t = 16$

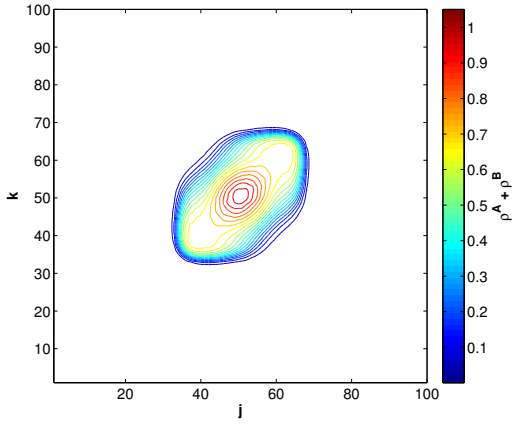

(e) Stochastic, $t = 20$

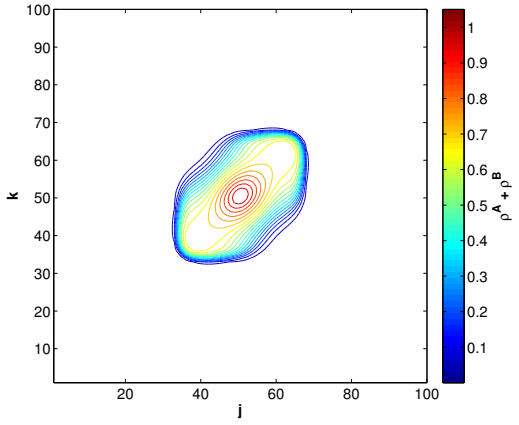

(f) Deterministic, $t = 20$

Figure 4.21: ρ^A and ρ^B, Stochastic and Deterministic, Times $t = 12, 16, 20$ $\alpha = 2$

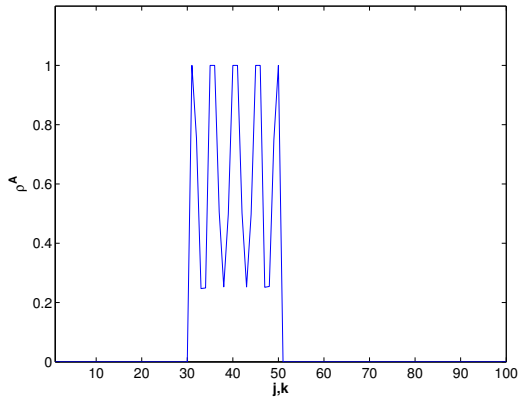

(a) Stochastic, $t = 0$

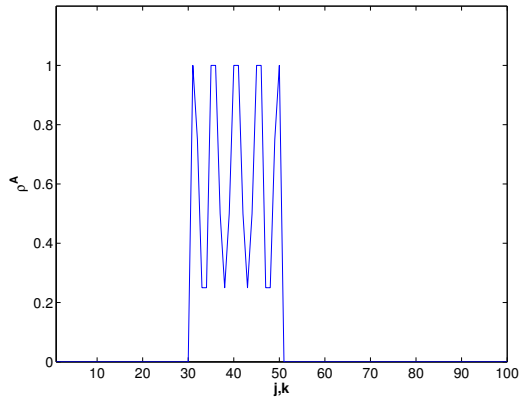

(b) Deterministic, $t = 0$

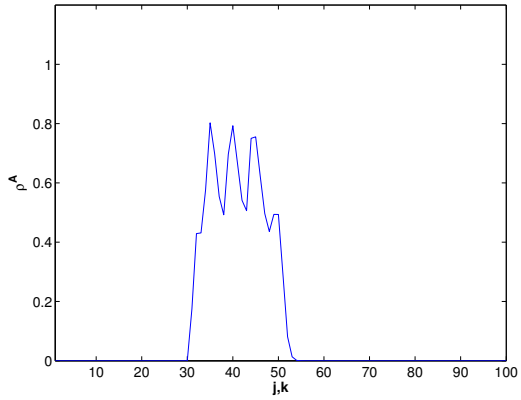

(c) Stochastic, $t = 4$

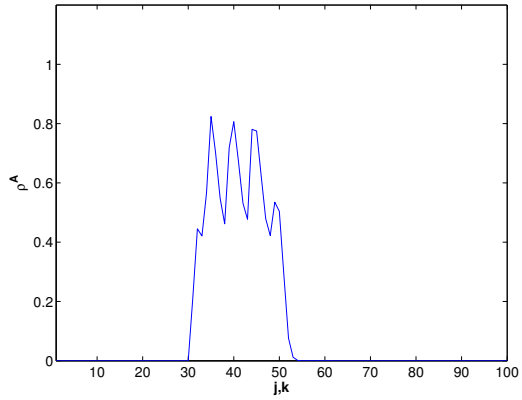

(d) Deterministic, $t = 4$

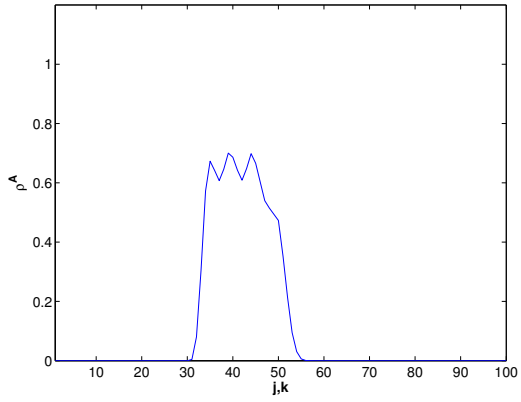

(e) Stochastic, $t = 8$

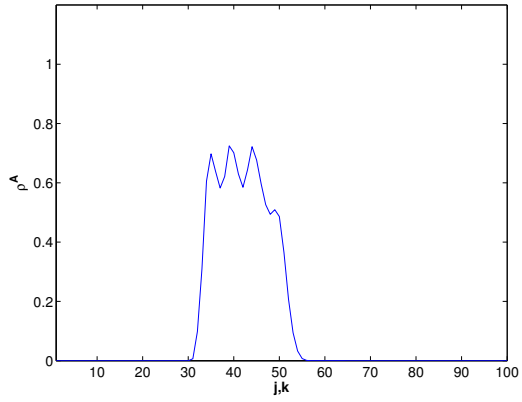

(f) Deterministic, $t = 8$

Figure 4.22: $\rho^A_{j,j,t}$, Stochastic and Deterministic, Times $t = 0, 4, 8$
$\alpha = 2$

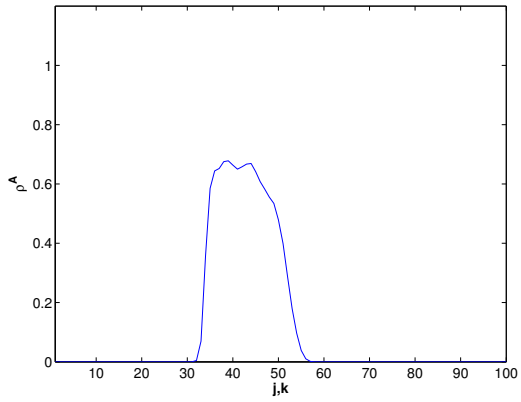

(a) Stochastic, $t = 12$

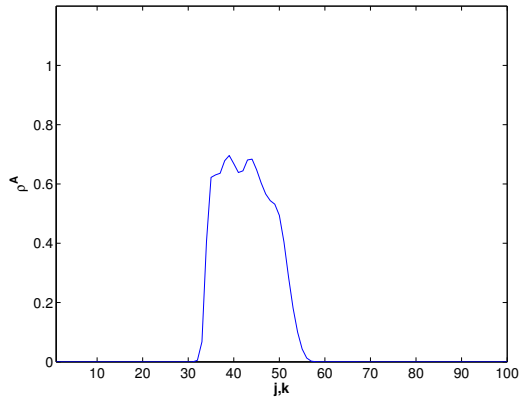

(b) Deterministic, $t = 12$

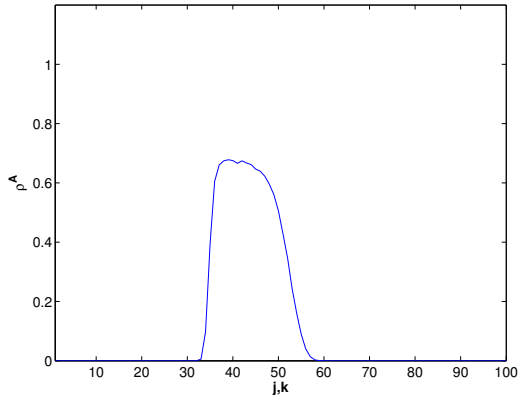

(c) Stochastic, $t = 16$

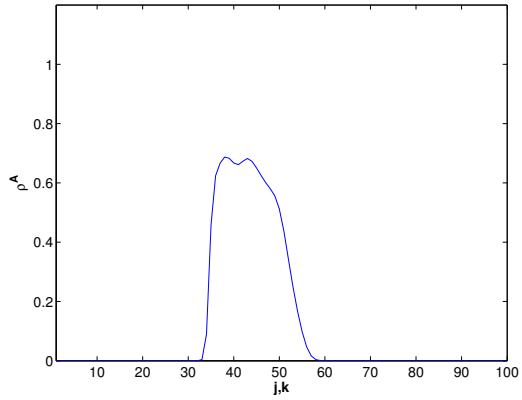

(d) Deterministic, $t = 16$

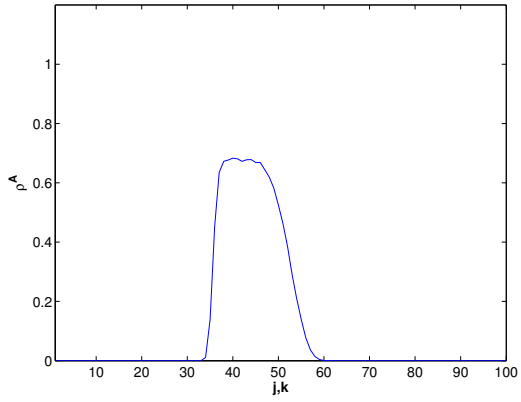

(e) Stochastic, $t = 20$

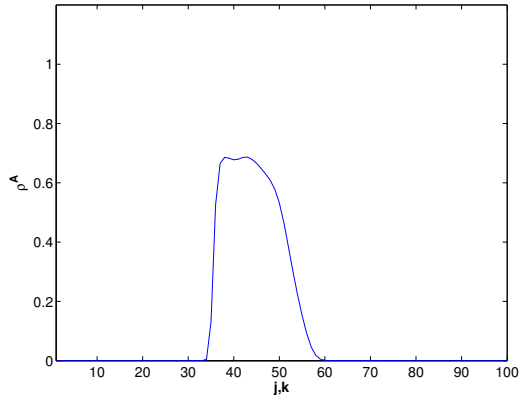

(f) Deterministic, $t = 20$

Figure 4.23: $\rho^A_{j,j,t}$, Stochastic and Deterministic, Times $t = 12, 16, 20$ $\alpha = 2$

was also the case in [14]. In Chapter 5, we will attempt to correct this difference by deriving a diffusive correction to the macroscopic model.

Chapter 5

Hyperbolicity and Diffusiveness of the Macroscopic Model

5.1 Hyperbolicity of the Macroscopic System

The system of PDEs given in equation 3.40 is only conditionally hyperbolic. Indeed, the hyperbolicity of the system depends not only on the values of the densities, but on the defined velocity fields and the values of the constants c_0, c_1, c_2, and c_3 as well. We will derive the necessary and sufficient conditions for the hyperbolicity of the model, and study the effects of different velocity fields and constant values on the hyperbolicity.

5.1.1 Hyperbolicity Conditions

By definition, this system is strictly hyperbolic exactly in the case that the matrix

$$A = \alpha_1 \begin{bmatrix} \phi_1^A f'(\rho^A) g(\rho^B) & \phi_1^A f(\rho^A) g'(\rho^B) \\ \phi_1^B f(\rho^B) g'(\rho^A) & \phi_1^B f'(\rho^B) g(\rho^A) \end{bmatrix} + \alpha_2 \begin{bmatrix} \phi_2^A f'(\rho^A) g(\rho^B) & \phi_2^A f(\rho^A) g'(\rho^B) \\ \phi_2^B f(\rho^B) g'(\rho^A) & \phi_2^B f'(\rho^B) g(\rho^A) \end{bmatrix} \tag{5.1}$$

has two distinct real eigenvalues for all $\alpha_1, \alpha_2 \in \mathbb{R}$. Letting $\boldsymbol{\alpha} = (\alpha_1, \alpha_2)$, Equation 5.1 can be rewritten as

$$= A = \begin{bmatrix} (\boldsymbol{\alpha} \cdot \phi^A) f'(\rho^A) g(\rho^B) & (\boldsymbol{\alpha} \cdot \phi^A) f(\rho^A) g'(\rho^B) \\ (\boldsymbol{\alpha} \cdot \phi^B) f(\rho^B) g'(\rho^A) & (\boldsymbol{\alpha} \cdot \phi^B) f'(\rho^B) g(\rho^A) \end{bmatrix}. \tag{5.2}$$

The eigenvalues of this matrix are those $\lambda \in \mathbb{C}$ that satisfy the equation

$$\begin{aligned} 0 = &\left[(\boldsymbol{\alpha} \cdot \phi^A) f'(\rho^A) g(\rho^B) - \lambda\right] \left[(\boldsymbol{\alpha} \cdot \phi^B) f'(\rho^B) g(\rho^A) - \lambda\right] \\ &- (\boldsymbol{\alpha} \cdot \phi^A)(\boldsymbol{\alpha} \cdot \phi^B) f(\rho^A) f(\rho^B) g'(\rho^A) g'(\rho^B). \end{aligned} \tag{5.3}$$

This equation can be rewritten as

$$\begin{aligned} 0 = &\lambda^2 - \left[(\boldsymbol{\alpha} \cdot \phi^B) f'(\rho^B) g(\rho^A) + (\boldsymbol{\alpha} \cdot \phi^A) f'(\rho^A) g(\rho^B)\right] \lambda \\ &+ (\boldsymbol{\alpha} \cdot \phi^A)(\boldsymbol{\alpha} \cdot \phi^B) \left[f'(\rho^A) f'(\rho^B) g(\rho^A) g(\rho^B) - f(\rho^A) f(\rho^B) g'(\rho^A) g'(\rho^B)\right], \end{aligned} \tag{5.4}$$

from which we can see that matrix A has two distinct real eigenvalues exactly in the case that

(5.5)

$$0 < \left[(\boldsymbol{\alpha}\cdot\phi^A)f'(\rho^A)g(\rho^B) + (\boldsymbol{\alpha}\cdot\phi^B)f'(\rho^B)g(\rho^A)\right]^2 - 4(\boldsymbol{\alpha}\cdot\phi^A)(\boldsymbol{\alpha}\cdot\phi^B)\left[f'(\rho^A)f'(\rho^B)g(\rho^A)g(\rho^B) - f(\rho^A)f(\rho^B)g'(\rho^A)g'(\rho^B)\right] \quad (5.6)$$

for all $\boldsymbol{\alpha} \in \mathbb{R}^2$, or equivalently, exactly in the case that

$$\begin{aligned} 0 < {} & \left[(\boldsymbol{\alpha}\cdot\phi^A)f'(\rho^A)g(\rho^B)\right]^2 + \left[(\boldsymbol{\alpha}\cdot\phi^B)f'(\rho^B)g(\rho^A)\right]^2 \\ & - 2(\boldsymbol{\alpha}\cdot\phi^A)(\boldsymbol{\alpha}\cdot\phi^B)f'(\rho^A)f'(\rho^B)g(\rho^A)g(\rho^B) \\ & + 4(\boldsymbol{\alpha}\cdot\phi^A)(\boldsymbol{\alpha}\cdot\phi^B)f(\rho^A)f(\rho^B)g'(\rho^A)g'(\rho^B) \end{aligned} \quad (5.7)$$

for all $\boldsymbol{\alpha} \in \mathbb{R}^2$.

5.1.2 Case 1: $\phi^A = \phi^B$

In the case that $\phi^A = \phi^B$, we would have that pedestrians from both groups were following the same velocity field, as could be the case in an evacuation scenario in which there was only one exit point. In this case, the hyperbolicity condition 5.7 simplifies to the form

$$\begin{aligned} 0 < {} & \left[f'(\rho^A)g(\rho^B)\right]^2 + \left[f'(\rho^B)g(\rho^A)\right]^2 - 2f'(\rho^A)f'(\rho^B)g(\rho^A)g(\rho^B) \\ & + 4f(\rho^A)f(\rho^B)g'(\rho^A)g'(\rho^B). \end{aligned} \quad (5.8)$$

Defining the function $h_1(x, y)$ by

$$\begin{aligned} h_1(x,y) = {} & [f'(x)g(y)]^2 + [f'(y)g(x)]^2 - 2f'(x)f'(y)g(x)g(y) \\ & + 4f(x)f(y)g'(x)g'(y). \end{aligned} \quad (5.9)$$

we plot the value of the $h(\rho^A, \rho^B)$ for $0 \leq \rho^A \leq 1$ and $0 \leq \rho^B \leq 1$ under various values of α in Figure 5.1. Under all values of α tested, there was never a case in which the inequality was false, and so the system admitted no non-hyperbolic regime. It is, indeed, provable that this system is always hyperbolic under the condition that $\phi^A = \phi^B$, but we omit the proof here.

5.1.3 Case 2: $\phi^A = -\phi^B$

In the case that $\phi^A = -\phi^B$, pedestrians from opposing groups are following velocity fields that point in opposite directions at every point on the lattice. An example of a model for which this type of configuration would be appropriate is two groups of pedestrians traversing a hallway in opposite directions. Indeed, this is analogous to the traffic model studied in [14]. The hyperbolicity condition 5.7 in this case simplifies to the form

$$\begin{aligned} 0 < \left[f'(\rho^A)g(\rho^B)\right]^2 + \left[f'(\rho^B)g(\rho^A)\right]^2 + 2f'(\rho^A)f'(\rho^B)g(\rho^A)g(\rho^B) \\ - 4f(\rho^A)f(\rho^B)g'(\rho^A)g'(\rho^B). \end{aligned} \tag{5.10}$$

Defining the function $h_2(x, y)$ by

$$\begin{aligned} h_2(x,y) = \left[f'(x)g(y)\right]^2 + \left[f'(y)g(x)\right]^2 + 2f'(x)f'(y)g(x)g(y) \\ - 4f(x)f(y)g'(x)g'(y). \end{aligned} \tag{5.11}$$

We plot the value of the $h_2(\rho^A, \rho^B)$ for $0 \leq \rho^A \leq 1$ and $0 \leq \rho^B \leq 1$ under various values of α in Figure 5.2, marking a bold line where $h(\rho^A, \rho^B) = 0$ and omitting contour levels below zero. Thus in each graph, the central blank region represents

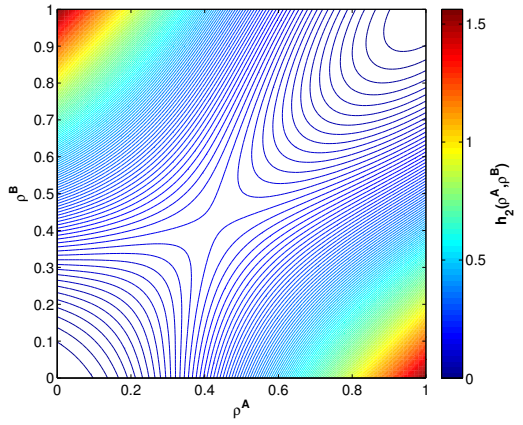

(a) $\alpha = 2$

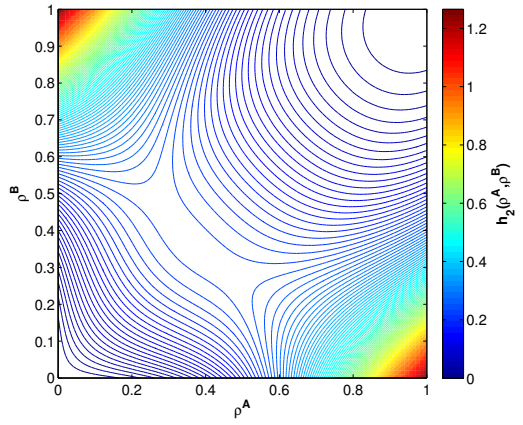

(b) $\alpha = 4$

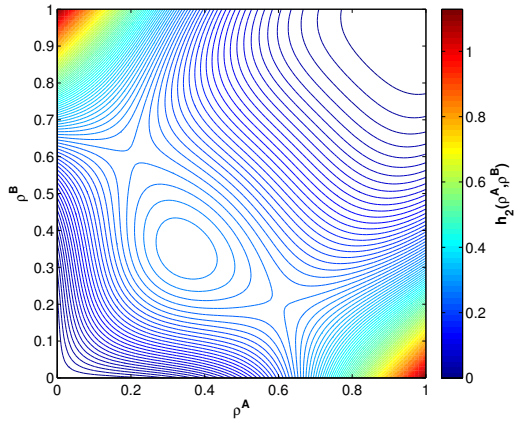

(c) $\alpha = 8$

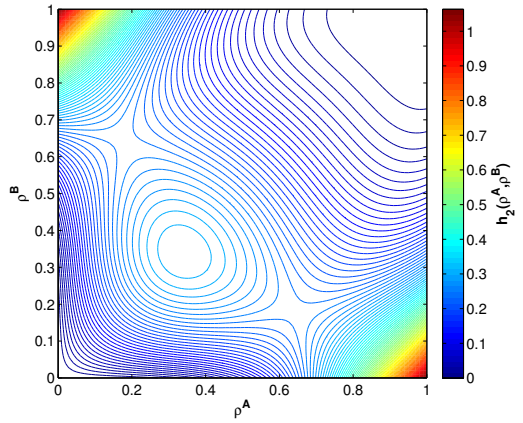

(d) $\alpha = 16$

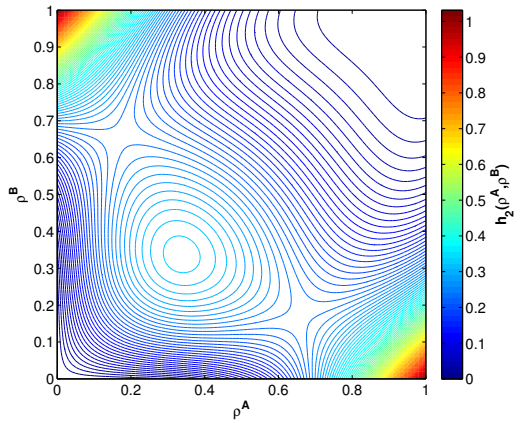

(e) $\alpha = 32$

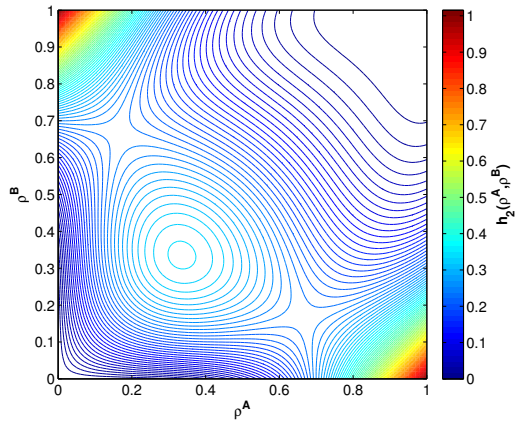

(f) $\alpha = 64$

Figure 5.1: $h_1(\rho^A, \rho^B)$, $\alpha = 2, 4, 8, 16, 32, 64$

those values of ρ^A and ρ^B for which $h_2(\rho^A, \rho^B) < 0$. In Figure 5.3, we plot the value of the $h_2(\rho^A, \rho^B)$ for $0 \leq \rho^A \leq 1$ and $0 \leq \rho^B \leq 1$ under various values of α, marking a bold line where $h(\rho^A, \rho^B) = 0$ and omitting contour levels above zero.

In these figures, we see that letting $\phi^A = -\phi^B$ produces large regions of non-hyperbolicity, with the size and shape of these regions dependent on the chosen value of α: as α, and therefore the strength of the slowdown interaction, increases, the likelihood of the system entering a non-hyperbolic regime expands.

5.1.4 Hyperbolicity of Simulated Models

In the simulations run in Section 4.2, we have that $\phi^A \approx -\phi^B$ in cells close to the center of the lattice. As this is region in which the central blockage occurs, we would expect that as the simulation progresses, the system of equations enters the non-hyperbolic regime in this region and remains in it for a non-trivial period of time. As shown in Figures 5.4 and 5.5, which plot the differences of the eigenvalues of the matrix in Equation 5.2 at various points on the lattice over the range of values of ρ^A and ρ^B, it is, in fact, quite easy to enter a non-hyperbolic regime in most cells in the lattice, where a non-hyperbolic regime corresponds to those central regions of most figures where there is empty space, these regions indicating where the eigenvalues are complex. Indeed, at all cells observed that lie on the interior of the square having cells $(21, 21)$ and $(180, 180)$ as opposite vetices, we see that roughly the same region of values of ρ^A and ρ^B will result in non-hyperbolicity. with the region again depending on α. We also see that in cell $(1, 1)$, where $\phi^A \approx \phi^B$, the system will be hyperbolic for any values of ρ^A and ρ^B.

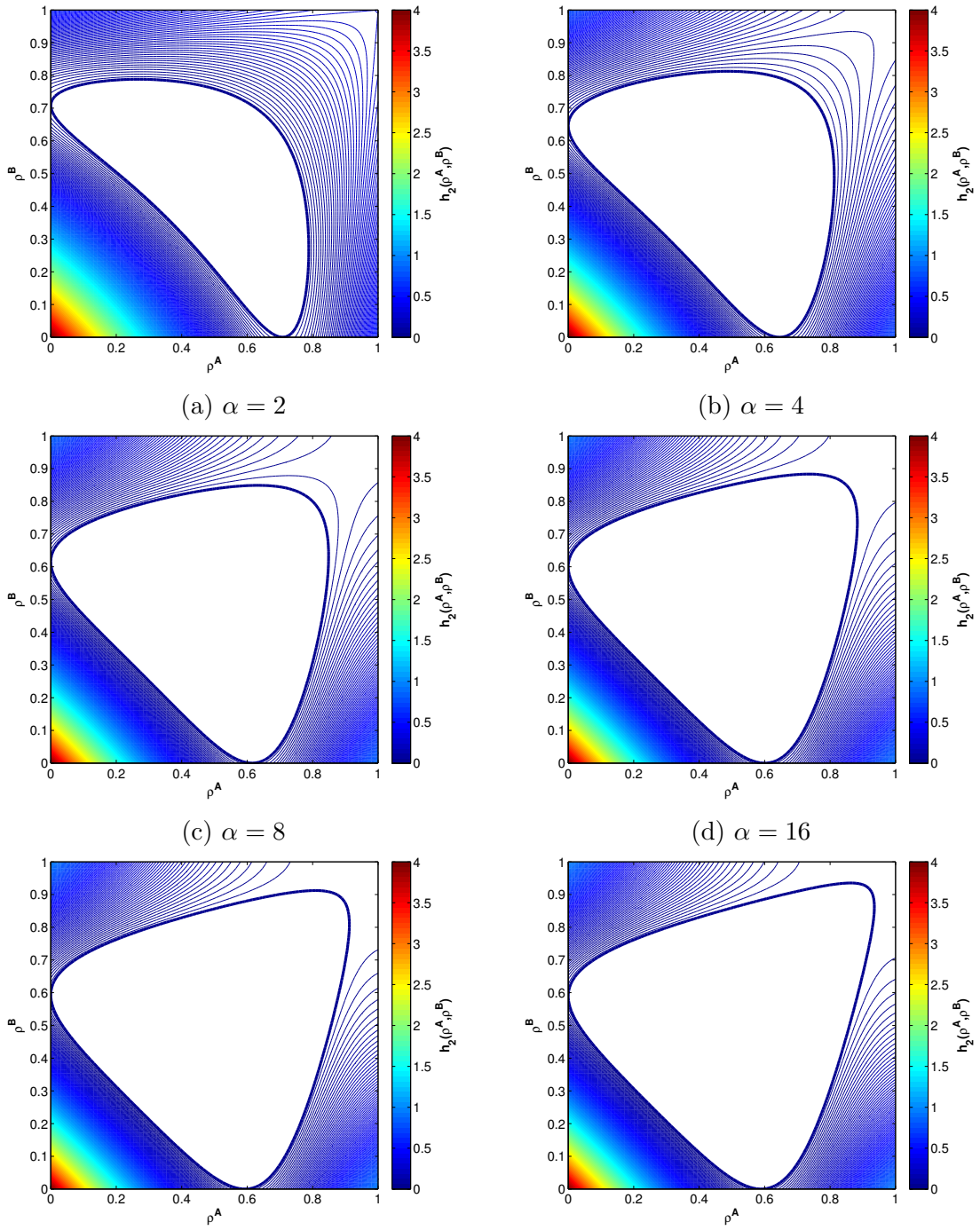

(a) $\alpha = 2$ (b) $\alpha = 4$

(c) $\alpha = 8$ (d) $\alpha = 16$

(e) $\alpha = 32$ (f) $\alpha = 64$

Figure 5.2: $h_2(\rho^A, \rho^B) \geq 0$, $\alpha = 2, 4, 8, 16, 32, 64$

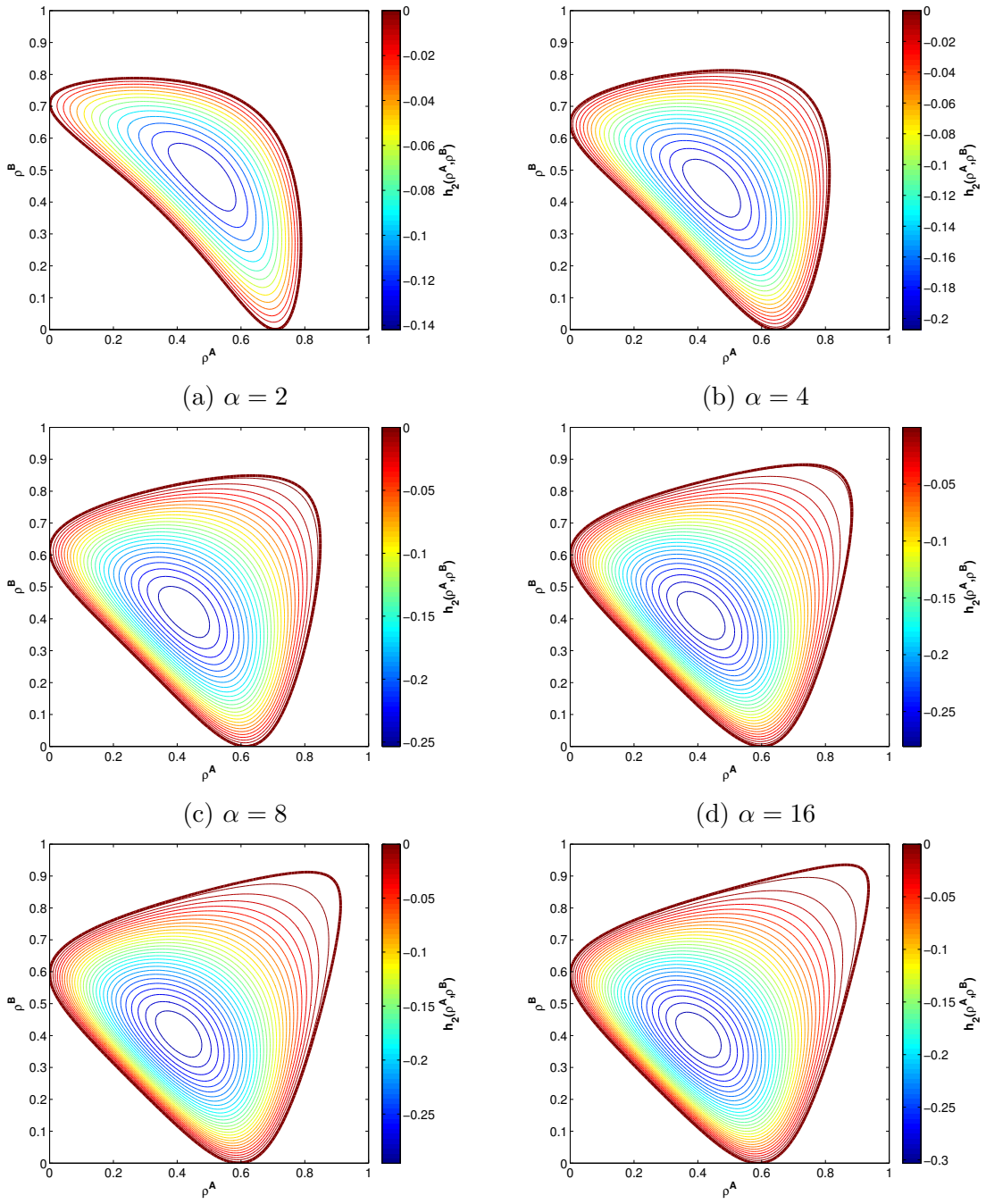

(a) $\alpha = 2$ (b) $\alpha = 4$

(c) $\alpha = 8$ (d) $\alpha = 16$

(e) $\alpha = 32$ (f) $\alpha = 64$

Figure 5.3: $h_2(\rho^A, \rho^B) \leq 0$, $\alpha = 2, 4, 8, 16, 32, 64$

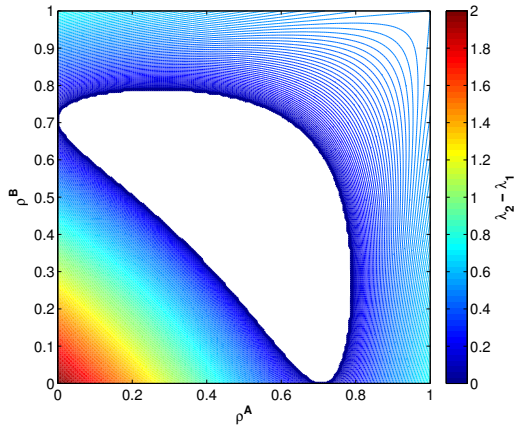

(a) Cell $(100, 100)$, $\alpha = 2$

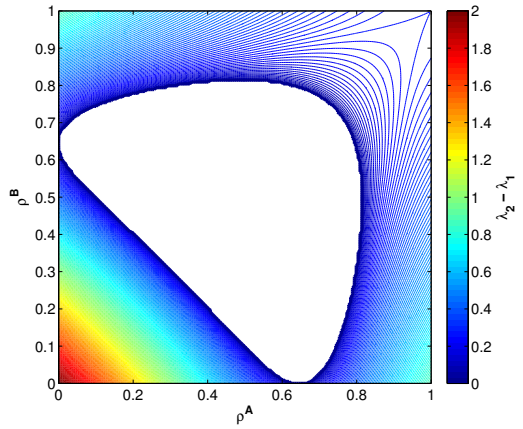

(b) Cell $(100, 100)$, $\alpha = 4$

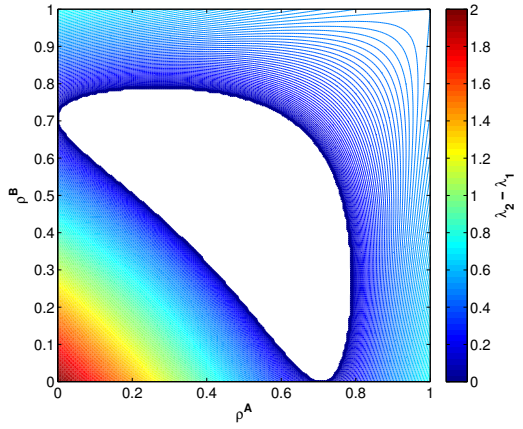

(c) Cell $(50, 100)$, $\alpha = 2$

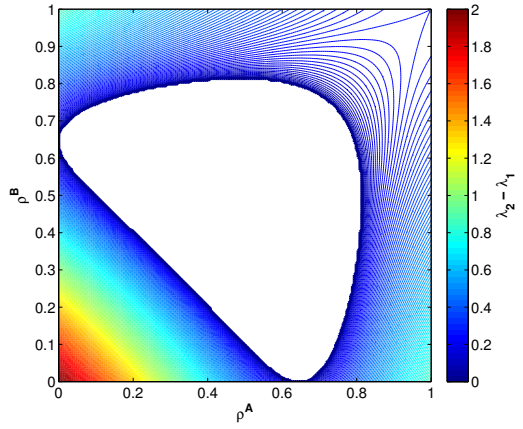

(d) Cell $(50, 100)$, $\alpha = 4$

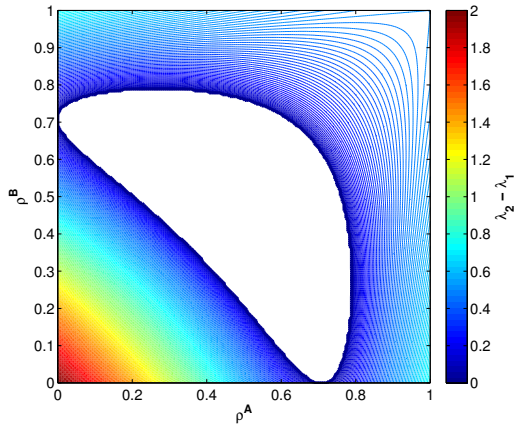

(e) Cell $(22, 22)$, $\alpha = 2$

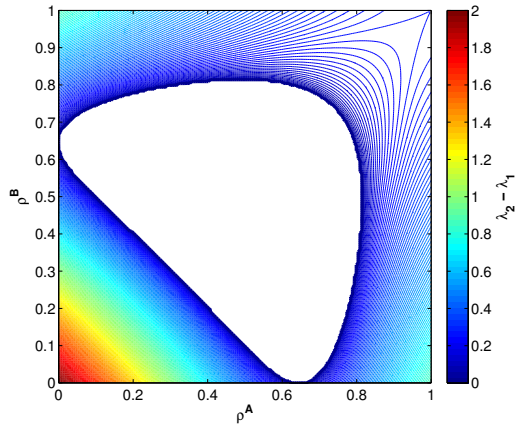

(f) Cell $(22, 22)$, $\alpha = 4$

Figure 5.4: Difference of Real Eigenvalues, $\alpha = 2, 4$, Various Cells

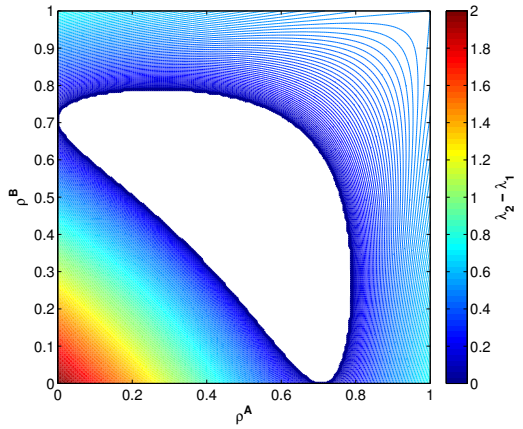

(a) Cell $(22, 179)$, $\alpha = 2$

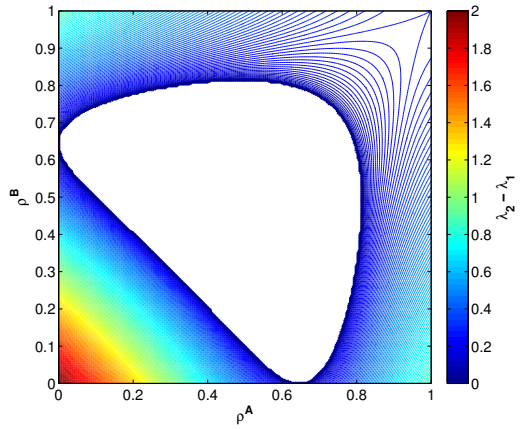

(b) Cell $(22, 179)$, $\alpha = 4$

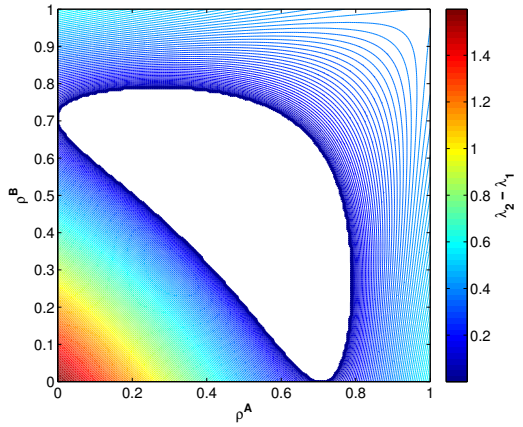

(c) Cell $(1, 200)$, $\alpha = 2$

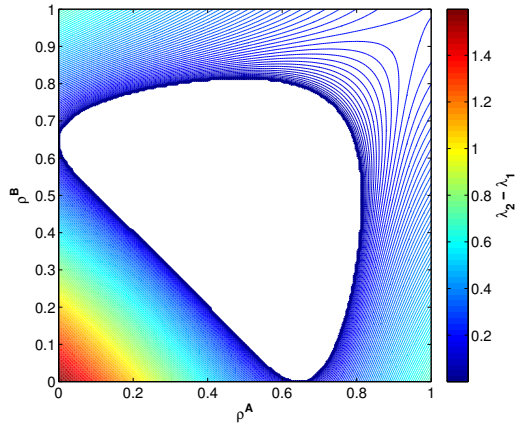

(d) Cell $(1, 200)$, $\alpha = 4$

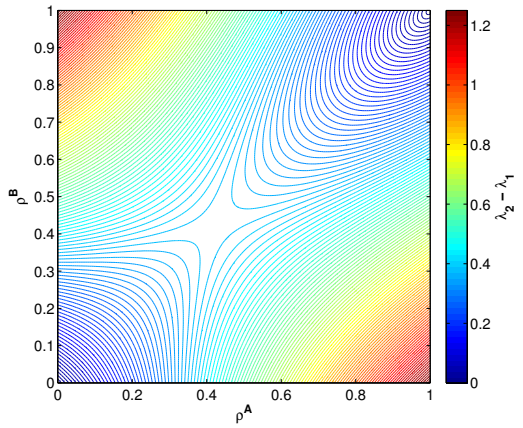

(e) Cell $(1, 1)$, $\alpha = 2$

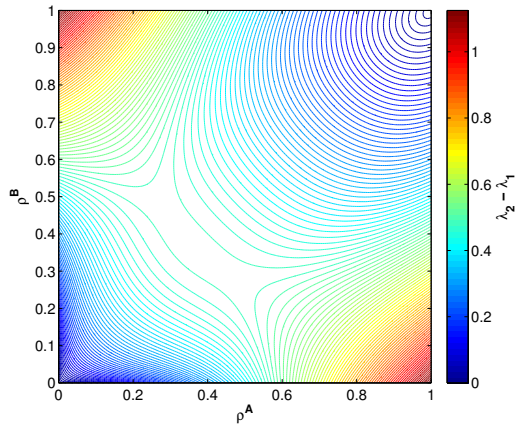

(f) Cell $(1, 1)$, $\alpha = 4$

Figure 5.5: Difference of Real Eigenvalues, $\alpha = 2, 4$, Various Cells

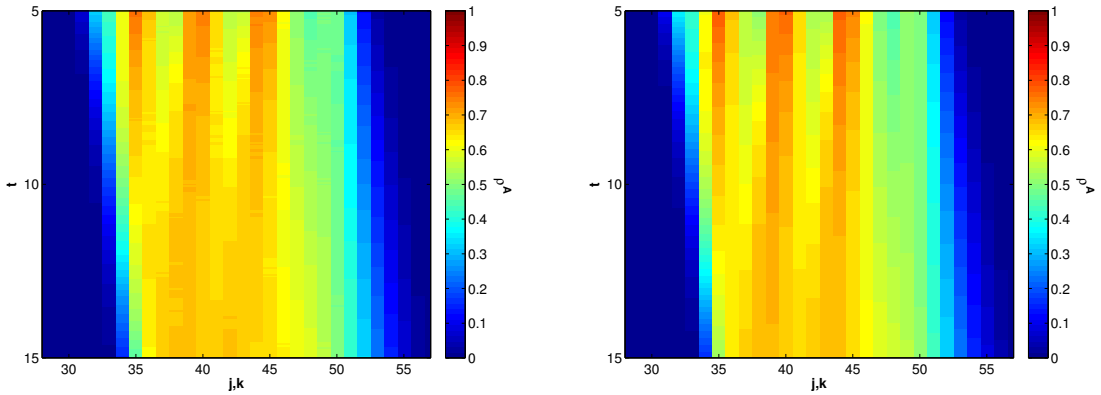

(a) Stochastic Model (b) Deterministic Model

Figure 5.6: ρ^A along the Diagonal $j = k$, Non-Uniform Model

5.2 Diffusiveness

5.2.1 Diffusiveness of Simulated Models

As we saw in Figures 4.22, and 4.23, the miscroscopic model appears to be more diffusive than the deterministic model under certain initial conditions. This difference is highlighted in Figure 5.6.This discrepancy also occurred in [14] when the initial data under fully mixed initial conditions. As in [14], this difference is due to the closure assumptions made in equation 3.24. As such, we will proceed as they did by deriving a diffusive correction for the macroscopic PDE.

5.2.2 Diffusive Correction

The formulation of the macroscopic model given in Equation 3.40 can also be obtained through the substitution of the Taylor expansions

$$\rho^A_{j\pm h,k} = \rho^A_{j,k} \pm h\frac{d}{dx}\rho^A_{j,k} + \frac{h^2}{2}\frac{d^2}{dx^2}\rho^A_{j,k} + \mathcal{O}(h^3), \tag{5.12}$$

$$\rho^A_{j,k\pm h} = \rho^A_{j,k} \pm h\frac{d}{dy}\rho^A_{j,k} + \frac{h^2}{2}\frac{d^2}{dy^2}\rho^A_{j,k} + \mathcal{O}(h^3), \tag{5.13}$$

$$\rho^B_{j\pm h,k} = \rho^B_{j,k} \pm h\frac{d}{dx}\rho^B_{j,k} + \frac{h^2}{2}\frac{d^2}{dx^2}\rho^B_{j,k} + \mathcal{O}(h^3), \tag{5.14}$$

$$\rho^B_{j,k\pm h} = \rho^B_{j,k} \pm h\frac{d}{dy}\rho^B_{j,k} + \frac{h^2}{2}\frac{d^2}{dy^2}\rho^B_{j,k} + \mathcal{O}(h^3), \tag{5.15}$$

into the flux equation given in Equation 3.25 and taking the limit as $h \to 0^+$.

If instead we let h be a small fixed number ϵ and disregard all terms of order h^3 or higher, we arrive at the following second order PDE system with diffusion terms:

$$\rho^A_t + [\phi^A_1 f(\rho^A)g(\rho^B)]_x + [\phi^A_2 f(\rho^A)g(\rho^B)]_y \tag{5.16}$$

$$= \frac{\epsilon}{2}\left[\left[\phi^A_x f(\rho^A)g(\rho^B) + \phi^A\left[\rho^A_x g(\rho^B) + (c_1 - c_2)f(\rho^A)\rho^B_x\right]\right]_x\right.$$

$$\left. + \left[\phi^A_y f(\rho^A)g(\rho^B) + \phi^A\left[\rho^A_y g(\rho^B) + (c_1 - c_2)f(\rho^A)\rho^B_y\right]\right]_y\right], \tag{5.17}$$

$$\rho^B_t + [\phi^B_1 f(\rho^B)g(\rho^A)]_x + [\phi^B_2 f(\rho^B)g(\rho^A)]_y \tag{5.18}$$

$$= \frac{\epsilon}{2}\left[\left[\phi^B_x f(\rho^B)g(\rho^A) + \phi^B\left[\rho^B_x g(\rho^A) + (c_1 - c_2)f(\rho^B)\rho^A_x\right]\right]_x\right.$$

$$\left. + \left[\phi^B_y f(\rho^B)g(\rho^A) + \phi^A\left[\rho^B_y g(\rho^A) + (c_1 - c_2)f(\rho^B)\rho^A_y\right]\right]_y\right], \tag{5.19}$$

with f and g as defined in Equation 3.35. Unfortunately, simulation of the diffusive equation is beyond the scope of the present work. However, it was found in [14] that the addition of the diffusive correction did mitigate the effects of the closure assumption in the case of fully mixed initial conditions in the one-dimensional case.

Chapter 6

Discussion

6.1 Summary of Results

From one- and two-group multi-agent models, we have been able to derive and simulate macroscopic PDE models that closely match the behavior of the microscopic stochastic models over relatively fair periods of time, though the closeness of the fit breaks down more rapidly as the strength of the slowdown interaction increases. This breakdown of the independence assumption is consistent with the results observed in [29]. For the two-group model, we also derived a diffusion correction to help the macroscopic model match the diffusiveness of the miscroscopic model observed under non-uniform initial conditions. The hyperbolicity of this model was also examined, and it was noted that the macroscopic model is likely to change from a hyperbolic to a non-hyperbolic regime and back over the course of its evolution, a change that has been observed in the past to lead to oscillations that are unlikely to arise in microscopic simulations or in nature.

As noted in Section 1.2.1, allowing multiple groups to move more realistically accord-

ing to both a preferred velocity field and a rule for interacting with an opposing group allows for much more interesting and realistic models to be studied by allowing for more complicated combinations of behavior. While we did not have sufficient time to study all implications of the expanded model, we will outline in the following section several potential areas of further research.

6.2 Recommendations for Future Work

6.2.1 Pedestrian Behavior Rules

The present work concerns itself with pedestrians whose behavior is determined by very simple rules involving only a velocity field and the pedestrian's immediate neighbors in a von Neumann neighborhood. Realistically, a pedestrian would incorporate more information into his or her behavior than just his or her immediate surroundings; for example, the pedestrian might change behavior based on not only the local density of pedestrians, but also on the density of pedestrians at the target point or at any point in between. It remains to be seen what effect deriving a macroscopic model from this type of miscroscopic interaction would have.

6.2.2 Group Switching

In an evacuation scenario, it is unlikely that people who are trying to evacuate a building will have a strong preference for one exit over another. As the situation evolves, a person may find herself in a scenario in which it would be wise to change which exit she is heading towards. This could be modeled at the microscopic level by a rule that allows a pedestrian to change groups, thereby changing velocity fields. A

study of a model with this type of rule could be interesting, as it would mean that the mass of a given group is no longer necessarily conserved, though the total mass would be.

6.2.3 Dynamic Velocity Field

In the models studied in this work, the velocity field is a function only of location on the lattice. In works such as [12], models are studied in which the defined floor fields change with time and are influenced by the passage of pedestrians. While the models studied in this work do not take into account changes in the velocity field, it is a logical extension of the studies presented herein.

6.2.4 Obstacle Avoidance

In [32], pedestrians are assigned behavior to navigate around obstacles on the lattice. In the models presented in this work, the only way for a pedestrian to do so would be to build obstacle avoidance into the defined velocity fields. A more interesting approach would be to define obstacle avoidance behavior at the level of the logic of the pedestrians themselves. One way to do so would be to create an additional group that a pedestrian could transfer into, with pedestrians of this group following specific obstacle avoidance commands and returning to the original group once the original obstacle was successfully avoided. This would then add additional equations to the macroscopic model describing the densities of the new groups.

6.2.5 Pedestrians with Memory

A potential way to deal obstacle avoidance is to have pedestrians track their previous behavior to some extent, thus giving them a sense of memory. Indeed, memory may be necessary to navigate some types of obstacles, as naively changing directions when a blockage is encountered and then returning to previous behavior was the obstacle has been passed could cause a pedestrian to walk directly back into the obstacle, leading to looping behavior. If the current state of a pedestrian is redefined to incorporate a series of remembered states, the system could still be viewed as a Markov chain, though one of much higher complexity, and the same methodology of study could still theoretically be employed.

6.2.6 Closure Assumptions

While the closure assumptions used to derive the mesoscopic model produce fairly good results, they rely on the assumption that adjacent cells and opposite groups are independent, which is not obvious. More work needs to be done to justify the closure used or to derive a more accurate close assumption. The closure assumption used in the present work should at least be verified numerically through simulation. As in [21], various closure assumptions should be examined and the resulting macroscopic models compared.

6.2.7 Further Analysis of Hyperbolicity Condition

In Section 5.1.4, we examined the hyperbolicity of the simulation from Section 4.2 and found that in the areas of interest for the given initial conditions, the values of ρ^A and ρ^B that produced non-hyperbolic results were almost identical for each

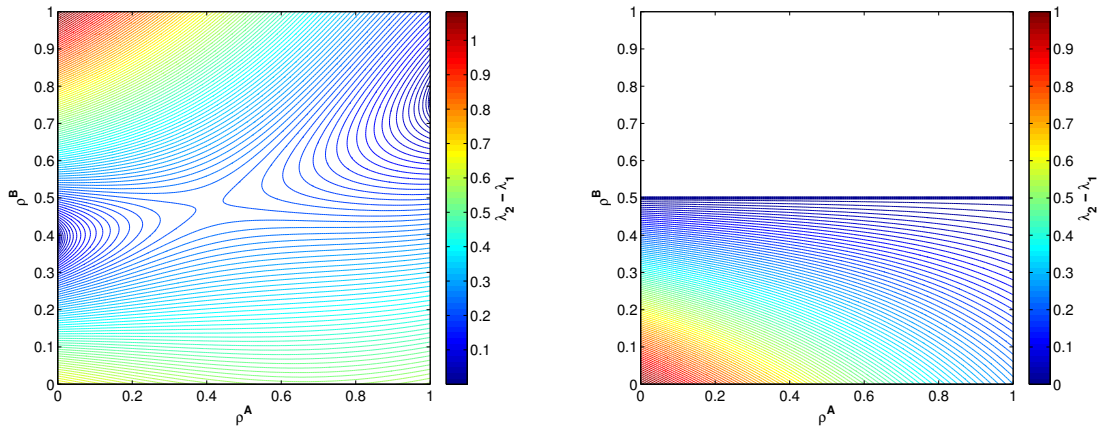

(a) Cell $(22, 19)$ (b) Cell $(22, 20)$

Figure 6.1: Difference of Real Eigenvalues, $\alpha = 2$

examined cell. If, however, we look at specific cells on the current lattice (Figure 6.1) or on an extended version of the lattice (Figure 6.2), we see that the hyperbolicity condition can vary greatly. The current theory is that the condition depends at least partly on the angle formed by the rays connecting the observed cell and the target point, but this has only been tested through observation. Further analysis of the hyperbolicity condition given in Equation 5.7 will be required to reveal whether or not this is actually the case.

6.2.8 Simulation of Diffusive Correction

In Section 5.2.2, a diffusive correction is derived in an attempt to correct for the lack of diffusiveness of the macroscopic model in comparison with the microscopic model. In [14], deriving such a correction was able to compensate for the lack of diffusiveness caused by the closure assumptions. We have hopes that this will also be the case here, but derivation of a discretization of Equation 5.16 and the simulation thereof is beyond the scope of the current work. It is hoped that a simulation of this equation

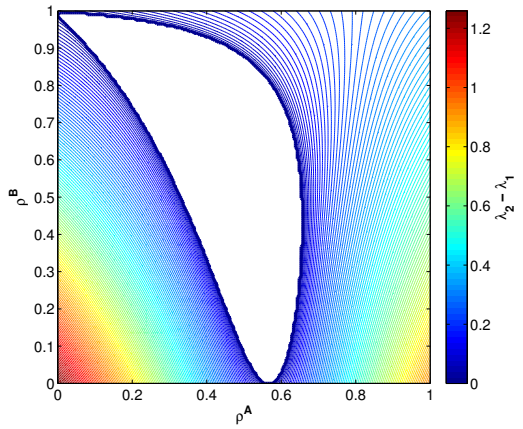

(a) Cell $(22, 273)$

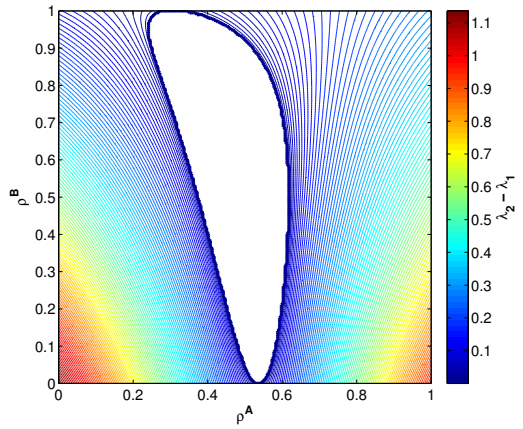

(b) Cell $(22, 300)$

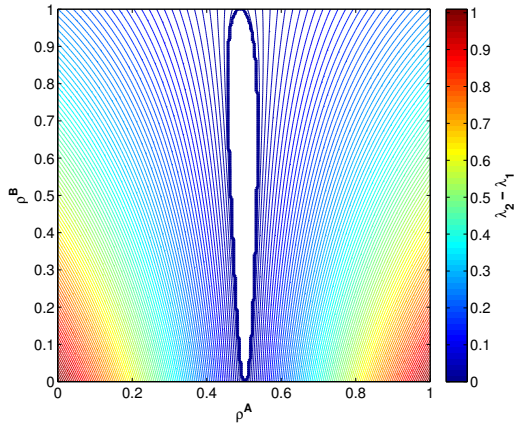

(c) Cell $(22, 335)$

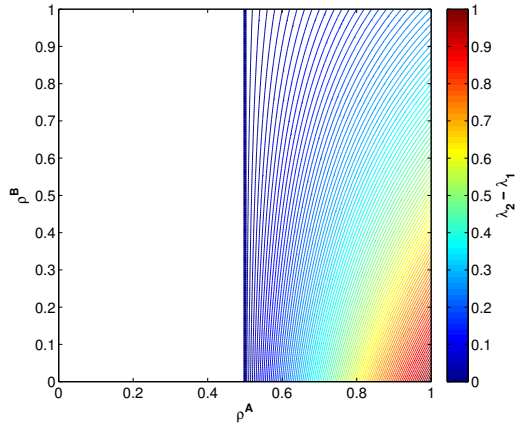

(d) Cell $(22, 338)$

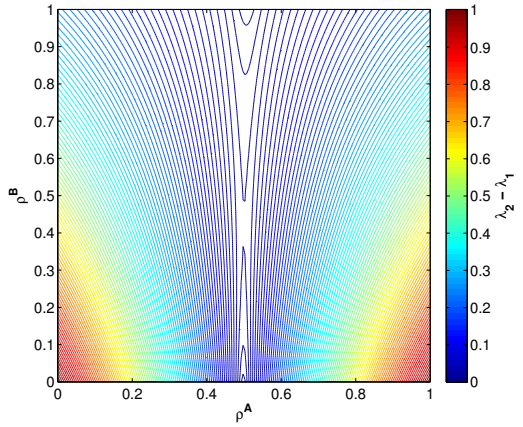

(e) Cell $(22, 340)$

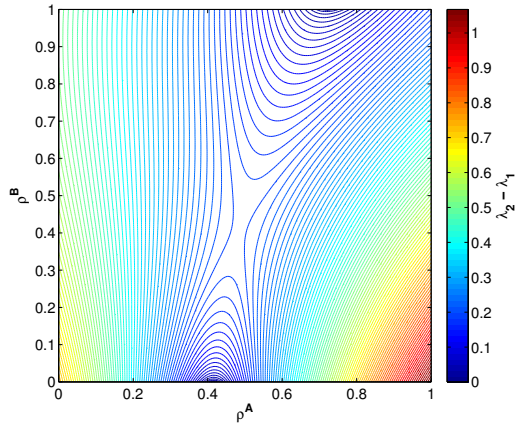

(f) Cell $(22, 455)$

Figure 6.2: Difference of Real Eigenvalues, $\alpha = 2$, Various Cells on Extended Lattice

with the non-uniform initial conditions outlined in Section 4.3 would result in a closer match for the agent-based model.

6.2.9 Real-World Observation

The scaling coefficients used in the simulations presented in this work are based not on real-world observation but on simplicity of use. Observation of actual pedestrian group interactions would be necessary to determine values for the scaling coefficients and would lead to more useful data.

Appendices

Appendix A

Comparison of Stochastic Simulation Methods

To lend legitimacy to the use of the Progressive Modified Tau-Leaping Method defined in Section 4.1, we here present a comparison of the results of simulating the model defined in Section 4.2.3 using both the Progressive Modified Tau-Leaping Method and the more traditional Kinetic Monte Carlo method, the algorithm for which is also defined in Section 4.1. Following the format of the results presented in Chapter 3, Figures A.1, A.2, and A.3 show the densities for the groups on the lattice at various times, and Figures A.4, A.5, and A.6 show the density of a single group along the diagonal of the lattice. Both simulations are run to a maximum time of $t = 250$, but while the Progressive Modified Tau-Leaping Method is averaged over 1000 realizations, the Kinetic Monte Carlo model is averaged over only 100 realizations, as it is much more time intensive to run.

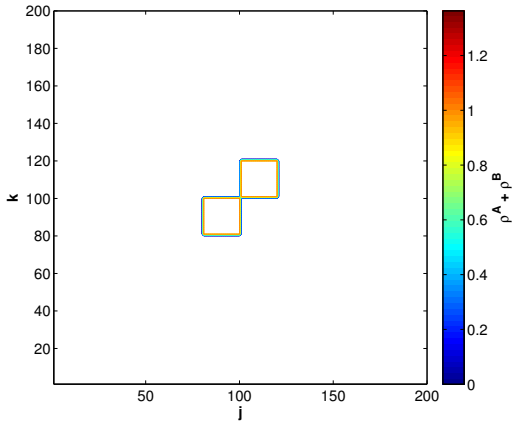

(a) Tau-Leaping, $t = 0$

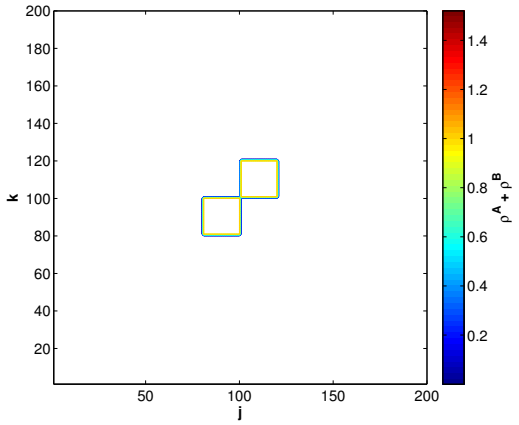

(b) KMC, $t = 0$

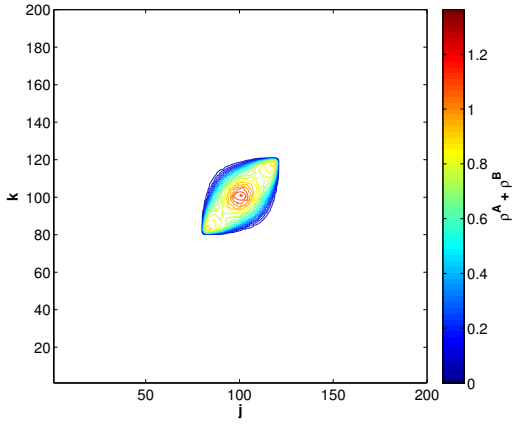

(c) Tau-Leaping, $t = 30$

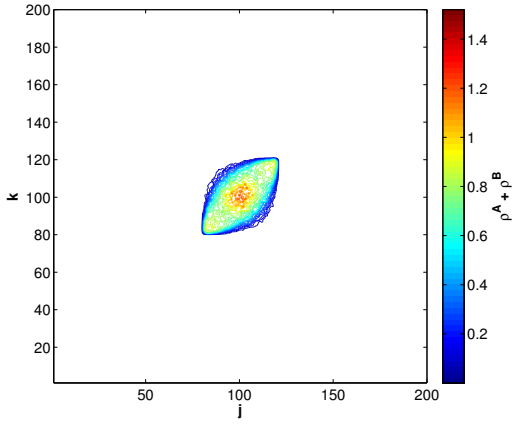

(d) KMC, $t = 30$

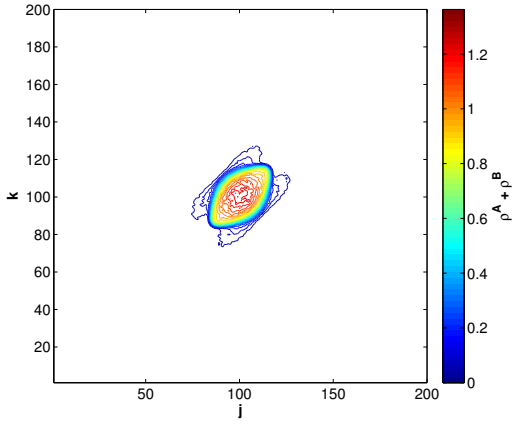

(e) Tau-Leaping, $t = 60$

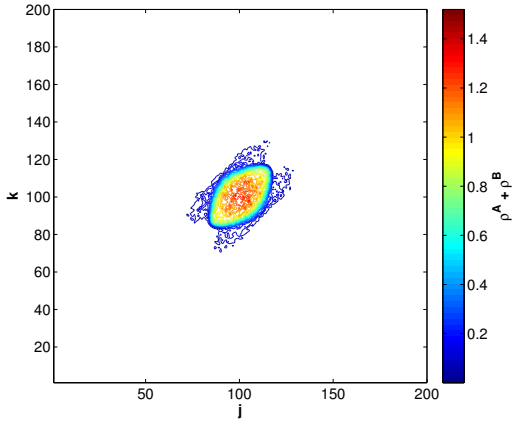

(f) KMC, $t = 60$

Figure A.1: ρ^A and ρ^B, Tau-Leaping and Kinetic Monte Carlo Models
Times $t = 0, 30, 60$, $\alpha = 2$

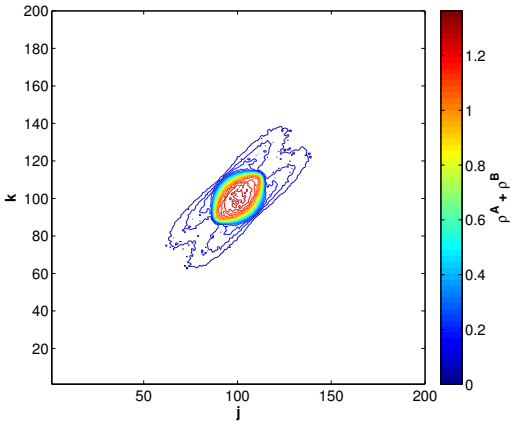

(a) Tau-Leaping, $t = 90$

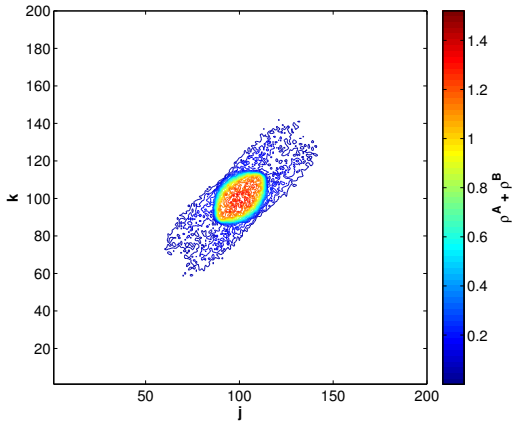

(b) KMC, $t = 90$

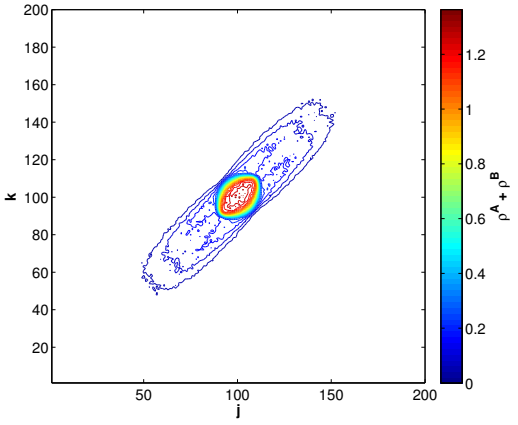

(c) Tau-Leaping, $t = 120$

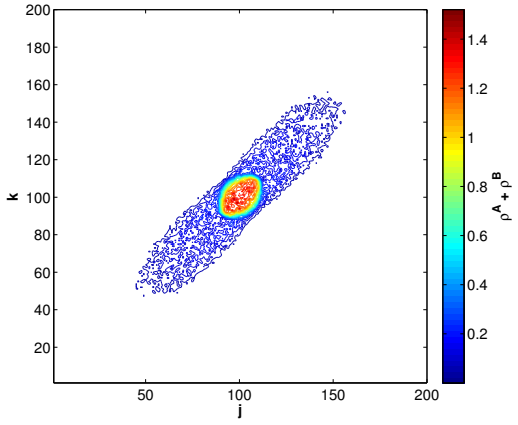

(d) KMC, $t = 120$

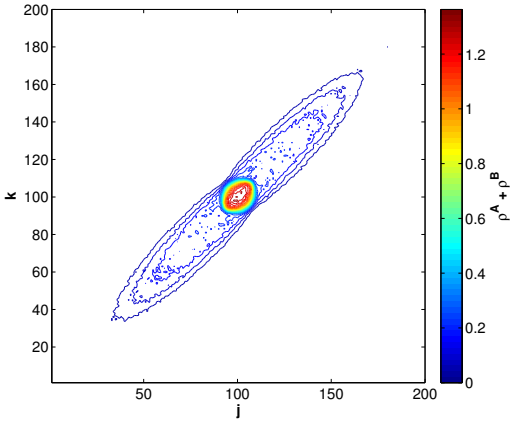

(e) Tau-Leaping, $t = 150$

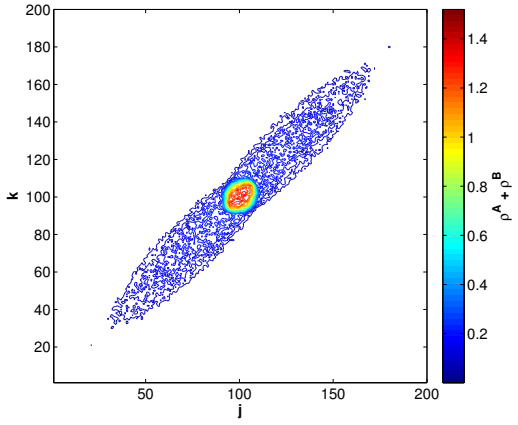

(f) KMC, $t = 150$

Figure A.2: ρ^A and ρ^B, Tau-Leaping and Kinetic Monte Carlo Models
Times $t = 90, 120, 150$, $\alpha = 2$

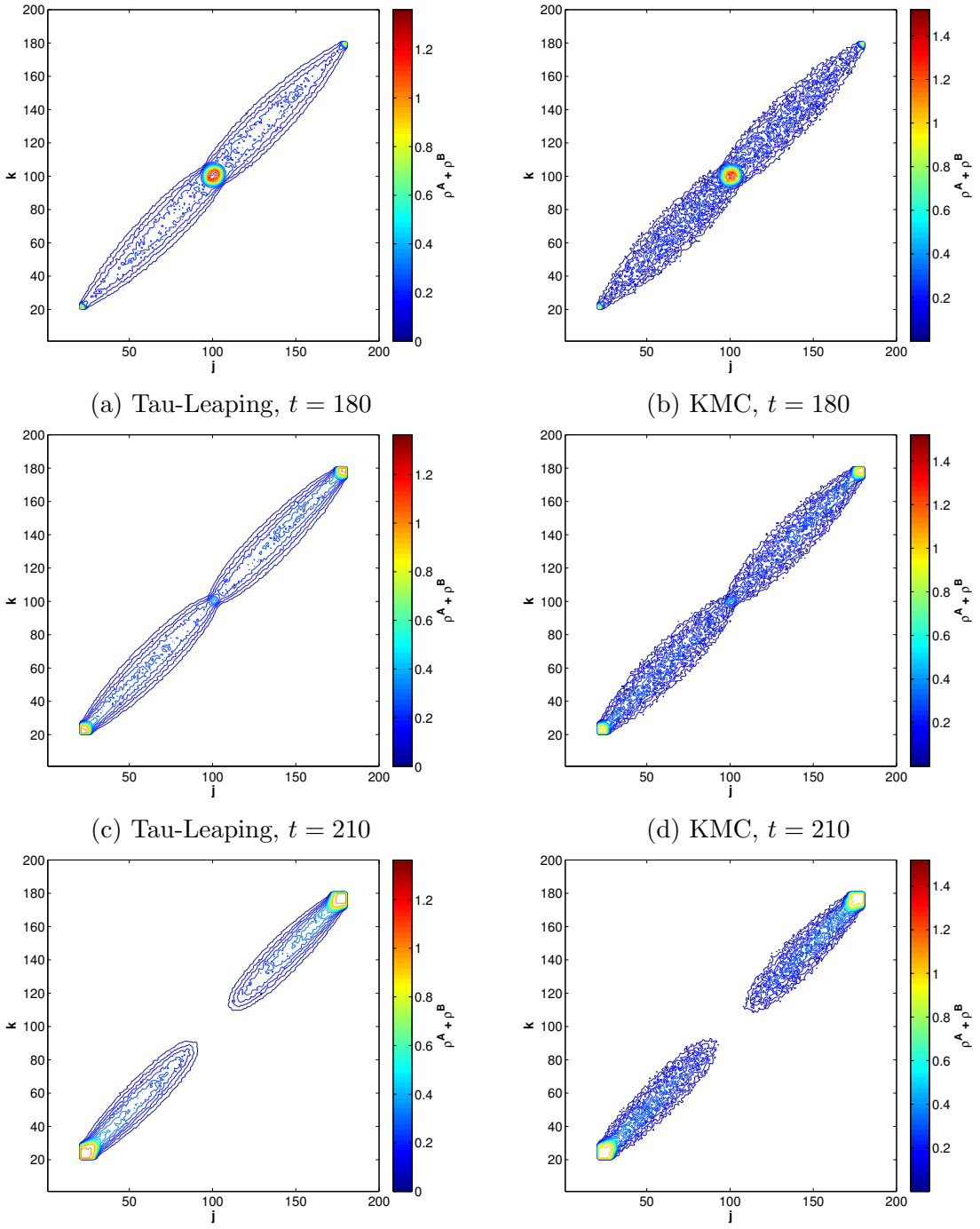

(a) Tau-Leaping, $t = 180$

(b) KMC, $t = 180$

(c) Tau-Leaping, $t = 210$

(d) KMC, $t = 210$

(e) Tau-Leaping, $t = 240$

(f) KMC, $t = 240$

Figure A.3: ρ^A and ρ^B, Tau-Leaping and Kinetic Monte Carlo Models
Times $t = 180, 210, 240$, $\alpha = 2$

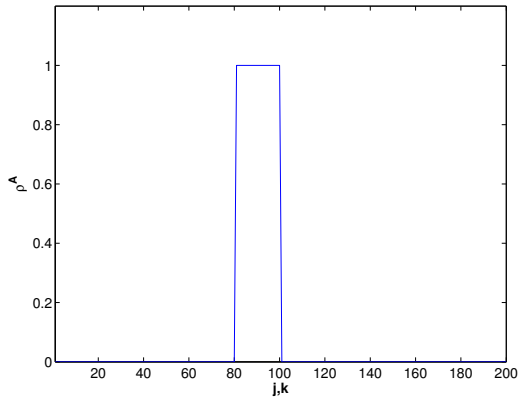

(a) Tau-Leaping, $t = 0$

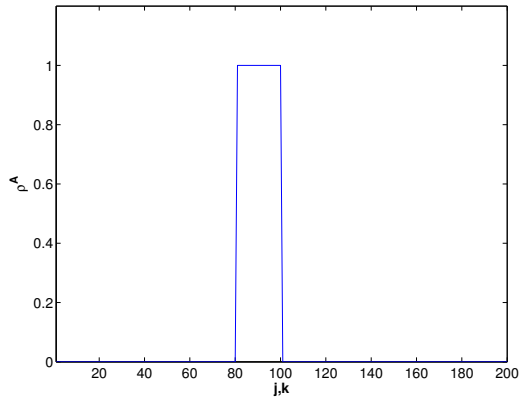

(b) KMC, $t = 0$

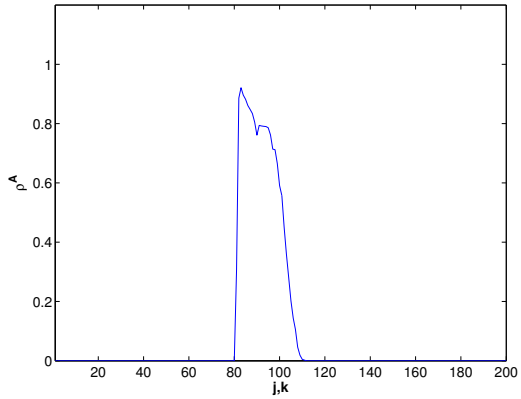

(c) Tau-Leaping, $t = 30$

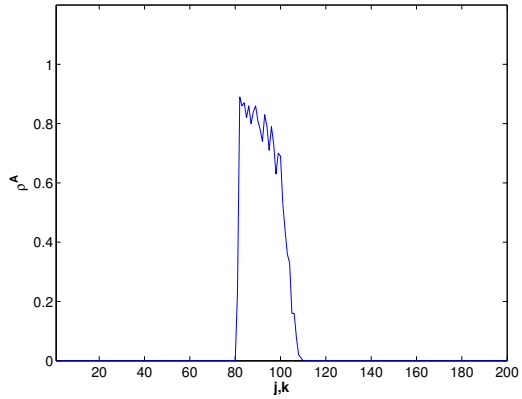

(d) KMC, $t = 30$

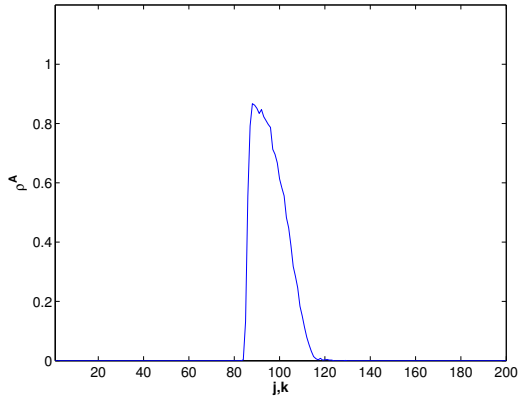

(e) Tau-Leaping, $t = 60$

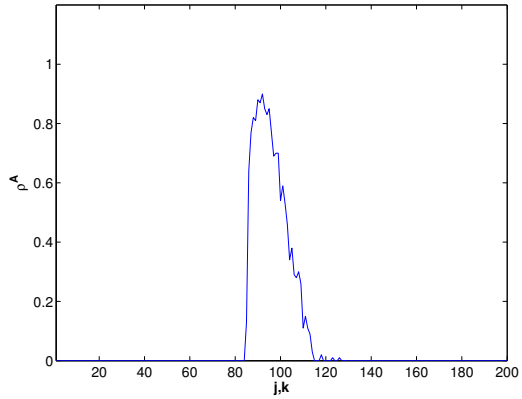

(f) KMC, $t = 60$

Figure A.4: $\rho^A_{j,j,t}$, Tau-Leaping and Kinetic Monte Carlo Models
Times $t = 0, 30, 60$, $\alpha = 2$

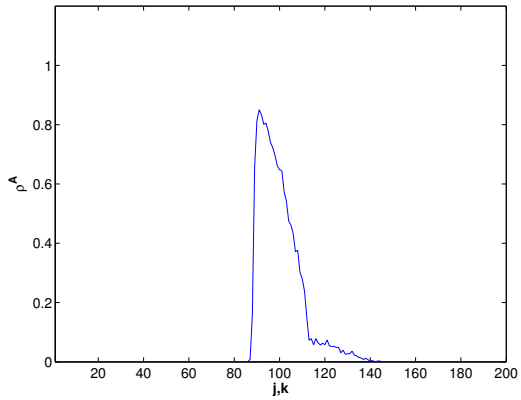

(a) Tau-Leaping, $t = 90$

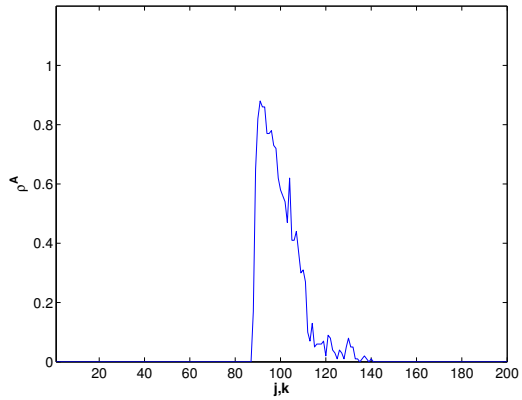

(b) KMC, $t = 90$

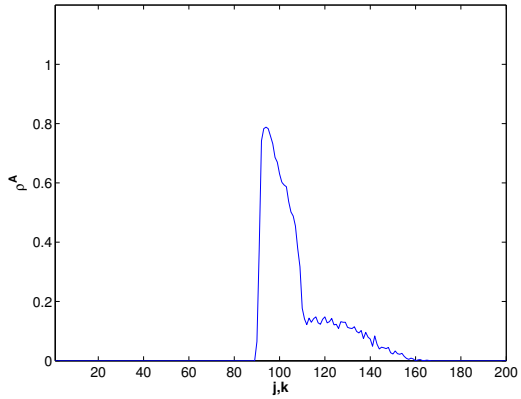

(c) Tau-Leaping, $t = 120$

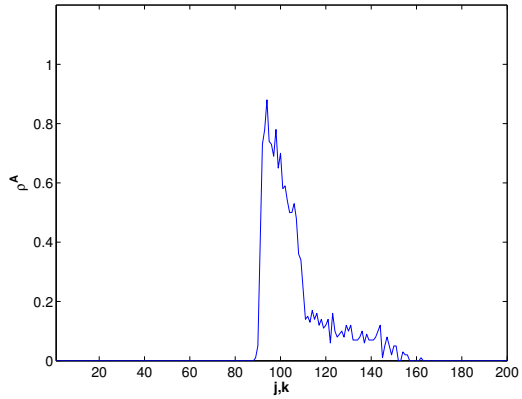

(d) KMC, $t = 120$

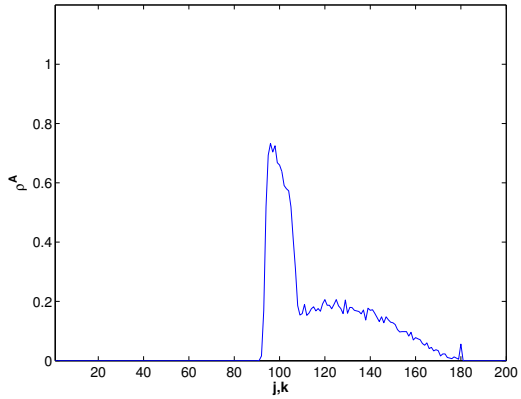

(e) Tau-Leaping, $t = 150$

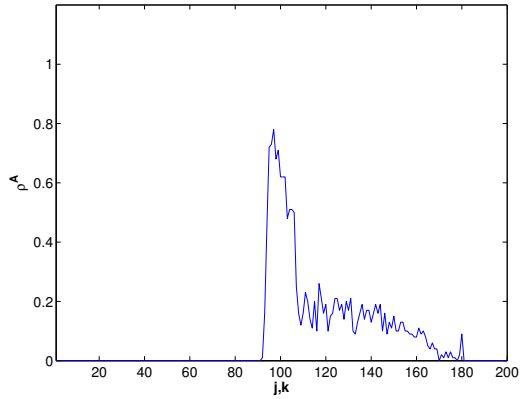

(f) KMC, $t = 150$

Figure A.5: $\rho^A_{j,j,t}$, Tau-Leaping and Kinetic Monte Carlo Models
Times $t = 90, 120, 150$, $\alpha = 2$

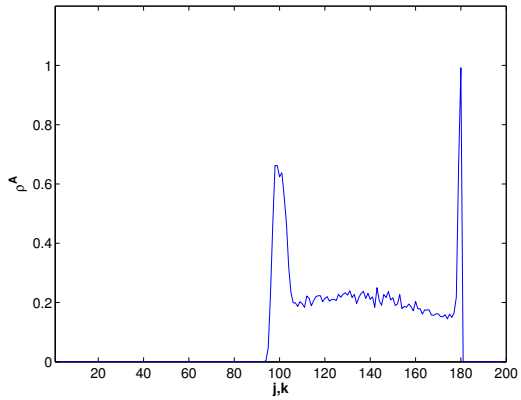

(a) Tau-Leaping, $t = 180$

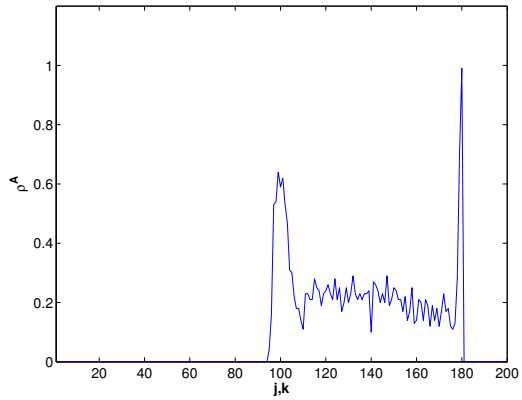

(b) KMC, $t = 180$

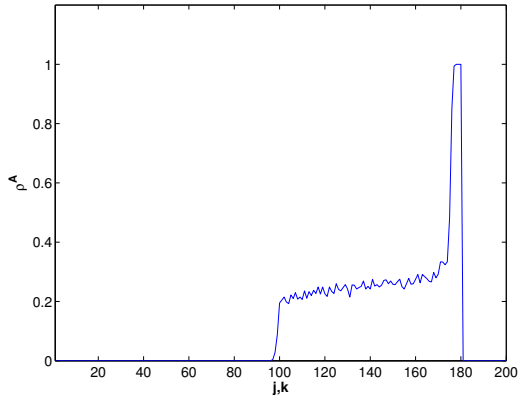

(c) Tau-Leaping, $t = 210$

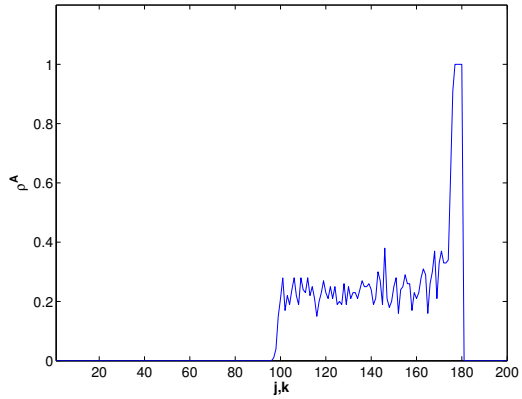

(d) KMC, $t = 210$

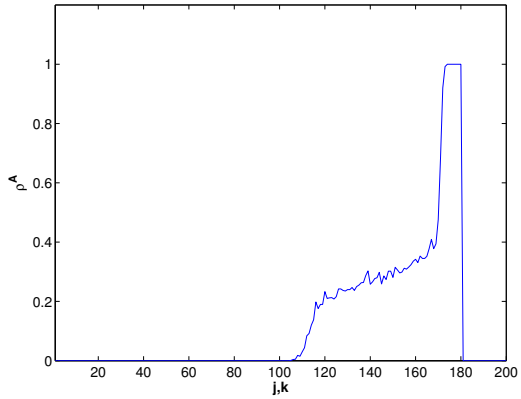

(e) Tau-Leaping, $t = 240$

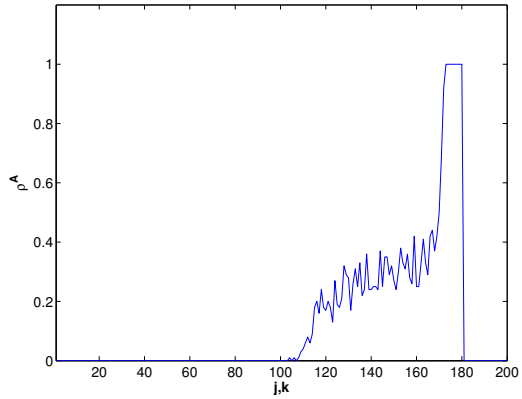

(f) KMC, $t = 240$

Figure A.6: $\rho^A_{j,j,t}$, Tau-Leaping and Kinetic Monte Carlo Models
Times $t = 180, 210, 240$, $\alpha = 2$

Bibliography

[1] Al-nasur, S. and P. Kashroo, "A microscopic-to-macroscopic crowd dynamic model", in *Proceedings of the IEEE Intelligent Transportation Systems Conference 2006*: 606611.

[2] Alperovich, T. and A. Sopasakis. "Modeling highway traffic with stochastic dynamics", in *J.Stat.Phys*, 133: 1083-1105, 2008.

[3] Appert-Rolland, C., J. Cividini, H.J. Hilhorst, and P. Degond. "Pedestrian Flows: From Individuals to Crowds", in *Transportation Research Procedia*, Volume 2: 468-476, 2014.

[4] Appert-Rolland, C., P. Degond, and S. Motsch. "Two-way multi-lane traffic model for pedestrians in corridors", in *Networks and Heterogeneous Media*, 6: 351381, 2011.

[5] Bando, M., K. Hasebe, A. Nakayama, A. Shibata and Y. Sugiyama. "Dynamical model of traffic congestion and numerical simulation", in *Physical Review E*, 51: 1035-1042, 1995.

[6] Bandyopadhyay, T., C. Jie, D. Hsu, J. Ang, Marcelo H. Ang Jr., D. Rus, and E. Frazzoli. "Intention-aware pedestrian avoidance", in *Experimental Robotics*, Edited by J. P. Desai, G. Dudek, O. Khatib, and V. Kumar, vol. 88 of *Springer Tracts in Advanced Robotics*: 963-977, Springer International Publishing, 2013.

[7] Bellomo, N., B. Piccoli, and A. Tosin. "Modeling dynamics from a complex system viewpoint", in *Mathematical Models and Methods in Applied Sciences*, 22(2): 1230004, 2012.

[8] Bellomo, Nicola and Christian Dogbe. "On the modelling crowd dynamics from scaling to hyperbolic macroscopic models", *Mathematical Models and Methods in Applied Sciences*, 18: 1317-1345, 2008.

[9] Bellomo, Nicola and Christian Dogbe. "On the Modeling of Traffic and Crowds: A Survey of Models, Speculations, and Perspectives", in *SIAM Review*, 53(3): 409-463, 2011.

[10] Blue, V. J. and J. L. Adler. "Cellular automata microsimulation for modeling bi-directional pedestrian walkways", in *Transportation Research Part B*, 35: 293312, 2001.

[11] Blue, V. J. and J. L. Adler. "Cellular automata microsimulation of bi-directional pedestrian flows", in *J. Trans. Research Board*, 1678: 135-141, 2000.

[12] Burstedde, C., K. Klauck, A. Schadschneider, and J. Zittarz. "Simulation of pedestrian dynamics using a 2-dimensional cellular automaton", in *Physica A*, 295: 507525, 2001.

[13] Castellano, C., S. Fortunato, and V. Loreto, "Statistical physics of social dynamics", in *Rev. Mod. Phys.*, 81: 591-646, 2009.

[14] Chertock, A., A. Kurganov, A. Polizzi, and I. Timofeyev. "Pedestrian Flow Models with Slowdown Interactions", in *Mathematical Models and Methods in Applied Sciences* 24(2): 249-275, 2014.

[15] Chopard, Bastien, Alexandre Dupuis, Alexandre Masselot, and Pascal Luthi. "Cellular Automata and Lattice Boltzmann Techniques: An Approach to Model and Simulate Complex Systems.", in *Advances In Complex Systems*, 5(2/3): 103-246, 2002.

[16] Chowdhury, D., V. Guttal, K. Nishinari, and A. Schadschneider. "A cellular-automata model of flow in ant trails: non-monotonic variation of speed with density", in *Journal of Physics A: Mathematical and General*, 35(41): L573, 2002.

[17] Chowdhury, D., L. Santen, and A. Schadschneider. "Statistical physics of vehicular traffic and some related systems", in *Physics Reports*, 329(46): 199-329, 2000.

[18] Cremer, M. and J. Ludwig. "A fast simulation model for traffic flow on the basis of Boolean operation", in *Mathematics and Computers in Simulation*, 28: 297-303, 1986.

[19] Degond, P. "Macroscopic limits of the Boltzmann equation: A review", in *Modeling and Computational Methods for Kinetic Equations*: 3-57, 2004.

[20] Degond, P., A. Frouvelle and J-G. Liu. "Macroscopic limits and phase transition in a system of self-propelled particles", in *J. Nonlinear Sci.*, 23: 427-456,2013.

[21] Degond, P., C. Appert-Rolland, J. Pettré, and G. Theraulaz. "Vision-based macroscopic pedestrian models", in *Kinetic and Related Models*, 6: 809-839, 2013.

[22] Degond, P., C. Appert-Rolland, M. Moussaïd, J. Pettré, and G. Theraulaz. "A Hierarchy of Heuristic-Based Models of Crowd Dynamics", in *Journal of Statistical Physics*, 152(6): 1033-1068, 2013.

[23] Degond, Pierre, Jian-Guo Liu, and Christian Ringhofer. "Large-scale dynamics of Mean-Field Games driven by local Nash equilibria", in *Journal of Nonlinear Science*, 24: 93-115, 2014.

[24] Dijkstra, J., A. Jessurun, and H. Timmermans. "A multi-agent cellular automata model of pedestrian movement", in *Pedestrian and Evacuation Dynamics*: 173-181, Edited by M. Schreckenberg and S.D. Sharma, Berlin: Springer-Verlag, 2001.

[25] Dundon, N. and A. Sopasakis. "Stochastic modeling and simulation of multi-lane traffic", in *Transportation and Traffic Theory 2007: Papers selected for presentation at ISTTT17*: 661-691, 2007.

[26] Ezaki, T., D. Yanagisawa, and K. Nishinari. "Pedestrian flow through multiple bottlenecks", in *Phys. Rev. E*, 86: 026118, 2012.

[27] Fukui, M. and Y. Ishibashi. "Self-organized phase transitions in cellular automaton models for pedestrians", in *J. Phys. Soc. Jpn.*, 68: 2861-2863, 1999.

[28] Gipps, P. G. and B. Marksjo. "A micro-simulation model for pedestrian flows", in *Mathematics and Computers in Simulation*, 27: 95-105, 1985.

[29] Hauck, C., Y. Sun and I. Timofeyev, "On Cellular Automata Models of Traffic Flow with Look-Ahead Potential", in *Stochastics and Dynamics* 14(3): 1350022, 2014.

[30] Helbing, D. "A fluid dynamic model for the movement of pedestrians", in *Complex Systems*, 6(5): 391-415, 1992.

[31] Helbing, D. "Traffic and related self-driven many-particle systems", in *Rev. Mod. Phys.*, 73: 1067-1141, 2001.

[32] Huang, Hai-Jun and Ren-Yong Guo. "Static floor field and exit choice for pedestrian evacuation in rooms with internal obstacles and multiple exits", in *Phys. Rev. E*, 78: 021131, 2008.

[33] Kirchner, A. and A. Schadschneider. "Simulation of evacuation processes using a bionics-inspired cellular automaton model for pedestrian dynamics", in *Physica A*, 312: 260276, 2002.

[34] Kneidl, A., M. Thiemann, A. Borrmann, S. Ruzika, G. K. H. W. Hamacher, and E. Rank. "Bidirectional coupling of macroscopic and microscopic approaches for pedestrian

behavior prediction", in *Pedestrian and Evacuation Dynamics*: 459-470, Edited by R. D. Peacock, E. D. Kuligowski and J. D. Averill. Springer, 2011.

[35] Knopse, Wolfgang, Ludger Santen, Andreas Schadschneider, and Michael Schreckenberg. "Towards a realistic microscopic description of highway traffic", in *Journal of Physics A: Mathematical and General*, 33(48): L477-85, 2000.

[36] Landim, C. and C. Kipnis, *Scaling Limits of Interacting Particle Systems*, Berlin: Springer, 1999.

[37] Liggett, Thomas. *Interacting Particle Systems*, New York: Springer-Verlag, 1985.

[38] Lighthill, M. J. and G.B.Whitham. "On kinematic waves II: A theory of traffic flow on long, crowded roads", in *Proceedings of The Royal Society of London Ser. A*, 229: 317-345, 1955.

[39] Lizhong, Y., F. Weifeng, H. Rui, and D. Zhihua. "Occupant evacuation model based on cellular automata in fire", in *Chinese Science Bulletin*, 47(17): 1484-1487, 2002.

[40] Muramatsu, M., T. Irie, and T. Nagatani. "Jamming transition in pedestrian counter flow", in *Physica A*, 267(34): 487-498, 1999.

[41] Muramatsu, M. and T. Nagatani. "Jamming transition in two-dimensional pedestrian traffic", in *Physica A: Statistical Mechanics and its Applications*, 275(12): 281-291, 2000.

[42] Nagel, Kai and Maya Paczuski. "Emergent traffic jams", in *Phys. Rev. E*, 51(4): 2909-2918, 1995.

[43] Nagel, Kai and Michael Schreckenberg. "A cellular automaton model for freeway traffic", in *J. Phys. I France*, 2: 2221-2229, 1992.

[44] Newell, G. F. "Nonlinear Effects in the Dynamics of Car Following", in Operations Research, 9(2): 209-229, 1961.

[45] Pipes, Louis. "An Operational Analysis of Traffic Dynamics", in *J. Appl. Phys.*, 24: 274-81, 1953.

[46] Rauch, E. M., M. M. Millonas, and D. R. Chialvo. "Pattern formation and functionality in swarm models", in *Physics Letters A*, 207(3-4): 185-193, 1995.

[47] Schadschneider, A., W. Klingsch, H. Klupfel, T. Kretz, C. Rogsch, and A. Seyfried. "Evacuation dynamics: Empirical results, modeling and applications", in *Encyclopedia of Complexity and Systems Science*: 3142-3176, Edited by R. Meyers, Berlin: Springer-Verlag, 2009.

[48] Schelhorn, T., D. OSullivan, M. Haklay, and M. Thurstain-Goodwin. "STREETS: An Agent-Based Pedestrian Model", Working Paper 9, London: Centre for Advanced Spatial Analysis, University College, 1999.

[49] Schelling, Thomas. "Models of Segregation", in *American Economic Review*, 59(2): 488-93, 1969.

[50] Sopasakis, A. and M. Katsoulakis, "Stochastic modeling and simulation of traffic flow: Asymmetric single exclusion process with arrhenius look-ahead dynamics", in*SIAM J. Appl. Math.*, 66: 921944, 2006.

[51] Spitzer, Frank. "Random processes defined through the interaction of an infinite particle system", in *Probability and Information Theory: Proceedings of the International Symposium at McMaster University, Canada, April, 1968*: 201-223, Edited by M. Behara, K. Krickeberg, and J. Wolfowitz, Berlin: Springer Berlin Heidelberg, 1969.

[52] Treiber, Martin and Arne Kesting. *Traffic Flow Dynamics: Data, Models and Simulation*, Translated by Martin Treiber and Christian Thiemann. New York: Springer-Verlag, 2013.

[53] von Neumann, John. "The General and Logical Theory of Automata", in *Cerebral Mechanisms in Behavior*, 1-41. New York: Wiley, 1941.

[54] Watmough, J. and L. Edelstin-Keshet. "Modelling the formation of trail networks by foraging ants", in *J. Theor. Biol*, 176: 357-371, 1995.

[55] Wong, G. C. K. and S. C. Wong. "A multi-class traffic flow model - an extension of LWR model with heterogeneous drivers", in *Transportation Research*, 36A(9): 827-841, 2002.

[56] Yang, L., K. Zhu, and S. Liu. "Cellular automata evacuation model considering information transfer in building with obstacles", in *Pedestrian and Evacuation Dynamics*: 317-326, Edited by R. D. Peacock, E. D. Kuligowski, and J. D. Averill. Springer, 2011.

[57] Yue, H., H. Hao, X. Chen, and C. Shao. "Simulation of pedestrian flow on square lattice based on cellular automata model", in *Physica A*, 384: 567-588, 2007.

[58] Zhang, H. M. "A non-equilibrium traffic model devoid of gas-like behaviour", in *Transportation Research Part B*, 36: 275-290, 2002.